

Development of an effective modelling method for the local mechanical analysis of submarine power cables

Fang, P.

DOI

[10.4233/uuid:acf6c625-1038-4e0e-b463-f5256cd803f9](https://doi.org/10.4233/uuid:acf6c625-1038-4e0e-b463-f5256cd803f9)

Publication date

2024

Document Version

Final published version

Citation (APA)

Fang, P. (2024). *Development of an effective modelling method for the local mechanical analysis of submarine power cables*. [Dissertation (TU Delft), Delft University of Technology].
<https://doi.org/10.4233/uuid:acf6c625-1038-4e0e-b463-f5256cd803f9>

Important note

To cite this publication, please use the final published version (if applicable).
Please check the document version above.

Copyright

Other than for strictly personal use, it is not permitted to download, forward or distribute the text or part of it, without the consent of the author(s) and/or copyright holder(s), unless the work is under an open content license such as Creative Commons.

Takedown policy

Please contact us and provide details if you believe this document breaches copyrights.
We will remove access to the work immediately and investigate your claim.

**DEVELOPMENT OF AN EFFECTIVE MODELLING
METHOD FOR THE LOCAL MECHANICAL ANALYSIS
OF SUBMARINE POWER CABLES**

**DEVELOPMENT OF AN EFFECTIVE MODELLING
METHOD FOR THE LOCAL MECHANICAL ANALYSIS
OF SUBMARINE POWER CABLES**

Dissertation

for the purpose of obtaining the degree of doctor
at Delft University of Technology
by the authority of the Rector Magnificus, prof. dr. ir. T.H.J.J. van der Hagen,
chair of the Board for Doctorates
to be defended publicly on
Monday 16th, December 2024 at 17:30 o'clock

by

Pan FANG

Master of Structural Engineering
Zhejiang University, Hangzhou, China
born in Jingdezhen, Jiangxi, China

This dissertation has been approved by the promotor.

Composition of the doctoral committee:

Rector Magnificus,	chairperson
Prof. dr. J.J. Hopman,	Delft University of Technology, <i>promotor</i>
Dr. X. Jiang,	Delft University of Technology, <i>copromotor</i>

Independent members:

Prof. dr. Svein Sævik	Norwegian University of Science and Technology
Prof. dr. Patrice Cartraud	Ecole Centrale Nantes, France
Prof. dr. Carey L. Walters	Delft University of Technology
Prof. dr. Lambertus J. Sluys	Delft University of Technology
Prof. dr. Chiara Bisagni	Delft University of Technology



The research leading to this dissertation is partly funded by Delft University of Technology (TU Delft) and China Scholarship Council (CSC) under the grant 201606950011.

Keywords: Submarine Power Cables; Periodical boundary conditions; Repetitive Unit Cell; Helical; Tension; Bending; Combined Tension and Bending

TRAIL Thesis Series no. T2024/17, the Netherlands TRAIL Research School

TRAIL

P.O. Box 5017

2600 GA Delft

The Netherlands

E-mail: info@rsTRAIL.nl

ISBN 978-90-5584-356-5

Copyright © 2024 by P. Fang

All rights reserved. No part of the material protected by this copyright notice may be reproduced or utilized in any form or by any means, electronic or mechanical, including photocopying, recording or by any information storage and retrieval system, without written permission from the author.

Printed in the Netherlands

满纸荒唐言，一把辛酸泪。
都云作者痴，谁解其中味。

曹雪芹

CONTENTS

Summary	xi
Samenvatting	xiii
Preface	xv
Nomenclature	xvii
1 Introduction	1
1.1 Background	2
1.2 Research objective and questions	6
1.3 Outline of the dissertation	6
2 Literature review	11
2.1 Cable configuration	12
2.1.1 Conductor	13
2.1.2 Insulation system	13
2.1.3 Armour layer	15
2.1.4 Serving	15
2.2 Cable design process	16
2.2.1 General cable design process	16
2.2.2 Mechanical design process for DPCs	16
2.3 Analytical method	19
2.3.1 Axisymmetric loadings	19
2.3.2 Bending	23
2.3.3 Remarks on analytical method	25
2.4 Numerical method	27
2.4.1 Axisymmetric loadings	27
2.4.2 Bending	29
2.4.3 Remarks on numerical method	35
2.5 Test method	35
2.5.1 Tension & Torsion tests	35
2.5.2 Bending tests	38
2.5.3 Remarks on test method	43
2.6 Summary	43
2.7 Chapter arrangement	45
3 Methodology	59
3.1 The Establishment of Finite Elements	60

3.2	The Setup of Contact	60
3.3	The Formulation of Boundary conditions	61
3.3.1	Macroscale problem	61
3.3.2	Microscale problem	63
3.3.3	Periodical boundary conditions	64
3.3.4	Boundary conditions for SPCs	70
3.4	CONCLUSIONS	71
4	Validation of the RUC model under tension	75
4.1	Tests	76
4.1.1	Material tests	76
4.1.2	Tension test	78
4.2	Validation of the RUC model under tension	80
4.3	Full-scale model	84
4.4	Results and discussions	84
4.4.1	Cable overall behaviour	85
4.4.2	Cable component behaviour	86
4.5	CONCLUSIONS	90
5	Validation of the RUC model under bending	93
5.1	Tests	94
5.1.1	Bending tests of the single-core SPC	94
5.1.2	Bending test of the three-core SPC	96
5.2	Validation of RUC Model under bending	97
5.2.1	Construction of the two types of SPCs	97
5.2.2	Calibration of the damping coefficient	99
5.2.3	Validation of the RUC model under bending	100
5.3	Full-scale models	103
5.3.1	Construction of the full-scale models	103
5.3.2	Discussions	104
5.4	Results and discussions	105
5.4.1	Cable overall behaviour	105
5.4.2	Cable component behaviour	109
5.5	CONCLUSIONS	112
6	Demonstration of the RUC model	117
6.1	Combined tension and bending	118
6.1.1	Construction of the RUC model	118
6.1.2	Cable overall behaviour	118
6.1.3	Cable component behaviour	120
6.2	Parametric studies	124
6.2.1	The local mechanical behaviours of the SPC without inner components	124
6.2.2	The local mechanical behaviours of the SPC with different pitch lengths regarding the inner components	125
6.2.3	The local mechanical behaviours of the SPC with different pitch lengths regarding the helical wires	126

6.3	CONCLUSIONS	127
7	Conclusions and Discussions	129
7.1	Conclusions	130
7.2	Limitations and Recommendations	133
7.3	Guidelines for employing the RUC model	134
	Acknowledgements	139
	Curriculum Vitæ	143
	List of Publications	145
	TRAIL Thesis Series	147

SUMMARY

Submarine power cables (SPCs) are vital for the offshore wind industry, particularly as wind farms expand into deeper and remoter ocean areas rich in wind resources. These environments subject SPCs, especially dynamic power cables (DPCs) connected to floating wind platforms, to repetitive loadings and consequent fatigue failures, posing substantial challenges within the industry.

Predicting the fatigue life of SPCs involves several critical steps, with local mechanical analysis acting as a pivotal bridge that significantly impacts overall fatigue life estimation. This analysis assesses overall cable behaviours, such as stiffness, and detailed component behaviours, such as stress and strain conditions. The accuracy of the local mechanical analysis crucially influences the ultimate fatigue life estimation. Currently, large safety factors are employed in engineering to compensate for uncertainties due to insufficient understanding of local mechanical behaviours. Therefore, there is a need for a modelling method that can accurately estimate the local mechanical behaviour of SPCs.

This PhD project is dedicated to developing an effective modelling method for the local mechanical analysis of SPCs. An extensive literature review on SPC configurations, design processes, and methods for determining mechanical behaviours is presented in Chapter 2. This chapter focuses on prevalent loadings of tension and bending and discusses the complexity of SPC structures, particularly due to their unbonded, multi-layer, helical component nature and associated stick-slip issues. Two approaches—analytical and numerical—are used to capture these behaviours, with numerical methods preferred for their ability to handle complex structures. However, these methods struggle with efficiency when detailed analysis is necessary. The balance between accuracy and efficiency in developing an effective numerical model hinges on resolving three specific issues: constructing appropriate finite element, managing contact issues, and establishing suitable boundary conditions.

Chapter 3 addresses the aforementioned challenges. First, it introduces an element combination—beam plus surface elements—to simulate the helical metals within SPCs, a method previously validated for accuracy and efficiency. This combination undergoes further verification in subsequent chapters. Secondly, the contact issue, particularly the initial residual stress from extruded polymers during manufacturing, is tackled using contact damping to simulate its effects, enhancing model efficiency and convergence. Lastly, the challenge of setting appropriate boundary conditions is addressed through periodic boundary conditions derived from the homogenization method, applied to a repetitive unit cell (RUC) whose length is reduced to increase computational efficiency. The resulting model, referred to as the RUC model, is applied to SPC samples and validated against test data on tension and bending.

The effectiveness of the RUC model under tension is confirmed in Chapter 4 through material tests and a tension test on a DPC sample. The model demonstrates superior

performance in terms of accuracy and efficiency compared to traditional full-scale models. Similarly, Chapter 5 validates the RUC model under bending conditions using tests on both three-core DPC and single-core SPCs. The model is verified against traditional full-scale models, affirming its robustness.

Subsequently, Chapter 6 explores the RUC model's application in analyzing the combined effects of tension and bending on DPCs. The study extends to parametric analysis of internal components and helical pitch lengths, providing crucial insights for cable design.

Finally, Chapter 7 concludes the dissertation by summarizing the key findings and offering recommendations for further research building on the current study. Additionally, it outlines guidelines for employing the proposed model in practical scenarios

SAMENVATTING

Onderzeese stroomkabels (SPC's) zijn van essentieel belang voor de offshore windindustrie, vooral nu windparken zich uitbreiden naar diepere zeeën en verder afgelegen zeegebieden die rijk zijn aan windbronnen. Deze omgevingen stellen SPC's, met name dynamische stroomkabels (DPC's) die verbonden zijn met drijvende windplatformen, bloot aan herhaaldelijke belastingen en daaruit voortvloeiende vermoeiingsbreuken, wat aanzienlijke uitdagingen binnen de industrie met zich meebrengt.

Het voorspellen van de vermoeiingslevensduur van SPC's omvat verschillende kritische stappen, waarbij lokale mechanische analyse een centrale rol speelt die de algehele schatting van de vermoeiingslevensduur sterk beïnvloedt. Deze analyse beoordeelt het algehele kabelgedrag, zoals stijfheid, en gedetailleerde componentgedragingen, zoals spanning- en rektoestanden. De nauwkeurigheid van de lokale mechanische analyse beïnvloedt de uiteindelijke schatting van de vermoeiingslevensduur op een cruciale manier. Momenteel worden in de techniek grote veiligheidsfactoren gehanteerd om onzekerheden door onvoldoende begrip van lokale mechanische gedragingen te compenseren. Daarom is er behoefte aan een modelleermethode die het lokale mechanische gedrag van SPC's nauwkeurig in kan schatten.

Dit promotieonderzoek is gericht op het ontwikkelen van een effectieve modelleermethode voor de lokale mechanische analyse van SPC's. Een uitgebreide literatuurstudie over SPC-configuraties, ontwerpprocessen en methoden voor het bepalen van mechanische eigenschappen wordt gepresenteerd in Hoofdstuk 2. Dit hoofdstuk richt zich op veelvoorkomende belastingen zoals trekkracht en buiging en bespreekt de complexiteit van SPC-structuren, met name vanwege hun ongelijkmatige, meerlagige, spiraalvormige componentstructuur en de bijbehorende stick-slip-problemen. Twee benaderingen – analytisch en numeriek – worden gebruikt om deze gedragingen vast te leggen, waarbij numerieke methoden de voorkeur genieten vanwege hun vermogen om complexe structuren aan te kunnen. Deze methoden worstelen echter met efficiëntie indien gedetailleerde analyse noodzakelijk is. De balans tussen nauwkeurigheid en efficiëntie bij het ontwikkelen van een effectief numeriek model hangt af van het oplossen van drie specifieke kwesties: het construeren van geschikte eindige elementen, het omgaan met contactproblemen en het vaststellen van passende randvoorwaarden.

Hoofdstuk 3 behandelt de bovengenoemde uitdagingen. Ten eerste introduceert het een elementcombinatie – balk- en oppervlakte-elementen – om de spiraalvormige metalen binnen SPC's te simuleren, een methode die eerder is gevalideerd op nauwkeurigheid en efficiëntie. Deze combinatie ondergaat verdere verificatie in de volgende hoofdstukken. Ten tweede wordt het contactprobleem, met name de initiële restspanning van geëxtrudeerde polymeren tijdens de productie, aangepakt door gebruik te maken van contactdamping om de effecten ervan te simuleren, wat de efficiëntie en convergentie van het model verbetert. Ten slotte wordt de uitdaging van het instellen van geschikte

randvoorwaarden aangepakt door periodieke randvoorwaarden af te leiden van de homogenisatiemethode, toegepast op een repetitieve eenheidscel (RUC) waarvan de lengte is verkort om de rekenefficiëntie te verhogen. Het resulterende model, het RUC-model genoemd, wordt toegepast op SPC-monsters en gevalideerd aan de hand van testgegevens voor trek- en buigbelastingen.

De effectiviteit van het RUC-model onder trekbelasting wordt bevestigd in Hoofdstuk 4 door middel van materiaaltesten en een trekproef op een DPC-monster. Het model toont veel betere prestaties op het gebied van nauwkeurigheid en efficiëntie in vergelijking met traditionele full-scale modellen. Op een vergelijkbare manier valideert Hoofdstuk 5 het RUC-model onder buigomstandigheden door middel van testen op zowel drie-aderige DPC's als een-aderige SPC's. Het model wordt vergeleken met traditionele full-scale modellen wat zijn robuustheid bevestigt.

Vervolgens onderzoekt Hoofdstuk 6 de toepassing van het RUC-model bij het analyseren van de gecombineerde effecten van trek- en buigbelastingen op DPC's. De studie wordt uitgebreid met een parametrische analyse van interne componenten en spiraal-spoedlengtes, wat cruciale inzichten oplevert voor kabelontwerpen.

Ten slotte vat Hoofdstuk 7 het proefschrift samen door de belangrijkste bevindingen te presenteren en aanbevelingen te doen voor verder onderzoek op basis van de huidige studie. Daarnaast biedt het richtlijnen voor het toepassen van het voorgestelde model in praktische scenario's.

PREFACE

After three years as a master's student specializing in flexible pipes under the guidance of Professor Yong Bai at Zhejiang University, I was afforded the opportunity in 2019 to further my research in a related area—submarine power cables (SPCs)—at Delft University of Technology. This new chapter was guided by Professor Hans Hopman and Dr. Xiaoli Jiang. To effectively transition into this field, I conducted an extensive literature review to familiarize myself with the subject and to identify significant research gaps that warranted further exploration.

In 2021, I visited a couple of well-known cable companies, discussing possible cooperation with them and applying for some cable samples for tests. Fortunately enough, I was invited to have a look at some of their laboratories and research departments. It was there I gained first-hand information on the design of SPCs. Although many European standards and reports have pointed out the serious issues that SPCs encounter in practical engineering and many organizations are calling for more research on the topic, I did not know exactly how a real cable company works on the challenges.

I still remember vividly when I was led into a room where a high-performance computer (HPC) was running. "So what are you guys running on the noisy computer?" I asked curiously. "A four-point bending test on an SPC sample. Come and have a look" an engineer replied. The monitor was turned on, and a quite long, colourful, elaborate SPC model floated on. Looking at the model, I knew the calculation is going to be extremely time-consuming because they tried to imitate almost every detail during the bending test. So I asked, "How long will it take to get a result?" "Well, on the computer with 32 cores, around a month, I guess, if the model is able to converge successfully. We have spent a long time debugging it already." he said in frustration. The answer did not astonish me much, as I had tried a few bending models of SPCs myself before I paid the visit. However, it was the first time that I realized the dilemma a practitioner faces in their work.

After this visit, I performed a few important tests, the results of which are utilized to validate the proposed model in my dissertation. Returning to TU Delft with the experience and the valuable test results, I started to figure out how to develop an effective analysis tool for such a complicated structure. The tool, in the end, should balance accuracy and efficiency. A numerical model that can take more details into account became our first choice. Given that a full-scale numerical model was built, the calculation resources became insufficient (The HPC Delft Blue was not available then, and I only had access to a lower-capable HPC). I conveyed this concern to my supervisor, Xiaoli Jiang, and she recommended her former PhD student, Xiao Li. Xiao has substantial simulation experience with flexible pipes and is now at the Institute of High-Performance Computing (IHPC) in Singapore. We were thinking more simulations could be conducted with that HPC. The moment he said, "Why don't you try to accelerate your calculation by using the RUC technique?" there was a voice in my head saying no!

I had read papers where the authors tried to simulate other multi-layer flexible structures by using this technique. However, this requires serious mathematical derivations and deep physical understanding before the corresponding FORTRAN code and Python code are inputted into the user-subroutine and the finite element method package. There is a lot of work only by reading this long sentence. I am quite familiar with these stuffs now, but back then, they were brand-new, and it seemed there was nobody around me whom I could ask for help on the coding and software manipulation. I did not realize that a qualified PhD needs to learn new skills all the time, and I was trying to stay in my comfort zone by relying on old techniques. Nevertheless, the limited calculation resources urged me to give it a try. After this attempt, I found how powerful the foundation of the RUC method (multi-scale analysis) is. It is such a potential mathematical tool rooted in many scientific and engineering fields, which makes me fascinated and just want to learn more in my future academia life. It is also the RUC method that imparts more scientific value to this dissertation.

A balance between scientific value and engineering value in a PhD project is hard to reach, similar to the difficulty in keeping a balance between accuracy and efficiency in a simulation of a complex structure. Thanks to my supervisors, I also had a couple of chances to connect with more cable engineers during the development of the model, which made my work align with the engineering requirements as much as possible. Apart from imitating SPCs under pure bending, there were also engineers who wanted to study the SPCs under combined tension and bending (more common in practical engineering); unlike the pure bending case, the test of the combined loading case is extremely difficult to carry out in real life, so an alternative to test methods is in need as well. I was not able to answer those engineers when they asked me how to deal with the combined loading case two years ago, but now I am confident to welcome them to try my model.

I do hope the proposed model (calculation time reduced to a few hours) in this dissertation is going to be used in practical engineering, and I hope the cable engineers find the content useful. I used to write down similar sentences at the end of my journal papers, but I do mean it.

Last but not the least, the source code and detailed documentation are made freely available to download at <https://pan-fang.github.io/Codes/>. Please feel free to try it!

*Pan Fang
Delft, April 2024*

NOMENCLATURE

LIST OF ACRONYMS AND ABBREVIATIONS

DOF	Degree of Freedom
DPC	Dynamic Power Cable
FE	Finite Element
FEA	Finite Element Analysis
FEM	Finite Element Method
HDPE	High-density Polyethylene
MDPE	Medium-density Polyethylene
MPC	Multi-point Constraint
ORE	Offshore renewable Energy
RP	Reference Point
RUC	Repeated Unit Cell
Single-core SPC	A power cable with only an insulated conductor
SPC	Submarine Power Cable
Three-core SPC	Three insulated conductors assembled into the same (armoured) protection, leading to one cable per 3-phase circuit
XDPE	Cross-linked Polyethylene

LIST OF MATHEMATICAL SYMBOLS

A	Cross section area
\mathbf{a}	Elastic moduli tensor
α	Winding angle of helical components
b	Width
δ	Axial strain
D	Diameter
E	Young's Modulus
\mathbf{e}	Strain operator
ε	Strain
f	Friction force
\mathbf{F}	Force vector
K	Stiffness
k	Curvature
l	Microscopic length
L	Macroscopic length
M	Moment
\mathbf{M}	Moment vector
N	Tension
n	Number of helix in current layer
p	Pitch length
P	Pressure
μ	Friction coefficient
ϕ	Rotation vector
φ	Torsion angle
\mathbf{R}	Rotation matrix
σ	Stress
t	Thickness
u	Displacement

\mathbf{U}, u	Displacement vector and its components
\mathbf{X}, X	Coordinate vector and its components
θ	Bending angle
V	Angular position

LIST OF STANDARDS AND DESIGN GUIDELINES

(CIGRE TB = International Council on Large Electric Systems Technical Brochure)

(IEC = International Electrotechnical Commission)

(ICEA = Insulated Cable Engineers Association)

(CENELEC = European Committee for Electrotechnical Standardization)

(DNV = Det Norske Veritas)

(IEEE = Institute of Electrical and Electronics Engineers)

(API = American Petroleum Institute)

(ISO = International Organization for Standardization)

CIGRE TB 862	Recommendations for mechanical testing of submarine cables for dynamic applications
CIGRE TB 610	Offshore generation cable connections
CIGRE TB 623	Recommendations for mechanical testing of submarine cables
CIGRE TB 669	Mechanical forces in large cross section cables systems
CIGRE TB 722	Recommendations for Additional Testing for Submarine Cables from 6kV ($U_m=7.2$ kV) up to 60 kV ($U_m = 72.5$ kV)
CIGRE TB 751	Electrical properties of insulating materials under VLF voltage
CIGRE TB 852	Recommendations for testing DC extruded cable systems for power transmission at a rated voltage up to and including 800 kV
CIGRE TB 496	Recommendations for Testing DC Extruded Cable Systems for Power Transmission at a Rated Voltage up to 500 kV
CIGRE TB 490	Recommendations for Testing of Long AC Submarine Cables with Extruded Insulation for System Voltage above 30 (36) to 500 (550) kV
CIGRE TB 446	Advanced Design of Metal Laminated Coverings: Recommendation for Tests, Guide to Use, Operational Feed Back

IEC 60840	Power cables with extruded insulation and their accessories for rated voltages above 30 kV ($U_m = 36$ kV) up to 150 kV ($U_m = 170$ kV) – Test methods and requirements
IEC 62067	Power cables with extruded insulation and their accessories for rated voltages above 150 kV ($U_m = 170$ kV) up to 500 kV ($U_m = 550$ kV) – Test methods and requirements
IEC 62895	High voltage direct current (HVDC) power transmission - Cables with extruded insulation 2017 and their accessories for rated voltages up to 320 kV for land applications - Test methods and requirements
IEC 63026	Submarine power cables with extruded insulation and their accessories for rated voltages from 6 kV ($U_m = 7,2$ kV) up to 60 kV ($U_m = 72,5$ kV) – Test methods and requirements
ICEA S-108-720	Extruded Insulation Power Cables Rated Above 46 through 500 KV AC
DNVGL-RP-0360	Subsea power cables in shallow water
DNV-ST-0359	Subsea power cables for wind power plants
DNV-RP-F401	Electrical power cables in subsea applications
DNVGL-ST-0119	Floating wind turbine structures
API RP 17B	Recommended Practice for Flexible Pipe
API 17E	Specification for Subsea Umbilicals
ISO 13628-5	Design and operation of subsea production systems – Part 5: Subsea Umbilicals
CENELEC	Electric cables - Additional test methods
IEEE	IEEE Guide for the Planning, Design, Installation, and Repair of Submarine Power Cable Systems

1

INTRODUCTION

Wind energy, esteemed as a stable source of renewable power, is increasingly being harnessed by humanity. A key strategy for optimizing abundant wind energy involves gaining access to the remoter and deeper expanses of the open sea, where winds are more bountiful, and wind turbines tend to be installed on floating platforms. Once wind energy is converted into electricity within wind farms, the need arises for submarine power cables (SPC) to transport the power. The floating platform requires a special type of SPC, i.e., the dynamic power cables (DPC) whose one end is suspended from the floating structure and the other end is lying on the seabed. As DPCs are suffering from constant repetitive loads from the environment and the movement of floating platforms, the wind industry has found that fatigue failure of this particular structure is becoming a great concern. An indispensable step in predicting fatigue life is the local analysis that aims to evaluate the stiffness of overall cables and the details of cable components such as their stress. Such a modelling method in performing the local mechanical analysis of DPCs is needed so that the black box can be unfolded in front of cable engineers.

1.1. BACKGROUND

OVER the past few decades, there have been significant advancements in offshore energy production technologies, including floating offshore wind farms and wave energy converter systems. Among these, wind energy has proven particularly promising, garnering increasing attention in the academic and industrial sectors [1–4]. Recent years have witnessed robust growth in offshore wind energy, a trend that is projected to continue, as depicted in Figure 1.1. In 2024, global offshore wind capacity is estimated at nearly 70 Gigawatts [5]. Specifically, in Europe, there are more than 100 offshore wind farm installations across eleven countries, boasting a combined capacity of approximately 23 Gigawatts [6].

A key strategy for harnessing significant wind energy involves exploiting more distant oceanic areas, where winds are plentiful. As Europe targets climate neutrality by 2050, achieving this goal requires the development of up to 150 GW of floating offshore wind capacity [7]. This endeavor is indeed considerable. Figure 1.2 illustrates this ongoing trend within the North Sea basin.

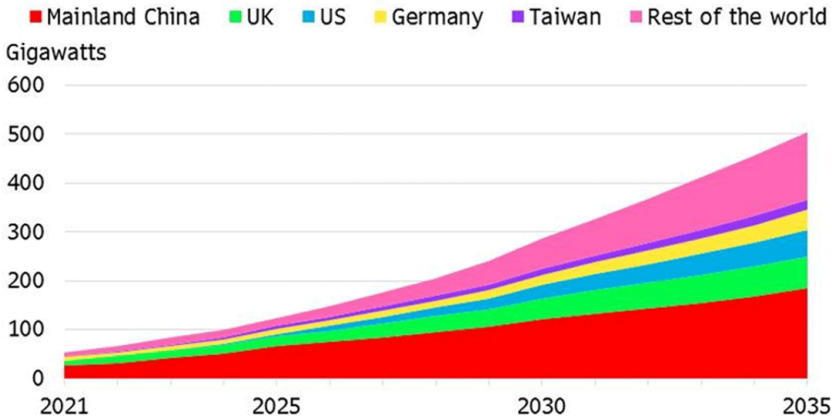


Figure 1.1: Cumulative offshore wind capacity around the world [8]

Wind farms are comprised of turbines dedicated to transforming wind energy into electricity. Figure 1.3 highlights a crucial element within these farms: submarine power cables (SPCs). Acting as the vital "lifeline," these cables are responsible for transmitting the electricity generated by wind turbines to consumers. The history of power cables extends over a century [10], though initially, they were confined to terrestrial and overhead uses. However, they eventually transitioned into maritime settings, adapting their structural designs to meet the evolving demands of the industry [11].

In the design of SPCs, strength and flexibility are paramount concerns from a mechanical perspective [13]. To ensure strength, sufficient metals are incorporated within the SPC, while flexibility is achieved by designing some internal components into a helical shape [14]. These helical components are intended to mitigate built-up

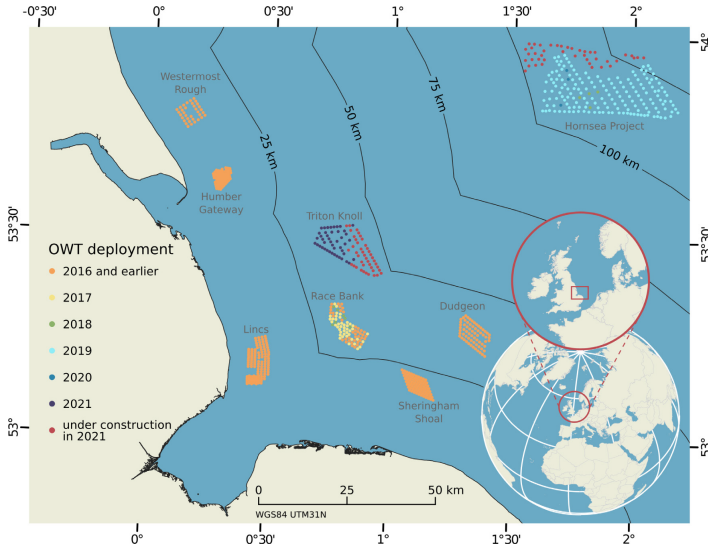


Figure 1.2: Offshore wind farms and their locations at the East England coast in the North Sea Basin [9]

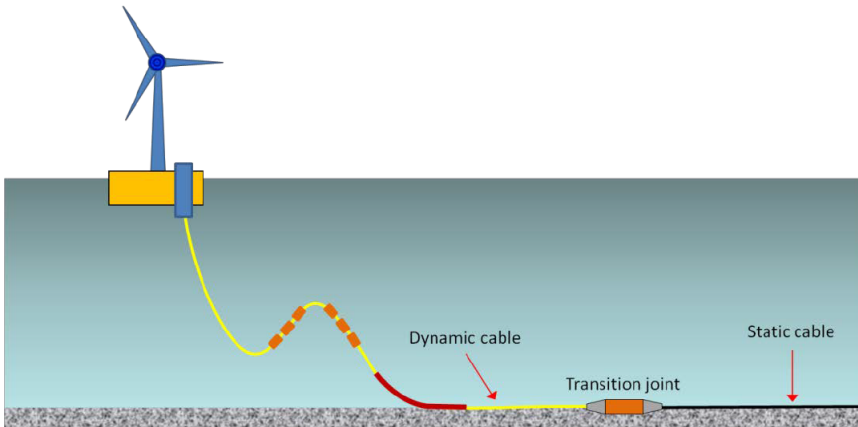


Figure 1.3: Facilities in floating wind system [12]

stress during loading by permitting the components to move apart. Although this design extends the cable's lifespan, it also increases complexity and renders the SPCs less comparable to the other flexible structures used in oil and gas industry, such as flexible pipes and umbilicals. A typical flexible pipe, shown in Figure 1.4(b), primarily designed to transport oil and gas, features a hollow centre to allow fluid flow. Unlike SPCs, the armour layers of a flexible pipe often consist of helical wires with rectangular cross-sections. Umbilicals used in the oil and gas industry, shown in Figure 1.4(c), combine pipes for transporting oil or gas with pipes for other liquids like hydraulic oils and cooling liquids as well as cables for electricity and data. However, the inner components in an umbilical distinguish significantly from SPCs. Particularly, SPCs contain solid and relatively large-diameter power cores made of copper or aluminium. These metallic cores provide a much larger contribution to the overall strength, stiffness and, therefore, a distinguished fatigue life of the cable than umbilicals. This issue has not been paid much attention to in the previous studies regarding both flexible pipes and umbilicals.

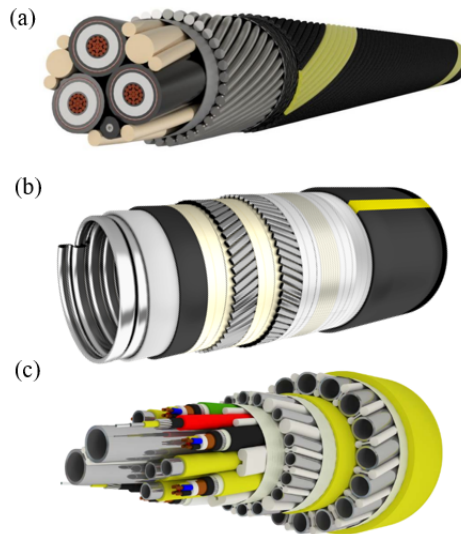


Figure 1.4: An SPC (a) [15] and a flexible pipe (b) [16] and an umbilical (c) [17]

Similar to the classification of traditional flexible structures in practical engineering, depending on the placement of the structures in their global configuration, SPCs are categorized as either:

- dynamic power cables (DPC), if suspended from floating platforms. This corresponds to flexible risers.
- static power cables, if laid upon the seabed [18]. This corresponds to static flexible pipes.

For instance, the cable depicted in Figure 1.3 is suspended from a floating platform, classifying it as a DPC. Unlike static power cables, DPCs are subject to repetitive loadings—dominantly tension, bending, and their combination—due to the motion of

floating platforms and environmental forces such as currents and waves [19, 20]. The wind industry regards the fatigue of DPCs as a significant concern, prompting calls for intensified research efforts to address this issue [14, 21, 22].

Fatigue analysis involves multiple complex steps and necessitates collaboration among engineers from various research fields. Typically, the fatigue life prediction process for DPCs encompasses three key phases [21]:

- global analysis,

This step requires inputs including environmental loadings and cable properties such as stiffnesses. A global model is first used to determine the cable's levels of loading in three modes: bending, twisting and tension for representative environmental conditions [23].

- local analysis,

In addition to the cable stiffness, this step also estimate the levels of stresses in the metal components of the cable. The helical metallic components and polymer layers are more forgiving against bending loads than a standard flexible pipe would be. Generally, the metallic layers are more susceptible to failure from dynamic loading and thus they are the focus of mechanical engineering investigation.

- and fatigue life prediction.

The fatigue life prediction requires the stress variation of the concerned components based on the global analysis and local analysis, as well as the fatigue properties of these components from fatigue tests.

The parameters used in the global analysis and fatigue life prediction, i.e., stiffnesses and the stress variations, are obtained from the local analysis. Therefore, it can be found that the local analysis plays a key role in the whole process. In practice, global analysis and fatigue life prediction are similar to those employed for traditional flexible structures [19, 20]. However, the local analysis of SPCs varies significantly from them due to their structure distinctions. The precision of local mechanical analysis is critical, as it substantially influences the evaluation of fatigue life. Nicholls et. al. [24] found that the stiffness from local analysis determines the global analysis that ultimately affects the fatigue life prediction. Furthermore, a minor discrepancy in stress prediction, as demonstrated by CIGRE [21], can significantly alter the predicted fatigue life.

Consequently, a more accurate local mechanical analysis of SPCs is essential to minimise uncertainties as much as possible. Several European projects from the wind industry, such as WIND EUROPE [25], CARBON TRUST [26, 27], and ETIPWind [28], are advocating for studies on DPCs. Notably, CARBON TRUST [26, 27] and ETIPWind [28] have emphasised the need for design tools specifically developed for the local mechanical analysis of DPCs, to demystify the complexities for cable engineers.

Two analysis methods, analytical and numerical, can be used to perform local mechanical analysis, while testing is employed to calibrate and validate these methods. Open standards and brochures reveal that only the test method is explicitly presented for SPCs [21]. Testing can ascertain the overall stiffness needed to validate the analysis methods; however, capturing specific component stresses and strains proves challenging due to the multi-layer property of this structure [24, 29–31]. Analytical

and numerical methods are good supplements, yet they are not given explicitly in current standards [21, 22, 32, 33]. The complexity of the multi-layer structure configuration of an SPC, especially its inner helical components and the stick-slip issue within contact interfaces, makes the local mechanical analysis challenging as no specific codes and standards are available on how to perform this analysis.

1.2. RESEARCH OBJECTIVE AND QUESTIONS

THE primary objective of this dissertation is:

Developing an effective modelling method for the local mechanical analysis of SPCs that provides both more accurate input parameters for the global analysis as well as detailed component data to be used in the fatigue life prediction.

To achieve this goal, the following research questions should be answered:

1. How are SPCs structured?
2. What are the methods used by industry for the local mechanical analysis of SPCs?
3. What are the requirements for the new modelling method to be effective in generating the required information?
4. What is the best modelling principle to be used as a starting point for the development of the new modelling method?
5. How can a modelling method be specifically developed for the local mechanical analysis of SPCs?
6. How can the accuracy of the proposed modelling method be validated?
7. How to demonstrate the modelling method for further application?

1.3. OUTLINE OF THE DISSERTATION

THE remainder of the dissertation is made up of five parts:

Part I introduces the detailed configuration and design process for SPCs, providing an overview of current methods used to perform the local mechanical analysis. It identifies research gaps and outlines the promising approach that will be employed in the dissertation. This part addresses sub-question 1-4.

Part II describes the development of an effective modelling method for the local mechanical analysis of SPCs. This method aims to enhance both accuracy and efficiency. The methodology developed in this part responds to sub-question 5.

In Part III, the proposed modelling method is applied to SPCs and rigorously validated against experimental results. The efficiency of the method is also carefully checked by proper means, directly addressing sub-question 6.

After successful validation, Part IV demonstrates the practical application of the modelling method in detailed local mechanical analysis of SPCs. The findings in this part answer sub-question 7.

Part V of the dissertation synthesizes the results obtained, summarises the conclusions, and offers recommendations for further research based on the findings. This part also presents guidelines for implementing the proposed modelling method in engineering applications.

REFERENCES

- [1] G. J. Herbert, S. Iniyan, E. Sreevalsan, and S. Rajapandian. “A review of wind energy technologies”. In: *Renewable and sustainable energy Reviews* 11.6 (2007), pp. 1117–1145.
- [2] M. Hannan, A. Q. Al-Shetwi, M. Mollik, P. J. Ker, M. Mannan, M. Mansor, H. M. Al-Masri, and T. I. Mahlia. “Wind Energy Conversions, Controls, and Applications: A Review for Sustainable Technologies and Directions”. In: *Sustainability* 15.5 (2023), p. 3986.
- [3] T. Letcher. *Wind energy engineering: a handbook for onshore and offshore wind turbines*. Elsevier, 2023.
- [4] Z. Zhang, X. Liu, D. Zhao, S. Post, and J. Chen. “Overview of the development and application of wind energy in New Zealand”. In: *Energy and Built Environment* 4.6 (2023), pp. 725–742.
- [5] TGS. *Global Offshore Wind Farm Database And Intelligence*. 2023. URL: <https://www.4coffshore.com/windfarms/> (visited on 08/31/2023).
- [6] WindEurope. *Offshore wind in Europe key trends and statistics 2019*. 2019. URL: <https://windeurope.org/wp-content/uploads/files/about-wind/statistics/WindEurope-Annual-Offshore-Statistics-2019.pdf> (visited on 08/31/2023).
- [7] ETIPWind. *Floating Offshore Wind: Delivering climate neutrality*. 2023. URL: <https://etipwind.eu/news/floating-offshore-wind-delivering-climate-neutrality/#:~:text=To%20become%20climate%2Dneutral%20by,and%20reliable%20energy%20society%20wants.> (visited on 08/31/2023).
- [8] Prysmian. *A closer look at 2023 worldwide Offshore Floating Wind Market Trends*. 2023. URL: <https://www.prysmiangroup.com/en/insight/projects/a-closer-look-at-2023-worldwide-offshore-floating-wind-market-trends> (visited on 08/31/2023).
- [9] T. Hoerer and C. Kuenzer. “Global dynamics of the offshore wind energy sector monitored with Sentinel-1: Turbine count, installed capacity and site specifications”. In: *International Journal of Applied Earth Observation and Geoinformation* 112 (2022), p. 102957.
- [10] H. Orton. “History of underground power cables”. In: *IEEE Electrical Insulation Magazine* 29.4 (2013), pp. 52–57.
- [11] R. M. Black. *The history of electric wires and cables*. 4. IET, 1983.

- [12] C. TB. *Offshore generation cable connections*. 2015. URL: https://www.researchgate.net/publication/338388640_CIGRE_TB_610_-_Offshore_generation_cable_connections/citations (visited on 03/16/2024).
- [13] T. Worzyk. *Submarine power cables: design, installation, repair, environmental aspects*. Springer Science & Business Media, 2009.
- [14] M. Ikhennicheu, M. Lynch, S. Doole, F. Borisade, F. Wendt, M.-A. Schwarzkopf, D. Matha, R. Vicente, H. Tim, L. Ramirez, *et al.* “Review of the State of the Art of Dynamic Cable System Design”. In: *COREWIND: Brussels, Belgium* (2020).
- [15] NEXANS. *SUBSEA CABLES | MV MEDIUM VOLTAGE POWER FIBRE OPTICS CABLES*. 2019. URL: <https://www.powerandcables.com/subsea-cables-joints-terminations/> (visited on 02/08/2024).
- [16] Ray Burke, Baker Hughes. *Power Generation*. 2020. URL: <https://www.offshore-mag.com/business-briefs/equipment-engineering/article/14168451/new-flexible-pipe-technology-designed-for-challenging-environments> (visited on 04/05/2024).
- [17] Ray Burke, Baker Hughes. *Subsea Distribution Products*. 2024. URL: <https://www.oceaneering.com/subsea-distribution-solutions/products/> (visited on 04/09/2024).
- [18] M. Marta, S. Mueller-Schuetze, H. Ottersberg, D. Isus, L. Johanning, and P. R. Thies. “Development of dynamic submarine MV power cable design solutions for floating offshore renewable energy applications”. In: (2015).
- [19] D. Young, C. Ng, S. Oterkus, Q. Li, and L. Johanning. “Assessing the mechanical stresses of dynamic cables for floating offshore wind applications”. In: *Journal of Physics: Conference Series*. Vol. 1102. 1. IOP Publishing. 2018, p. 012016.
- [20] M. U. Rentschler, F. Adam, and P. Chainho. “Design optimization of dynamic inter-array cable systems for floating offshore wind turbines”. In: *Renewable and Sustainable Energy Reviews* 111 (2019), pp. 622–635.
- [21] M. Jeroense. “Recommendations for Mechanical Testing of Submarine Cables (and Their Accessories)”. In: *Accessories for HV and EHV Extruded Cables: Volume 2: Land and Submarine AC/DC Applications*. Ed. by P. Argaut. Cham: Springer International Publishing, 2023, pp. 351–424. ISBN: 978-3-030-80406-0. DOI: [10.1007/978-3-030-80406-0_5](https://doi.org/10.1007/978-3-030-80406-0_5). URL: https://doi.org/10.1007/978-3-030-80406-0_5.
- [22] DNVGL. *Subsea power cables for wind power plants*. 2020. URL: <https://www.dnv.com/energy/standards-guidelines/dnv-st-0359-subsea-power-cables-for-wind-power-plants.html> (visited on 08/31/2023).
- [23] WFO. *Floating Offshore Wind Dynamic Cables: Overview of Design and Risks*. 2024. URL: <https://wfo-global.org/wp-content/uploads/2024/02/WFO-Cables-and-FOSS-White-Paper.pdf> (visited on 05/31/2024).
- [24] R. Nicholls-Lee, P. R. Thies, and L. Johanning. “Coupled modelling for dynamic submarine power cables: interface sensitivity analysis of global response and local structural engineering models”. In: (2021).

- [25] WindEurope. *The EU Offshore Renewable Energy Strategy*. 2020. URL: <https://windeurope.org/policy/position-papers/the-eu-offshore-renewable-energy-strategy/> (visited on 08/31/2023).
- [26] C. TRUST. *Floating wind joint industry project – phase 2 summary report*. URL: <https://www.carbontrust.com/our-work-and-impact/guides-reports-and-tools/floating-wind-joint-industry-project-phase-2-summary-report> (visited on 08/31/2023).
- [27] C. TRUST. *Floating wind joint industry programme – phase IV summary report*. URL: <https://www.carbontrust.com/our-work-and-impact/guides-reports-and-tools/floating-wind-joint-industry-programme-phase-iv-summary-report> (visited on 08/31/2023).
- [28] ETIPWind. *Roadmap*. 2019. URL: <https://etipwind.eu/roadmap/> (visited on 08/31/2023).
- [29] C. T. Poon, C. Mullins, L. Radziunas, E. O’Connell, A. Connolly, and S. Leen. “Finite Element Design Study of Dynamics in Submarine Power Cables for Offshore Renewable Wind Energy”. In: *International Conference on Offshore Mechanics and Arctic Engineering*. Vol. 86618. American Society of Mechanical Engineers. 2022, V001T01A023.
- [30] CATAPULT. *FLOATING OFFSHORE WIND CENTRE OF EXCELLENCE - DYNAMIC CABLE TECHNOLOGY QUALIFICATION FRAMEWORK AND CASE STUDIES*. 2022. URL: <https://ore.catapult.org.uk/wp-content/uploads/2022/10/Dynamic-Cable-Technology-Qualification-Oct-2022.pdf> (visited on 08/31/2023).
- [31] H.-T. Thai and S.-E. Kim. “Nonlinear static and dynamic analysis of cable structures”. In: *Finite elements in analysis and design* 47.3 (2011), pp. 237–246.
- [32] DNV-RP-F401. *Electrical power cables in subsea applications*. 2022. URL: <https://www.dnv.com/oilgas/download/dnv-rp-f401-electrical-power-cables-in-subsea-applications.htm> (visited on 08/31/2023).
- [33] C. RILEY *et al.* “HV CABLE QUALIFICATIONS TO IEC 62067-2006 AND ICEA S-108-720-2004”. In: *Jicable Conf.* 2011.

2

LITERATURE REVIEW

This chapter provides a comprehensive review of the existing methods for the local mechanical analysis of SPCs. Before that, a review of cable configuration and its design process is presented to provide a better understanding of the following content. Detailed descriptions of SPC configurations are covered in Section 2.1, answering sub-question 1. The design process unfolds in Section 2.2, highlighting existing gaps in current practices and answering sub-question 2 and 3. This is followed by an examination of the analytical (Section 2.3) and numerical methods (Section 2.4) that are potential to fill up the gaps. Section 2.5 then presents the experimental method, which aims to guide the tests that help to calibrate and validate the proposed modelling method. Section 2.6 synthesises these discussions, identifying key challenges that must be addressed to develop an effective method and defining the research scope. Sub-question 4 is answered in this section. Finally, Section 2.7 presents the chapter arrangement of the dissertation.

Parts of this chapter are based on the following papers:

- [1] P. Fang, X. Jiang, H. Hopman, and Y. Bai. "A review of mechanical analysis of submarine power cables". In: *Maritime Technology and Engineering 5 Volume 2* (2021), pp. 559–568.
- [2] P. Fang, X. Li, X. Jiang, H. Hopman, and Y. Bai. "A review of the analysis tools in the local mechanical study of submarine power cables". In: *Marine Structures* (Under review).

2.1. CABLE CONFIGURATION

THIS section provides crucial background information on cable configurations, which is fundamental for understanding the subsequent content. From a mechanical perspective, a cable comprises four main components: conductor, insulation system, armour wire, and serving, as detailed in Table 2.1, which lists their materials and functions. For a multi-core SPC, such as the three-core SPC in Figure 2.1(b), there could also be extra components, e.g., fillers. Additionally, thin screens or tapes exist among each main layer. They will be discussed later on if necessary.

Examples of a single-core SPC and a three-core SPC are shown in Figure 2.1. As indicated in Chapter 1, the design of Dynamic Power Cables (DPCs) prioritises strength and flexibility, which are critical mechanical considerations [1]. Flexibility is achieved by designing the inner components into helical shapes, which help to mitigate built-up stress during loading by allowing the components to move relative to each other [2]. For example, the armour layer typically features a helical structure made up of numerous wires wound around the cable in helical shapes. Similarly, the components within a multi-core SPC are often designed and assembled into helical configurations, as seen with the helical shapes in the three-core SPC.

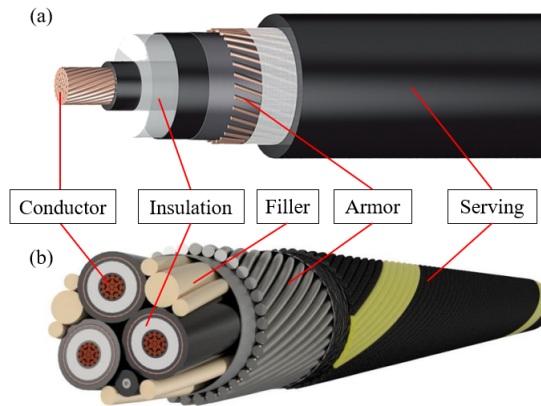


Figure 2.1: Typical configuration of a one-core SPC (a) [3] and a three-core SPC (b) [4]

Table 2.1: Main components inside a cable

Component	Material	Function
Conductor	Copper/Aluminium	Electricity transportation
Insulation	Cross-linked polyethylene	Prevent electrical leakage
Armor	Steel	Provide mechanical protection
Serving	Polymer	Anti-corrosion

2.1.1. CONDUCTOR

Theoretically, a variety of traditional metals, such as zinc, nickel, iron, aluminium, copper, lead, silver, and gold, can serve as conductive materials. Recent research has also investigated the potential of innovative materials like superconducting conductors [5–7]. However, the choice of conductor material must meet several criteria beyond conductivity, including cost and availability. In commercial SPCs, aluminium and copper are predominantly used, with copper being particularly favoured despite its higher cost per unit volume compared to aluminium. Copper's advantage lies in its ability to carry more current per unit cross-section, thereby reducing the material requirement for the outer layers of the cable [1].

The shape of the conductor is another critical consideration, chosen to optimise both electrical and mechanical properties. Factors influencing the conductor shape include voltage levels, cross-sectional area, requirements for water tightness, and the need for specific holes. Various conductor shapes are currently available, with the most common shapes illustrated in Figure 2.2. Among these, the stranded round conductor is most frequently used, as documented in recent literature [7–11]. This type of conductor undergoes compression by dies or roller sets, layer by layer, which deforms each individual wire and complicates the conductor's mechanical properties. A comprehensive overview of the design and manufacturing processes for each conductor type can be found in references [1, 12].

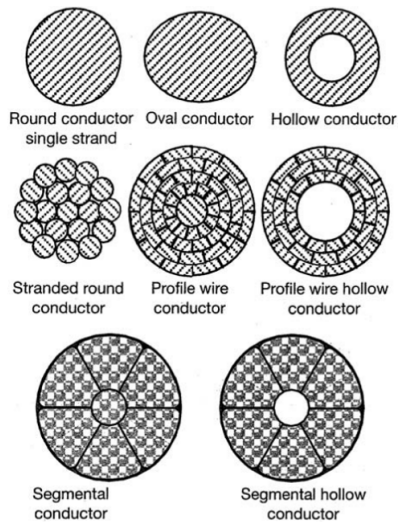


Figure 2.2: Common conductor shape [12]

2.1.2. INSULATION SYSTEM

The insulation system of an SPC consists of three key components: the conductor screen, the insulation, and the insulation screen, with insulation being the most

critical layer to prevent electrical leakage [13]. The commonly used insulation materials and their characteristics are detailed in Table 2.2. Among these, cross-linked polyethylene (XLPE) has become increasingly popular due to its superior properties, as highlighted by recent research [14–16]. Despite its advantages, the widespread commercial adoption of new XLPE formulations is still developing.

XLPE is currently the predominant material for insulation in SPCs, consisting of cross-linked long molecular chains from low-density polyethylene that form a three-dimensional network. This cross-linking is irreversible, preventing melting when subjected to high temperatures [1].

The manufacturing process of the insulation layer is intricate, often ending with the cable being cooled to room temperature by circulating water or gas around it. This cooling causes the material to shrink, inducing residual stresses within it. Studies, such as those by Amyot [17], have documented that these residual stresses can vary, and are challenging to measure accurately in practice. These stresses can significantly impact the mechanical and electrical properties of the SPC.

To mitigate dielectric strength losses caused by the rough surface of the conductor, a semi-conductive XLPE conductor screen is employed between the conductor and insulation. This layer smoothens the interface, effectively removing local electrical stresses. Additionally, a semi-conductive XLPE insulation screen is placed between the insulation and the swelling tape to protect the outer layers and maintain a stable dielectric surface. Electrical tree and water tree [18, 19] appearing in the insulation can be diminished as much as possible by these manipulations. These three layers are typically produced simultaneously via a triple-extrusion process, ensuring a high-quality insulation system. Detailed manufacturing processes for these dielectric systems can be found in [12].

Table 2.2: Frequently-used insulation materials

Material types	Specialities
Polyethylene(PE)	Subsequently been replaced by XLPE due to low temperature resistance
Cross-linked Polyethylene(XLPE)	Standard XLPE is not suitable for HVDC applications because of space charge phenomena
Extruded HVDC cable(special XLPE formulation)	Special XLPE formulations can cope with the space charge problem
Paper-Insulated Oil-Filled	Today, XLPE cables are qualified for very voltages and leave little room for fluid-filled cables
Gas-filled	Similar as oil-filled
Paper-Mass Insulation	Mass-impregnated cables are available for up to 500 kV d.c. For this voltage, there is no alternative to the well-proven mass-impregnated cables

2.1.3. ARMOUR LAYER

The armour layer plays a critical role in SPCs, as it provides essential strength against external loadings while maintaining flexibility [20–25]. This layer is primarily composed of numerous metal wires, typically steel, which are helically wrapped around the cable. Two key variables in this configuration are the lay length and the lay angle. Lay length refers to the distance a wire travels after one complete revolution around the cable at a specified lay angle, as shown in Figure 2.3. Both the lay length and the number of wires in the armour layer are tailored to achieve the desired mechanical properties.

Moreover, it is important to note that, in some manufacturing processes, hot bitumen is applied to the armour layer to prevent corrosion. The addition of this temperature-sensitive material can significantly alter the mechanical behaviour of the armour layer, especially under extreme environmental conditions [26, 27]. This treatment not only enhances durability but also influences the flexibility and strength characteristics of the armour, which are critical for the cable's overall performance.

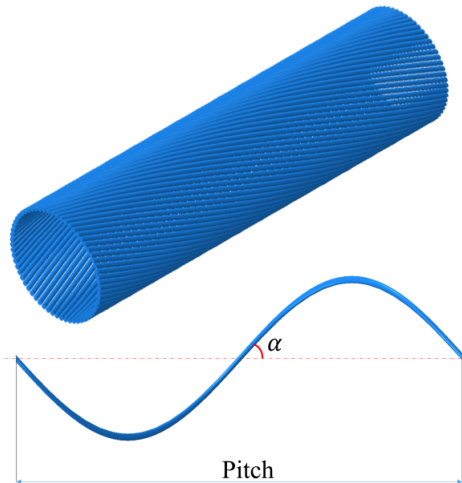


Figure 2.3: Helical wires in an armour layer (upper) and the definition of the basic parameters of the wire (down)

2.1.4. SERVING

The outer serving forms the final layer of an SPC and is crucial for protecting the armour from scratches, external stresses, and corrosion during the cable's loading, laying, and burial processes. Commonly, polymers are used for the outer serving. The cooling process of this sheath additionally induces residual stresses within the SPCs, which can affect their long-term durability [17].

2.2. CABLE DESIGN PROCESS

AN SPC plays a critical role in transmitting electricity within the offshore wind industry. In addition to conducting electricity, the current flowing through an SPC generates heat, thereby raising the cable's temperature. Furthermore, SPCs, and particularly DPCs, are continually subjected to mechanical loadings from environmental forces. Consequently, designing an SPC involves addressing a multi-physical problem that spans several research disciplines.

2.2.1. GENERAL CABLE DESIGN PROCESS

According to the design process outlined by DNVGL [28] and CIGRE [29], the flowchart summarized in Figure 2.4 illustrates that analyses of different physical fields are conducted separately. Below is a concise description of the entire design process:

The design process initiates with the establishment of functional project requirements, including specifications for power transmission capacity, environmental considerations, physical constraints, and regulatory compliance [1, 29].

Following requirement setting, the Cable Design phase begins. This involves the initial design of the cable, material selection, and construction determinations to meet the project's needs [1, 2, 30]. Key considerations during this phase include conductor size, insulation type, and protective layering.

The next step is the Thermal/Electrical Analysis phase, where the cable's ability to handle the expected electrical load without overheating is assessed [1, 31, 32]. Thermal analysis predicts temperature distribution during operation [33, 34], while electrical analysis ensures efficient power transmission by evaluating electrical performance factors such as resistance, capacitance, and inductance [35]. This stage is iterative, with findings used to refine the cable design for optimal parameters and performance.

Subsequently, mechanical analysis is conducted. This analysis is broad, encompassing the evaluation of the SPC's strength against external loadings, stiffness, fatigue life under repetitive loadings, and component stresses [36–39]. Given the dynamic nature of DPCs, which are subject to repetitive and severe environmental loadings that could induce fatigue failure, this phase is critical. DPCs are under higher mechanical stresses and must meet specialized requirements not typically necessary for static submarine cables [2, 13]. CIGRE [29] and DNVGL [28] provide extensive details on the mechanical analysis process for dynamic cables, emphasizing its importance in the design phase.

2.2.2. MECHANICAL DESIGN PROCESS FOR DPCs

According to the literature on DPCs [1, 13, 29], the flowchart of the mechanical analysis process is illustrated in Figure 2.5. One primary objective of conducting mechanical analysis on DPCs is to evaluate whether the cable's fatigue life meets the project requirements [2]. This involves initially determining the stress variation within the components of the DPC by conducting both global and local analyses.

Global Analysis: Global analysis requires inputs such as environmental loads and stiffness values derived from the local model. It outputs the curvature and tension values that are subsequently used in the local model. The approach to global analysis

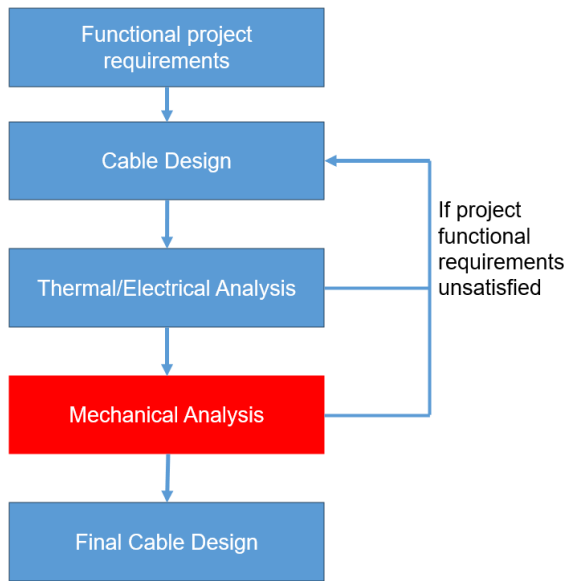


Figure 2.4: Example of general cable design process [29]

for DPCs closely resembles that used for flexible risers, as both are considered slender beams subjected to environmental loads. For further details on the global analysis of flexible structures, interested readers are referred to [40–42].

Local Analysis: Performing a local analysis is essential to ensure that the DPC can withstand the required stress and strain over its entire lifespan without premature failure such as fatigue. As depicted in Figure 2.5, local analysis is conducted both before and after the global analysis. It not only provides stiffness data necessary for global analysis but also assesses the stress variations in components crucial for fatigue analysis. Essential parameters for local analysis are outlined in Table 2.3, which includes material properties and component geometry provided by cable manufacturers, and global load calculations based on environmental loadings and the DPC’s configuration [40, 43]. The initial local analysis involves these material and geometric data as mandatory inputs, whereas the subsequent analysis integrates additional global load data to furnish necessary stress information for fatigue assessment.

CIGRE highlights through an example [29] that even minor uncertainties in stress calculations can significantly amplify uncertainties in predicted fatigue damage, underscoring the need for high safety factors in fatigue assessments. This exemplifies why achieving precise stress predictions from local analysis is crucial for reducing uncertainties and enhancing safety in cable design.

Analytical and numerical methods are recommended to perform the local mechanical analysis of SPCs in the industry [28]. The analysis tool in performing the

local mechanical analysis for SPCs must meet specific criteria, as outlined by CIGRE [29]:

- a. Geometrical and Material Description: The tool should accurately represent the geometrical arrangement of components within the cable cross-section and include material properties such as Young's modulus and friction coefficient.
- b. Load Sharing and Stress Calculation: It should calculate how loads are distributed among the components and the resultant stresses within each component.
- c. Inter-layer Friction: The tool must account for the effects of inter-layer friction on component stress during bending, incorporating the contact pressure between layers.
- d. Overall Stiffness Properties: It should be capable of calculating the overall stiffness properties of the cable.

The first three features focus on the mechanical analysis at the component level, while the last addresses the overall level. Local mechanical analysis of flexible structures, which have faced complex loadings in marine environments, has been conducted extensively due to safety considerations [44, 45]. While the configuration of SPCs has evolved, diverging from typical flexible structures like flexible pipes, significant overlap remains in the underlying principles. Thus, this review will also incorporate some historical research and standards related to typical flexible structures.

Given that tension, bending, and their combinations are dominant in practical engineering and frequently addressed in standards, the review will primarily focus on these loading scenarios. In practice, SPCs are also subjected to torsion, thus analyses of torsion will also be included when relevant. In Section 2.3 and Section 2.4, the potential methods for developing such an analysis tool—both analytical and numerical—are reviewed.

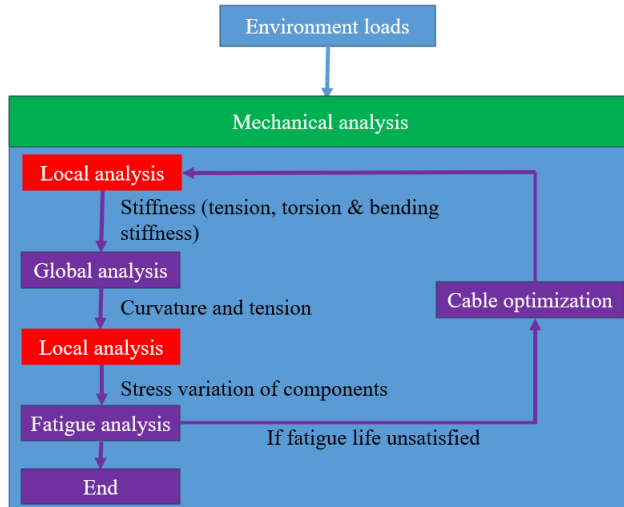


Figure 2.5: Example of the mechanical design process for DPCs

Table 2.3: Typical input parameters for local analysis

Input parameters	Details
Material properties	Young's Modulus/Stress-strain relation, Yield strength, Friction coefficient
Component geometry	Number of components, Size of components, Pitch length component radius, radial pressure resulting from extruded sheath, etc.
Global loads	Spectra of tension & curvature or classes of tension & curvature variations

2.3. ANALYTICAL METHOD

THIS section explores the analytical methods used to perform local mechanical analyses on flexible structures, focusing on SPCs. In the analysis of SPCs, tension, torsion, and external pressure are often grouped together as axisymmetric loadings. To facilitate understanding, the discussion is divided into subsections dealing with axisymmetric loadings and bending separately.

Before diving into specific methodologies, it is important to establish the common assumptions applied in the analytical study of SPCs:

- Strain Consistency: The strain of each component is assumed to be constant along the length of the structure.
- Small Deformations: Only small deformations are considered, aligning with the linear elastic framework.
- Helical Wire Spacing: Helical wires in any layer are assumed to be equally spaced around the cable's circumference, simplifying the analysis by ignoring the contact between wires in the same layer.
- Helical wire stress: Helical wires are assumed to have stress only in their axial direction; their stresses in other direction are ignored.
- Simplification of Components: Copper conductors and steel strands are modelled as solid cylinders, which simplifies complex real-world geometries into more manageable forms for mathematical analysis.

These assumptions are crucial for applying analytical methods effectively and are supported by references [25, 46–48]. Please be mind that these assumptions might cause difference in the analysis results as compared to practice. They set the foundational conditions under which the subsequent analyses are conducted, ensuring that the complexities of SPC behaviours are addressed within manageable and realistic constraints.

By setting these premises, the section prepares to delve into the detailed mechanical analysis of SPCs under specified loading conditions, providing a framework that supports robust and precise mechanical predictions.

2.3.1. AXISYMMETRIC LOADINGS

The tension stiffness in analytical methods is derived based on the principle of superposition, where the contributions from all components are cumulatively added. According to this principle, the equation for tension stiffness is expressed as follows:

$$K = A_c E_c + K_w \quad (2.1)$$

In this equation, the subscript c denotes cylinders and w denotes wires, which include helical wires and other helical components. Here, A_c represents the cross-sectional area, and E_c is the Young's modulus of the cylinders. Helical components, being structurally complex, have been the focus of several studies [25, 46, 47] due to their unique mechanical behaviours. Given that their cross-sectional area is significantly smaller than their length, helical wires are typically modelled as thin curved rods in analytical assessments. The complexities introduced by the helical configuration have garnered considerable research interest, highlighting the need for meticulous analysis to understand their influence on overall cable stiffness.

The foundational theory of thin curved rods can be attributed to Kirchhoff, who developed the linear theory of slender curved rods in the mid-19th century [49]. This seminal work is further explored in Love's comprehensive treatise [50] and elaborated upon by Ericksen and Truesdell [51]. Kirchhoff's theory posits that an elastic rod's centerline is inextensible and that its cross-sections remain plane and normal to the centerline throughout deformation [52].

An illustration of a Kirchhoff rod, depicted in Figure 2.6, demonstrates the rod's three translational degrees of freedom (DOFs) and three rotational DOFs. The unit vectors \mathbf{e}_t , \mathbf{e}_n and \mathbf{e}_b represent the directions tangent, normal, and binormal to the curve, respectively. The vector \mathbf{r} denotes the position of the target point of the wire relative to the origin of the Cartesian coordinate system.

Under Kirchhoff's theory, several critical assumptions are made to simplify the analysis:

- a. Cross-sections of the rod remain planar and perpendicular to the neutral axis during any deformation.
- b. Strain within the rod is minimal, allowing the material to maintain its linear elastic properties throughout deformation.
- c. Shear deformation effects are considered negligible, focusing analysis purely on bending and twisting responses.

Kirchhoff's theory is particularly applicable when the rod's length significantly exceeds its diameter, a condition referred to as a high slenderness ratio, and when deformations remain minimal. A comprehensive theoretical exploration of Kirchhoff's rod theory was provided by Dill [54]. Due to its generality, this theory has been extensively applied across diverse research fields that involve helical structures, as evidenced by its application in studies by Schlick et al. [55], Goyal et al. [56, 57], Yang [58], and Wang [59].

Focusing on the behaviour of single wires, Dong et al. [60, 61] conducted detailed analyses of the curvature variations of a single helical wire interacting with a neighbouring cylinder. These studies are crucial for understanding the local mechanical interactions within layered helical systems.

Additionally, Knapp [62] developed a stiffness matrix for helically armoured cables using the energy method, addressing the interaction between tension and torsion. His findings reveal that axial tension in cables can induce torsional forces, although his

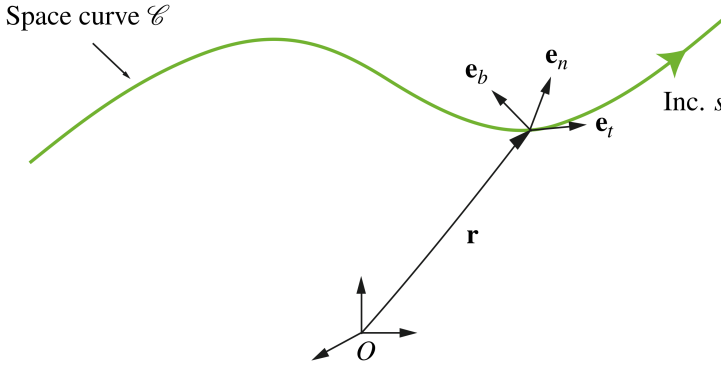


Figure 2.6: Kirchhoff rod illustration [53]

model simplifies the analysis by omitting the curvature variations of helical wires in their three local directions.

Despite the breadth of research in flexible structures, analytical models tailored specifically for SPCs are notably rare. To date, only a few studies, including those by Chang et al. [47], Nam et al. [25], and Delizisis et al. [46], have provided analytical formulas for SPCs under axisymmetric loadings. The methodologies from these studies are detailed in Table 2.4, highlighting the translational and rotational degrees of freedom (DOFs 1-6) that correspond to the vectors e_t , e_n and e_b illustrated in Figure 2.6.

Table 2.4: The information of available analytical studies on SPCs under axisymmetric loadings

Author	Cable types	Wire DOFs	Contact	Thickness variation
Grant et al. [46]	Three-core SPC	u_1	No	No
Chang et al. [47]	Three-core SPC	u_1, u_3, u_6	No	No
Nam et al. [25]	Three-core SPC	u_1, u_3, u_4, u_6	Normal contact	Yes

Grant et al. [46] obtained the stiffness contributed by the helical wires by superposing the contributions from all the wires, using the formula in Eq. 2.2, where the subscript j means the layer number, n is the number of wires in the corresponding layer, E is Young's modulus, A is the wire cross section and α is the winding angle. These parameters are illustrated in Figure 2.7. Only the deformation in the u_1 direction is considered in this formula. Grant et al. also gave the torsional stiffness K_4 [46], shown in Eq. 2.3. In this case, the wire axial stress σ_j is the product of Young's modulus E , the axial strain of the cable δ and $\cos^2 \alpha_j$, given in Eq. 2.4.

$$K_1 = n_j E_j A \cos^3 \alpha_j \quad (2.2)$$

$$K_4 = n_j E_j A r_i^2 \cos \alpha_j \sin^2 \alpha_j \quad (2.3)$$

$$\sigma_j = E \delta \cos^2 \alpha_j \quad (2.4)$$

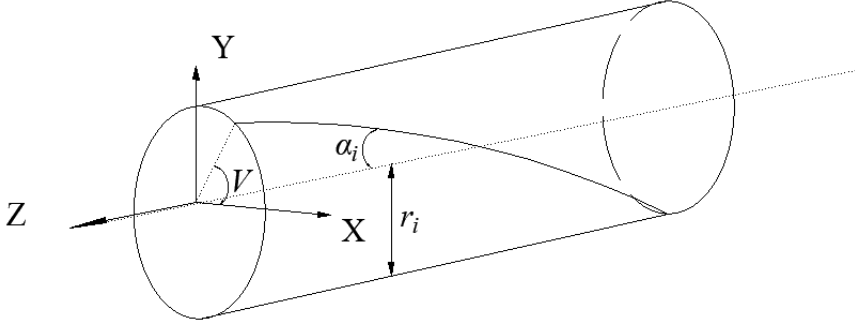


Figure 2.7: Helical wire on a cylinder

Chang et al. [47] further considered the deformation of helical wire in u_3 and u_6 directions based on Knapp's derivation [62]. Assuming no torsion coupling the axial stiffness thus becomes:

$$K_1 = n_j E_j A \left(\cos^3 \alpha_j - \frac{u_R}{r_j \delta} \sin^2 \alpha_j \cos \alpha_j \right) \quad (2.5)$$

The physical meaning of the newly-added term $-n_j E_j A \frac{u_R}{r_j \delta} \sin^2 \alpha_j \cos \alpha_j$ is the effect from radial strain on the axial stiffness, where u_R is radial displacement in the cable radial direction. The torsional stiffness given by Chang et al. [47] is the same as that given by Grant [46] in Eq. 2.3. In this case, the wire stress is given by the following equation, where θ is the rotation angle of the cable in unit length.

$$\sigma_j = E \left(\delta \cos^2 \alpha_j - \frac{u_R}{r_j} \sin^2 \alpha_j + r_j \theta \sin \alpha_j \cos \alpha_j \right) \quad (2.6)$$

Nam et al. [25] developed analytical methods that account for the curvature changes of helical wires and variations in the thickness of all layers. Their approach, rooted in the principle of minimum virtual work, is compiled into a matrix framework for analysis [63]. However, due to the complexity and number of deformations considered, their model often requires supplementation with numerical methods for direct solution.

Despite these advances, current models [25, 46, 47] generally overlook the specific contributions of inner helical components to the overall mechanical properties of the cable. This oversight is significant as the helical shape of these inner components can profoundly influence cable tension behaviours. Historically, these inner helical components are assumed to be straight during tension analyses [17], a simplification that may not accurately reflect their actual mechanical contributions.

2.3.2. BENDING

Analytical methods tailored specifically for SPCs are notably lacking, particularly concerning bending scenarios. Existing models from related fields, such as flexible pipes, cannot be directly applied to SPCs for several reasons. Flexible pipes are designed with a hollow cross-section to facilitate the transportation of oil and gas.

In contrast, SPCs incorporate metal components within their core, significantly influencing their structural properties. These central metal components are often helical and involve intense contact interactions, adding complexity to their local mechanical analysis.

One of the critical issues in the bending analysis of SPCs is the stick-slip phenomenon, which is influenced by contact pressure and the friction coefficient. These factors are intrinsic properties of an SPC and should be provided by cable manufacturers. The contact itself is often a result of radial initial pressure combined with residual stresses in the polyethylene (PE) sheath from the extrusion process. Currently, there are four main approaches to model the effects of these factors: using equivalent external pressure, equivalent internal pressure, tension force, or stresses induced by thermal variations in the polymer materials [64–66]. These methods will be explored further in Section 2.4.

Furthermore, the determination of when and how wires begin to slip during bending is governed by the contact pressure and friction coefficient. There are two classical assumptions about the path of slip in the literature, visualized in Figure 2.8:

Geodesic Path: This path is defined as the shortest path between the intrados and extrados on the neighbouring cylinder, as depicted in Figure 2.9. Under this assumption, a transverse slip occurs without any curvature change in this direction.

Loxodromic Path: This assumes that the wire maintains its position relative to its neighbouring layers during bending, potentially causing curvature variations in this direction.

The debate between adopting a geodesic or loxodromic path underlies many studies in the analysis of flexible pipes under bending. The actual response of a wire is likely to lie between these two theoretical paths. The representative research adopting different slip path assumptions is summarized in Table 2.5.

Table 2.5: The slip path assumptions in analytical studies

Slip path assumptions	Papers
Geodesic	Feret & Bournazel, 1987 [67]
	Feret & Momplot, 1991 [68]
Loxodromic	Berge, et al., 1992 [69]
	Saevik, 1992 [70]
	Kebadze & Kraincanic, 2000 [71]
	Saevik, 1993 [72]
	Lukassen, 2019 [73]
Others	Estrier, 1992 [74]
	TAN, et al., 2005 [75]
	Fergestad & Lotveit, 2014 [76]

Existing research found that the assumption of the loxodromic path is closer to reality after comparison with test results and thus is used more frequently in studies [69–73]. Based on the assumption of the loxodromic path and the Kirchhoff rod theory, the axial stress of the wire before it starts to slip can be given as:

$$\sigma_i^{stick} = E_i \cdot \kappa \cdot r_i \cdot \sin V \cdot \cos^2 \alpha_i \quad (2.7)$$

where κ is the cable curvature. As long as the friction stress along the wire is greater than σ_i^{stick} , the wire will continue to adhere to its neighbouring layers. Otherwise, the wire starts to slip. The friction force exists only when there is inner normal stress caused by, for example, residual stress, an external pressure or the normal contact stress component resulting from a tension force. Feret gives the pressure differential contributed by tension through each layer [67], as shown below:

$$\Delta P_j = \frac{n_j \sigma_j A_j \sin \alpha_j \tan \alpha_j}{2\pi r_j^2} \quad (2.8)$$

Therefrom, the contact pressure P between two neighbouring layers after considering an external pressure P_{ext} becomes:

$$P_j = \Delta P_j + P_{ext} \quad (2.9)$$

As there are gaps among wires in armour layers, the pressure needs to be distributed to each wire using a fill factor F_f . Saevik [77] defined this value for rectangular wires used in flexible pipes as:

$$F_{f,j} = \frac{n_j b_j}{2\pi r_j \cos \alpha_j} \quad (2.10)$$

where b is the width of wires with rectangular cross-sections. Nevertheless, the wires used in SPCs are mainly made into round cross-sections where the fill factor needs to be adjusted. Assuming the fill factor is satisfied for round helical wires, the contact pressure on each wire is given by:

$$P_j = \frac{P_j}{F_{f,j}} \quad (2.11)$$

Once the contact pressure is known, the friction force can be derived as:

$$f = \mu P_j \quad (2.12)$$

where μ is the friction coefficient. Therefore, as long as $f = \sigma_i^{stick}$, slip starts to appear. Wires on a region of a cross-section slip while wires on the other region still stick, as shown in Figure 2.10. The limit curvature is thus obtained:

$$\kappa_{limit} = \frac{\mu P_j}{Et \cos V \cos^2 \alpha_j \sin \alpha_j} \quad (2.13)$$

where t is the thickness of wires with rectangular cross-sections, and V is the wire position around the circular direction, as shown in Figure 2.9. It can be derived from

Eq. 2.13 that the slip first appears at the angular position $V = 0; V = \pi$. After the applied curvature surpasses κ_{limit} , the slip area will enlarge and gradually progress, then there will be a slip area and a stick area, as shown in Figure 2.10. The transition angle V^* between these two areas can be obtained:

$$V^* = \arccos\left(\frac{\mu P_j}{E t \cos^2 \alpha_j \sin \alpha_j k}\right) \quad (2.14)$$

In the slip area, the wire stress is:

$$\sigma_i^{slip} = \frac{\mu P_j r_j}{t \sin \alpha} V \quad (2.15)$$

The axial slip displacement is also mentioned in the literature [67, 78] by a simplified equation as:

$$u_{slip} = r_j^2 \frac{\cos^2 \alpha_j}{\sin \alpha_j} \kappa \cos V \quad (2.16)$$

Finally, the bending moment contributed by all the helical wires can be integrated over the cable cross-section as:

$$M_w = 4 \left(\int_0^{V^*} \sigma_{slip} A_j dV + \int_{V^*}^{\pi/2} \sigma_{stick} A_j dV \right) \quad (2.17)$$

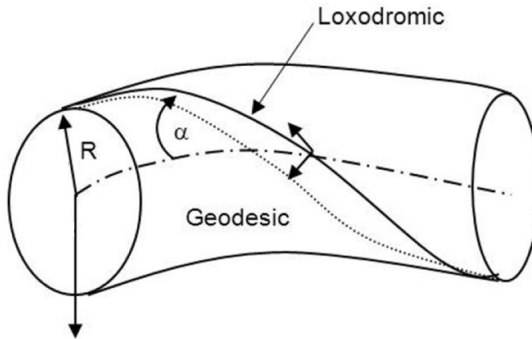


Figure 2.8: Geodesic and Loxodromic curves [79]

2.3.3. REMARKS ON ANALYTICAL METHOD

To date, only a limited number of studies, such as the one by Tjahjanto et al. [48], have attempted to provide an analytical method for evaluating the stress in an SPC, particularly addressing the effects of helical components. Although these components, including inner helical conductors, are crucial in influencing component stresses, the study does not comprehensively address the overall stiffness of the SPC. Additionally, the method for managing pressure across each layer remains unspecified, highlighting a gap in the analytical approach.

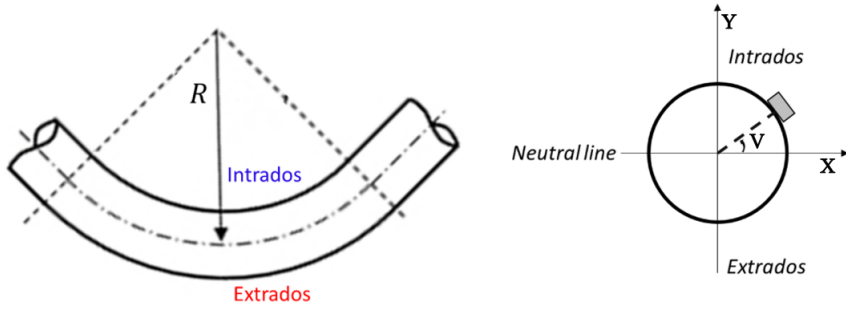


Figure 2.9: Illustration of the intrados and extrados [79]

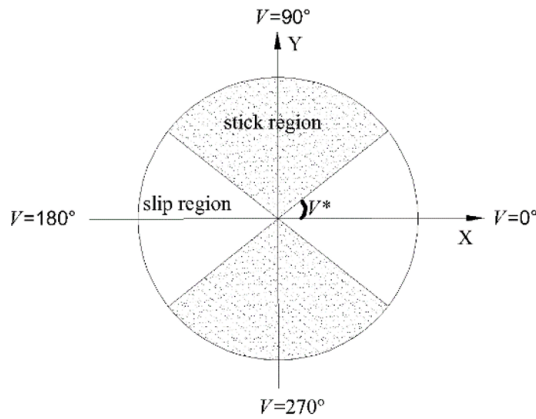


Figure 2.10: Stick and slip zones on a cross section

In summary, while analytical methods offer a framework to predict the overall stiffness of SPCs, several challenges emerge, particularly at the component level:

1. **Complex Contact Pressure:** Analytical methods struggle to accurately capture the complex contact pressures among layers, which are critical in the local mechanical analysis of SPCs under bending. This is largely due to the dense arrangement of helical components within the cable.

2. **Simplification of Helical components:** Previous studies often simplify the helical wires in the armour layers as Kirchhoff rods and make specific assumptions about their slip paths. However, inner helical components, which differ from slender beam-like structures, are not adequately studied, and analytical insights into these components are lacking.

3. **Limitations of Closed-form Solutions:** When the model incorporates many detailed features, deriving simple closed-form solutions becomes impractical.

Consequently, such complex models require numerical solutions to resolve [80], pushing the boundaries of traditional analytical methods.

2.4. NUMERICAL METHOD

WHEN considering the intricate details necessary for accurately modelling SPCs, a large number of partial differential equations (PDEs) emerge, necessitating numerical solutions. Common numerical methods employed include the finite difference method, finite volume method, boundary element method, and notably, the finite element method (FEM). FEM is particularly adept at addressing problems characterized by complex geometries, diverse material properties, and intricate contact interactions, making it the preferred choice for solving PDEs in this domain. Enhanced computational capabilities of modern computers have facilitated efficient PDE solutions via FEM, allowing designers to visually explore mechanical behaviours at both the overall and component levels of SPCs.

Both 2D [81, 82] and 3D models [47, 72] have been developed to analyze flexible structures. However, the greater detail and superior contact simulation abilities of 3D models have driven their increasing adoption in practical engineering. A notable challenge in these simulations is the modelling of numerous helical wires. Researchers have simplified these wires in armour layers of flexible pipes into equivalent tubular layers (orthotropic layer materials) [79, 83, 84], a process underpinned by equating the axial and bending stiffness of these simplified materials with those of actual layers, drawing on theories from Timoshenko et al. [85].

However, helical wires in SPCs typically differ significantly from those in flexible pipes; they are round with more gaps between them, as opposed to the closely arranged rectangular wires found in flexible pipes, as depicted in Figure 1.4(b). This structural difference raises concerns about the accuracy of stress predictions when using simplifications designed for flexible pipes, potentially leading to incorrect stress estimations. Furthermore, such simplifications are less useful when detailed stress analysis of each helical wire is required, thus they have not been widely implemented even in flexible pipe studies.

Constructing each helical wire individually in a detailed 3D model introduces considerable complexity. This approach requires careful selection of element types, meticulous setup of boundary conditions, and precise management of contact properties among interfaces, posing significant challenges in model construction.

2.4.1. AXISYMMETRIC LOADINGS

Numerical models that address axisymmetric loadings in SPCs are relatively rare in the open literature, with only a few studies addressing this specific challenge. Information on these models is summarised in Table 2.6.

Chang et al. [47] built a 3D model to study the mechanical behaviour of an SPC under coupled tension, torsion and compressive loads. Solid elements are used to simulate all the components within the cable, including the helical wires. Both ends of the cross sections in this model are set as rigid planes with all the nodes coupled

Table 2.6: The numerical models of SPCs under axisymmetric loadings

Author	Chang et al. [47]	Hsieh et al. [86]	Lu et al. [24]
Cable types	Three-core SPC	Three-core SPC	Umbilical cable
Pitch length	552.4 mm	-	-
Model length	941 mm	971 mm	-
Element types	Solid	Solid	Shell + beam + solid
Interaction	Normal direction	Normal direction	Normal direction
Algorithms	Static analysis	Static analysis	-

'-' means the information is unavailable.

to the middle node in the corresponding plane. One end is fully constrained while the loads are applied on the other end.

The interaction normally involves normal contact and tangential contact properties. The former, also known as normal or perpendicular penetration, refers to the interaction between surfaces along their normal direction. The latter, also known as shear or frictional contact, involves forces exchanged in the tangential direction along the contact surfaces. The most basic method of introducing contacts is to add springs between two contact interfaces. Sævik [72], for example, introduced hyperelastic and elastoplastic springs in the normal and transverse directions to simulate contact in flexible pipes. This is similar to the penalty method used in general FEM software. This method introduces a penalty term into the formulation to enforce contact conditions or constraints when bodies interact. The penalty term acts as a stiffness term that increases as the contact conditions are violated [87, 88].

Only the contact in the normal direction is considered in this model, where the pure penalty method is utilized. The contact between the cable layers is set to “no separation” for surface contact. Adjacent layers can slide horizontally but not vertically. To avoid the dynamic effect from the loading process, static analysis is selected for the simulation, where the effect from the time item in the dynamic algorithm is eliminated.

There is still no recommendation about how long a 3D model should be to eliminate boundary effects. The model length is 941 mm, nearly twice the pitch length of the outermost helical wire layer, according to the data provided by the authors. The authors tested the influence of the model length on its tension stiffness, and it was found that the model length stops affecting the tension stiffness significantly even when it is near the pitch length of the outermost helical wire layer. Nevertheless, one thing that should be noticed about this model is that the helical shapes of the inner components are disregarded. The other paper studying SPCs under tension is authored by Hsieh et al. [86], who further investigated the influence of the number of cores on the mechanical properties of SPCs under axisymmetric loadings based on the work of Chang et al. [47]. The details of the model are similar to Chang et al. [47], and the helical inner cores are simplified into straight cylinders again.

Apart from the studies on SPCs, Lu et al. [24] established a simplified 3D FE model to predict the axial structural behaviours of an umbilical cable. The original configuration of the umbilical cable is extremely complicated. In order to enable the

simulation, the authors homogenize the inner helical components into an equivalent column. The equivalent property parameter of the column is obtained by abandoning all the layers outside the inner sheath layer. After the parameter is obtained, it is then inputted back into the homogeneous column of the 3D FE model. The final 3D FE model is shown in Figure 2.11. Beam elements are also selected for the modelling of the helical wires. Meanwhile, solid elements and surface elements are utilized to simulate the rest layers. The boundary conditions in this model are also similar to those in Chang et al. [47]. Both cross-sections are coupled to a corresponding reference point (RP). One RP is fully fixed while the load is applied on the other RP. Likewise, only the contact in the normal direction is paid attention to in this model.

In conclusion, the numerical models developed for SPCs under tension are scarce. The aforementioned models do not consider the details of the inner helical components for the sake of efficiency. Solid elements are frequently selected for the analysis. The boundary conditions are the same as those in the tension test, where one end is fully fixed while the load is applied on the other end. The contact property in the normal direction is more paid attention to.

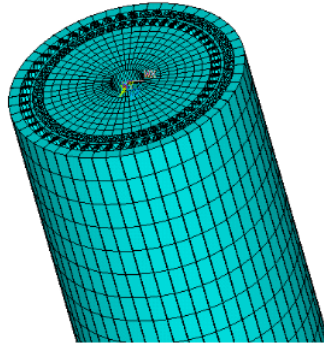


Figure 2.11: The 3-D FE model of the umbilical cable [24]

2.4.2. BENDING

Three seminal papers provide detailed 3D numerical models for SPCs specifically under bending conditions, with their findings summarized in Table 2.7. Each of these models, developed for three-core SPCs, varies in terms of how inner helical shapes are accounted for [48, 89, 90]. The analysis of these models will focus on three critical simulation challenges: elements, boundary conditions, and interactions.

Finite Element Type

Solid elements are the most commonly used element type in the mechanical analysis of bending across all three models [48, 89, 90]. Menard et al. [89], however, incorporated beam and surface elements alongside solid elements to address the computational challenges posed by the large model size and numerous helical wires.

Table 2.7: The reviewed numerical study of SPCs under bending

Author	Tyrberg et al. [48]	Leroy et al. [90]	Menard et al. [89]
Cable types	Three-core SPC	Three-core SPC	Three-core SPC
Pitch length	-	-	383 mm
Model length	1/3 core pitch	decided by wire	234.2 mm
Element types	Solid	Solid	Solid & beam & surface
Interaction	Normal + Tangential	Normal + Tangential	Normal + Tangential
Algorithms	-	-	Dynamic analysis

'-' means the information is unavailable.

The differentiation of wires using solid elements can lead to an overly dense mesh, which is computationally expensive. Inspired by advancements in modelling helical ropes [91], Menard et al. employed a hybrid approach using beam and surface elements to simulate the helical wires effectively. This approach is illustrated in Figure 2.12, where beams are meshed using Timoshenko beam elements and the surface, lacking thickness or stiffness, is coupled at the nodes with the beams. This method has been shown to offer a balance between computational efficiency and accuracy [91, 92].

In addition to typical commercial FEM program beam elements, special beam elements have been developed for helical wires in flexible structures. SÆVIK [72] introduced an eight-DOF curved beam element that restricts transverse translation, based on Kirchhoff rod theory [49, 50]. This element allows the wire to follow a loxodromic slip path, enhancing the model's fidelity to actual helical behaviors. The numerical program incorporating similar elements has been maturely developed and commercialized, as demonstrated in studies by Skeie [93, 94], indicating their practical applicability in industry.

Contact

Contact in the bending case is more complicated than that in the tension case, not only because both the normal and tangential directions need to be taken into account, but also due to the initial residual stress [29] which is gradually regarded as one of the factors that dominate the stick-slip phenomenon in a multi-layer flexible structure [43, 95, 96]. Kraincanic [43] made it clear that the initial (manufacturing) interlayer pressures are important for the described analysis and should be given alongside the pipe construction data. Yet this value is hard to obtain directly [29]. Fernando [97] listed methods to measure the value in pressure/tensile armour wires of flexible pipes, for example, by neutron diffraction. The values of the maximum mechanical stress observed in five transmission cables studied by Amyot et al. [17] varied from 4.5 MPa to 6 MPa. However, the initial residual stresses vary everywhere within an SPC, thus in practice, the curvature-bending moment curve from a bending test is recommended to calibrate an equivalent external pressure that imitates the effect from the initial residual stress [29, 89]. In the study of other flexible structures, alternatives to deal with the initial residual stress include applying an internal pressure, a tension force or introducing a thermal field that induces radial stresses within the structure [64–66].

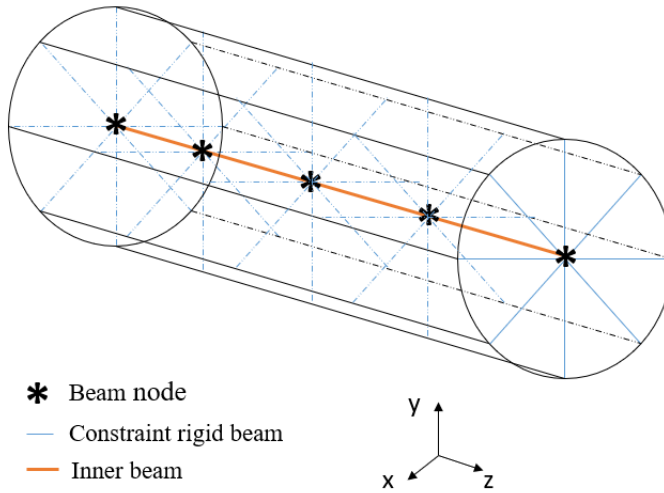


Figure 2.12: The combination of beam and surface elements

Applying external and internal pressure enables the radial stress to propagate among layers. A tension force also generates radial stresses due to the Poisson effect and the existence of helical components, while the expansion induced by thermal variation causes the radial stress by applying a thermal field.

To date, applying an equivalent external pressure is the most popular way that scholars have done in many flexible structures [48, 89, 98]. The values given by the previous studies are summarized in Table 2.8. Notice that out of the three papers about SPCs, Leroy et al. [90] and Tyberg et al. [48] pioneered the simulation of this particular structure, yet they did not provide a bending test to calibrate the equivalent external pressure. Therefore, the equivalent external pressure is not considered in Leroy's work while the value provided by Tybery is out of their industry experiences. It was not until 2023 that Menard et al. [89] first managed to calibrate the equivalent external pressure for a three-core SPC by the curvature-bending moment curve from his bending test, and the value for his SPC is 0.3 MPa. In their work [89], Menard et al. did a sensitivity study of the external pressure on the bending behaviour of the SPC. It is found that when the pressure is set as 0, the curvature-bending moment curve becomes a straight line instead of a hysteresis curve, as shown in Figure 2.13. In this case, the components within the SPC directly slip away from each other without the initial stresses that retard the slippage. When the equivalent external pressure increases, the stick section of the curve becomes longer as larger radial stresses introduce larger friction forces that make the slippage more difficult. This phenomenon can also be explained by Eq. 2.13 and Eq. 2.17 in the analytical section, which states that the slip curvature and the total moment are affected by the friction coefficient and the contact pressure among the contact interfaces. The same phenomenon was also observed by Zhang et al. [98], who studied a flexible

pipe with the test data provided by Witz [99]. Based on the proposed model by Zhang et al. [98], the equivalent external pressure calibrated by the test data on the curvature-bending moment curve is 1.9 MPa, as summarized in Table 2.8.

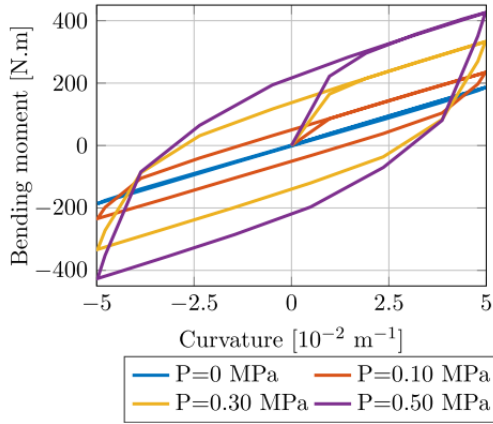


Figure 2.13: Evolution as a function of the external pressure on the curvature-bending moment curves [89]

Table 2.8: The friction coefficients and equivalent external pressure used in previous studies regarding flexible structures

Author	Structure types	Friction coefficient	Equivalent external pressure
Leroy [90]	Three-core SPC	0.15	0
Tyrberg [48]	Three-core SPC	0.25	0.2 MPa
Menard [89]	Three-core SPC	0.2	0.3 MPa
Zhang [98]	Flexible pipe	0.05 - 0.2	1.9 MPa

As compared with the tension case, the interaction properties in the tangential direction have received more attention in the bending case. Stick-slip behaviours within flexible structures strongly relate to the contact property in the tangential direction. Coulomb friction is a classical friction method in describing the interaction of contacting surfaces. The model characterizes the frictional behaviour between the surfaces using a coefficient of friction [100] and has been applied in many models [90, 101–103]. Scholars have also investigated friction methods other than the traditional Coulomb friction method. For example, Tianjiao et al. [104] studied the mechanical behaviour of a flexible pipe by using four different friction models, finding that the pipe exhibits different behaviours. It should be noted that the friction properties are different even in the same flexible structure because the contact interfaces are not the same. For example, the friction coefficients between two polymer interfaces differ from those between polymer and metals. In addition, the friction coefficient can also be affected by many other factors, such as temperature [105], air moisture content

[106], etc. Measurement of friction coefficients is also a cumbersome task. Therefore, the structure's equivalent unified friction coefficient is adopted normally.

Another factor affecting contact behaviour is the damping among interfaces [107, 108]. Damping in a physical system essentially refers to the loss of energy or, alternatively, energy dissipation. This means the energy is either redistributed to the surroundings or converted into other forms of energy, usually heat, that cannot be recovered. Consequently, this process diminishes the system's motion. Silva [109] classified the damping sources in mechanical systems as three: internal/material damping, structural damping, and fluid damping. The contact damping among the interfaces here refers to the structural damping that occurs in structural assemblies due to plasticity, dry friction (Coulomb damping), contact and interaction between structural components, typically in joints, connections, supports and other contact surfaces and interfaces. The contact damping itself is a complex subject that receives more and more attention [107, 108], however, in the previous studies about multi-layer flexible structures [110, 111], the contact damping is merely set as a tool to reduce solution noise and stabilize the structure for numerical consideration. In their studies [110, 111], the energy dissipated by contact damping is extremely tiny as compared to other types of energy, such as the internal energy or strain energy, which means that the contribution of the contact damping in the overall structure can be ignored and the mechanical behaviour is not affected too much by the artificially introduced damping.

Boundary Conditions

When it comes to the boundary conditions, the other problem that comes with it is how to choose a proper length for the bending simulation to eliminate the boundary effects, which is still an open question that no paper gives an explicit answer to. Theoretically, the longer the model, the more the boundary effect is eliminated. However, the contact effect becomes intensive based on the experience from bending tests, and a numerical model with a long length makes a simulation extremely time-consuming. Although comprehensive models for flexible pipes, spanning several meters and accounting for non-uniform curvature along their length, are prevalent in the literature [103, 112–115], no paper to date has provided detailed simulations of 3D bending numerical models with sample lengths matching those used in SPC tests in the available literature. Researchers are trying to propose reliable and efficient simulation models requiring less computational cost by applying appropriate boundary conditions. Thanks to the periodical structure pattern of helical components, a few numerical models based on the technique of periodical boundary conditions have been proposed [48, 89, 90].

The technique of periodical boundary conditions can be traced back to the multi-scale analysis, an approach used in various scientific and engineering disciplines to study and model phenomena that occur at multiple scales. It involves analyzing a system or process at different levels of detail, from microscale to macroscale, to understand its behaviour comprehensively. Homogenization is a common technique to bridge the different levels of scales where the mathematical tool of asymptotic expansion theory has been adopted frequently. On the macroscale level, SPCs can

be regarded as a type of beam-like structures that find significant applications in aerospace engineering, civil engineering, ocean engineering, etc. Helical ropes, lattice, cable-stayed bridges, SPCs, etc., are practical examples. These beam-like structures are characterized by having relatively small dimensions compared to their length. A conventional numerical simulation of these structures leads to heavy computations; therefore, researchers have been using homogenization theory to finish the simulation by bridging the macroscale beam-like structures to corresponding microscale homogeneous continuous medium.

The theory of the homogenization method applied to slender beam-like structures has been thoroughly developed by Buannic and Cartraud [116, 117]. The derived formulas are also used to study slender structures, from simple beam-like structures such as repetitive lattices to more complicated heterogeneous structures such as helical ropes in the past 30 years. A well-known model based on the theory used in practice is presented by Lukassen et al. [110]. Since the model is developed using a repeated unit cell (RUC), it is named the RUC model, as also referred to in [118]. Occasionally, readers might find the developed model called the RVE model [119, 120], which stands for representative volume element. Regardless of the terminology used, the core of these models is the application of periodic boundary conditions.

The periodical boundary conditions derived for slender beam-like structures by Buannic and Cartraud [116, 117] are found in the papers about SPCs during the recent years [48, 89, 90]. The model length is reduced and it is calculated as:

$$l = k \frac{p_i}{m_i} \quad (2.18)$$

where $k \in \mathbb{N}$, p is the pitch length, m is the number of helices, and the index i is the sequence of the current layer. The first two proposed models for SPCs that take advantage of the periodical boundary conditions are given by Tyrberg et al. (2017) [48] and Dupend et al. (2017) [90]. The equations of the periodical boundary conditions in these two papers are quite similar. However, the constituents of their numerical models differ from each other. Dupend et al. (2017) [90] divided the structure types in the SPC as helical wires and cylinders. The periodical boundary conditions are applied on the helical wires while a new set of constraint equations are derived and applied on the cylinders in order to obtain a constant curvature along the SPC. Besides, the helical shapes of the inner helical components, such as the copper conductors, are not considered and are simplified into straight structures. Tyrberg et al. (2017) [48], instead, chose to consider the inner components' helical configurations. Therefore, his model is much longer, with the inner helical shapes considered based on the length calculated through Eq. 2.18. The periodical boundary conditions are applied on both sides of the SPC for helical and cylinder components. Neither of the two models presents the overall behaviour of SPCs, nor are they validated by experimental data. Very recently, Fabien et al. [89] developed a model for a 3-core SPC based on Tyrberg's work. The helical shapes of the inner conductor cores with longer pitch lengths than the helical wires are considered. A bending test is performed, and the hysteretic curve has been observed through the test and the numerical model. The model requires an input of equivalent external pressure, and the combined tension and bending case is not studied.

2.4.3. REMARKS ON NUMERICAL METHOD

To sum up, the numerical method enables cable designers to gain more insights into the local mechanical behaviour of SPCs, especially at the component level. However, when a large amount of details are taken into account in the numerical model, the efficiency is infringed with the increase of accuracy. Three challenges need to be addressed to balance these two factors:

1. How to establish proper element types that are able to balance the accuracy and efficiency due to the existence of numerous helical structures and intensive contact within an SPC.
2. How to deal with the contact among the interfaces within an SPC and how to take into account the initial residual stresses generated in the manufacturing process.
3. How to set appropriate boundary conditions for SPCs.

2.5. TEST METHOD

IN order to calibrate and validate the developed modelling method, test data are needed, and the test method is thus reviewed. The purpose of common tests regarding flexible structures is to observe and obtain the mechanical response of the target structures under the loadings that the structures might encounter in real-life scenarios. In addition, the observations and data from tests can guide the research and development of analytical models and numerical models, finally validating their credibility and reliability.

2.5.1. TENSION & TORSION TESTS

API RP 17B [121] lists the procedure for performing tension tests. One end of the sample is fixed, and an axial load is applied to the other end. The load application should be sufficiently slow to avoid dynamic amplification. The maximum loading rate should not exceed 5% of the expected maximum load per minute. As a guideline, the load application should be completed in approximately 5 min. Unless otherwise specified in the details for particular tests, the tests shall be carried out at an ambient temperature of $(20 \pm 15)^{\circ}\text{C}$ [29].

The sketch of a typical tension sample is shown in Figure 2.14. The end effects can be reduced as much as possible if the sample length is as long as possible. However, the cost and laboratory conditions should also be considered. In the test recommendation given by the CIGRE guidelines [29], it is required that the length of the test cables be at least five times the pitch length of the outer armour layer. It is required that the minimum length of the test sample, excluding end fittings, i.e., the effective length in Figure 2.14, should be two times the pitch length of the outer armour layer [121]. A few examples of flexible structure tests are organised in Table 2.9 for a reference, where the key information such as the sample length, pitch and loading rate is given if available.

As tension tests regarding SPCs are scarce in the open literature, relevant information is found in four papers [25, 46, 122, 123]. Unlike flexible pipes, a power cable is usually preloaded before a tension test starts due to the existence of more gaps caused by the magnitude of helical components within this structure.

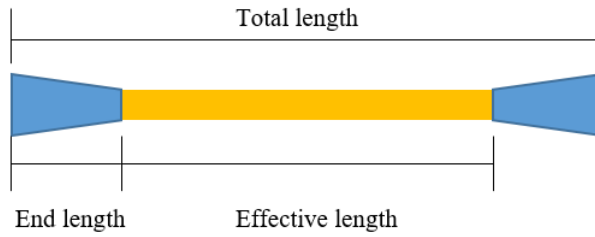


Figure 2.14: Sketch of tension test

Table 2.9: The available tension tests in the literature

Structure type	Diameter	Total length	Effective length	Pitch length	Loading rate
Three-core SPC [46]	-	63000	-	<30000/5	-
Fiber glass reinforced flexible pipes [20]	76	1800	1000	4.26	1 mm/s
Metallic strip flexible pipes [102]	74	1780	1100	57	1 mm/s
Umbilicals [23]	104	3000	-	125	slowly
Umbilicals cable [24]	95.7	2500	-	237	0.008 mm/s, 0.017 mm/s and 0.033 mm/s
Three-core SPC [25]	-	6500	-	-	force loading
Three-core SPC [122]	158.2	10000	-	-	0.108 KN/s
Three-core SPC [46]	-	30000	-	<30000/5	force loading

The unit is in mm if not written explicitly; '-' means the information is unavailable.



Figure 2.15: Tension test facility [25]

Helical components induce substantial gaps that need to be eliminated by the preloading process. After this manipulation, the stiffness will not be the same. As an example, after the cables are loaded and unloaded three times, according to the axial tension-axial displacement curves from Nam et. al [25], it is observed that the tension stiffness, i.e., the slope of the curve, is basically linear for the tests. Noteworthy, Nam et al. [25] applied an initial longitudinal displacement of 0.5 mm (a load of approximately 20 kN) on the cable prior to the test to minimise the deflection caused by the self-weight. They found that the stiffness in the first loading is slightly lower, then the stiffness in the next two loading rounds becomes larger and tends to a stable value. This is due to the presence of small gaps between each component layer after the fabrication of SPCs [124]. The gap was minimised or removed substantially after the first uniaxial tensile test. Consequently, the axial stiffness measured from the second and third loadings became constant.

Similarly, Guo et al. [122] also concluded that the degrees of stiffness in the later two rounds become larger than the first loading. The authors also observed that the axial stiffness during the unloading period is slightly smaller (about 3%) than during the loading period. Paiva et al. [123] performed a series of tests to validate the stress of the helical wires by inserting sensors into their cable. The cable sample used by Paiva et al. is a three-core SPC with bitumen sticking to the armour layers. The strain gauges were attached through small windows on the outer sheath to measure the variation in the deformation of the helical wires, as shown in Figure 2.16. The detailed values from the gauges are extracted and validated against their simulation results.

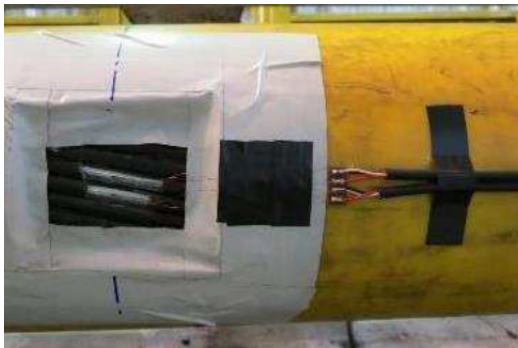


Figure 2.16: Strain gauges installation [123]

As SPCs also suffer from torsion, which affects the behaviour during the actual situation. CIGRE [29] points out that torsional stiffness is also an important parameter during cable design, so is the importance in the design of flexible pipes [121]. However, the test setup details are not given in either standard [29, 121]. Pure torsion tests regarding SPCs are quite scarce. In fact, up till the review, there is no pure torsion test on SPCs in the open literature. Although Delizisis et al. [46] obtained the torsional stiffness from a tension test where one end of the sample is freed in the rotation direction, this is not a true pure torsion test. Torsion tests on other flexible structures are reviewed, and their information is given in Table 2.10. Most flexible

structures are designed to be torsion-balanced, i.e., the degrees of torsional stiffness in both rotations need to be quite near. However, as the inner components within an SPC are helix wound around in one direction, it is hard to conclude that it is torsion-balanced without a test beforehand. If this point is not considered during the design, it is very likely that the torsional stiffness in one direction is much higher than that in the other. Performing a torsion test with respect to SPCs is necessary to evaluate their torsion behaviour.

Table 2.10: The available torsion tests in the literature

Structure type	Diameter	Total length	Effective length	Pitch length	Loading rate
Fiber glass reinforced flexible pipes [125]	76	-	1000	4.26	0.003 deg/s
Metallic strip flexible pipes [21]	78	1690	1010	61	0.1 deg/s
Reinforced thermoplastic pipes [126]	<167	1000	-	-	0.1 deg/s
Umbilicals [127]	93	-	6300	-	-

The unit is in mm if not written explicitly. '-' means the information is not available.

2.5.2. BENDING TESTS

Several test methods can be used to measure the bending stiffness of an SPC. CIGRE TB 669 [29] and Coser et al. [128] described three common test principles on which bending tests on SPCs are based: the three-point bending method (also termed single-point load method), four-point bending method (termed two-point load method) or moment method. The first two are more common in the open literature. For the three-point bending, a concentrated force is applied to the middle of a structure, which might cause structural collapse. This test facility is more recommended to obtain the critical bending loading, though it can also be used to predict bending stiffness. The four-point bending test facility, instead, prevents abrupt structural collapse as much as possible.

A classical four-point bending test sketch is given by CIGRE [29], as shown in Figure 2.17. A cable is supported by two rotating fixtures, enabling axial sliding with minimal friction. This capability is facilitated by either rollers or supports crafted from materials with low-friction properties. Consequently, a uniform bending moment, devoid of shear force, can be attained between the two inner supports. The test normally generates a curvature-bending moment curve that needs to be calculated based on the configuration of test setups. The resulting moment M over the cable between the inner supports is given by:

$$M = \frac{FL_2}{2} \quad (2.19)$$

Where F is the applied force and L_2 is the distance between the inner and outer supports. The curvature can be estimated from the displacement of the cable and the two supports that are connected to the moving frame by:

$$\kappa = \frac{8(S_1 - \frac{S_2}{2} - \frac{S_3}{2})}{L_1^2 + 4(S_1 - \frac{S_2}{2} - \frac{S_3}{2})^2} \quad (2.20)$$

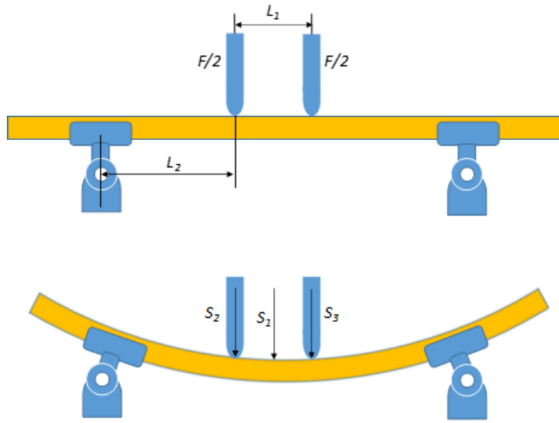


Figure 2.17: Illustration of test setup utilizing four-point bend method [29]

where κ is the cable curvature, S_1 is the displacement of the centre of the sample relative to a straight position, S_2 & S_3 are the displacements of the two supports relative to when the sample is in a straight position, and L_1 is the distance between the two inner supports. Should a dynamic bending stiffness be measured, the loading supports should be specially designed to satisfy the cyclic bending in two opposite directions. A typical dedicated test-rig for a full-scale four-point bend test can be found in, for example, Tyberg et al. [101], as shown in Figure 2.18.

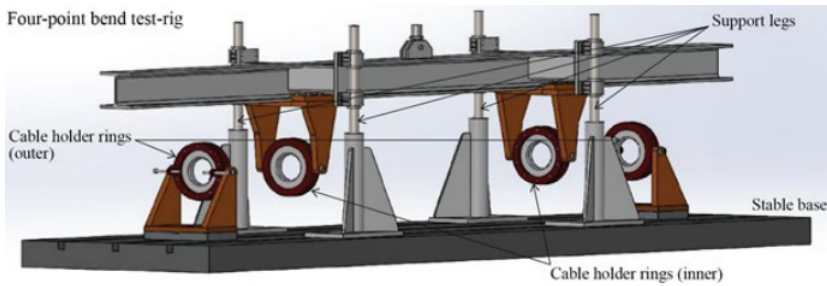


Figure 2.18: Dedicated test-rig for full-scale four-point bend test [101]

The length is crucial in preparing bending samples as it affects the predicted stiffness significantly. Although sample lengths are recommended to have at least one pitch length of the outer armour layer [29], actual physical lengths chosen by experimenters are usually much longer [89]. Table 2.11 shows detailed information on bending tests done by scholars. Unlike those in the tension test, the influences from temperature and loading rate have been more investigated by the experimenters. Whether or not the influence from these two factors is tested is summarized in Table 2.11. Tests are usually performed in a cyclic manner to measure bending

stiffnesses until a stable hysteretic response is achieved. This results in a hysteretic curvature-bending moment curve, as Figure 2.19.

Table 2.11: The reviewed bending tests in the literature

Author	Test method	L/D	L/Pitch	Thermal	Loading rate
Maioli [129]	Three-point bending	>20	-	Yes	Yes
Tyrberg et al. [101]	Four-point bending	-	-	Yes	No
Komperød et al. [130]	Four-point bending	-	-	Yes	Yes
Fabien et al. [89]	Four-point bending	25	3.42	No	No
Coser et al. [128]	Cantilever beam and three-point bending	17.77 and 46.6	-	No	No
Delizisis et.al. [46]	Three-point bending	-	-	No	No

'-' means the information is unavailable.

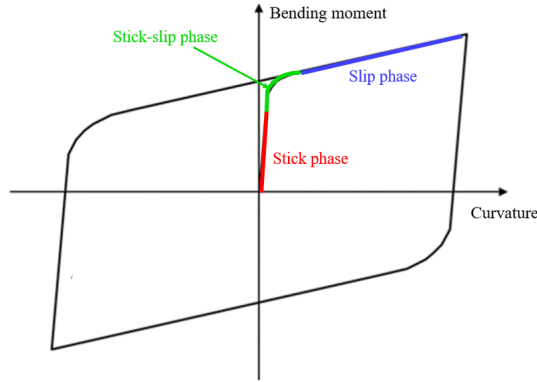


Figure 2.19: Hysteretic curvature-bending moment curve [29]

When the curvature is low, friction among the components is sufficient to resist slippage, resulting in a relatively higher stiffness, i.e., the slope of the curve. Stiffness in this scenario is called stick stiffness. However, as the curvature increases, a point is reached where the friction is not enough to prevent the components from slipping, slowing down the increased speed of the bending moment and reaching the slip stiffness. These phenomena can be observed from Figure 2.19. Slip stiffness can be several orders of magnitude lower than stick stiffness [29]. When the bending direction is reversed, friction needs to be overcome in the opposite direction, resulting in a hysteretic curvature-moment relationship. In this example, the cable is first bent to a positive curvature, then to a negative curvature, and then back to a positive curvature again, creating a hysteresis loop. This type of curvature is observed by bending tests on cables [46, 89, 101, 129], as well as on copper conductors [131, 132], flexible pipes [43, 133–135] and umbilicals [127, 136].

As the temperature variation during the service scenarios ranges substantially and there is polymer material whose material property is strongly affected by the

temperature variation, CIGRE [29] and IEC[137] recommend that the bending test should also be performed under different temperature to obtain the corresponding bending stiffness. Maioli et al. [129], Tyrberg et al. [101], Komperød and Magnus [130] took the thermal effect into account in their tests, and it is found that the thermal effect is indeed a significant factor in determining the bending stiffness. The curvature-moment curves obtained by Komperød et al. [130] are shown in Figure 2.20 for an example. The test was performed at two different temperatures and two different loading rates. When the ambient temperature changes from 5° C to 20° C, the moment becomes twice smaller. This might cause the notorious overbending failure [28] if not considered properly. The influence of loading rate can also be observed from Figure 2.20.

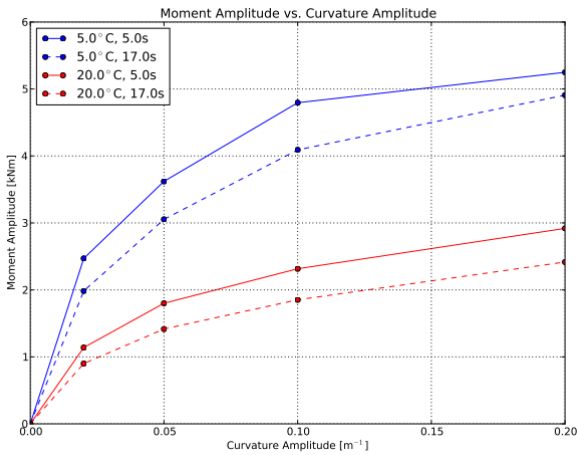


Figure 2.20: Curvature-bending moment curve under different temperature and loading speed [130]

It is commonly known from the flexible pipe industry that stiffness can be affected by combined loadings. For example, tension significantly affects the bending stiffness [138], so does external pressure on bending and torsional stiffnesses. Plus, they are all very common combination styles that a cable suffers from in real life. However, these combination loading tests require specially designed test facilities, which are not easily attainable [139]. There is only one paper presented by Coser et al. [128] that introduces the setup of the facility for SPCs under combined loadings. The test results show that the bending stiffness is significantly affected by tension forces. The setup of their test facility is shown in Figure 2.21. The test rig had two hydraulic actuators: an axial actuator and a transversal actuator. The former generates a tension force, while the latter bends the test sample. With this test setup, it was possible to obtain the bending stiffness of the cable under different axial tensions.

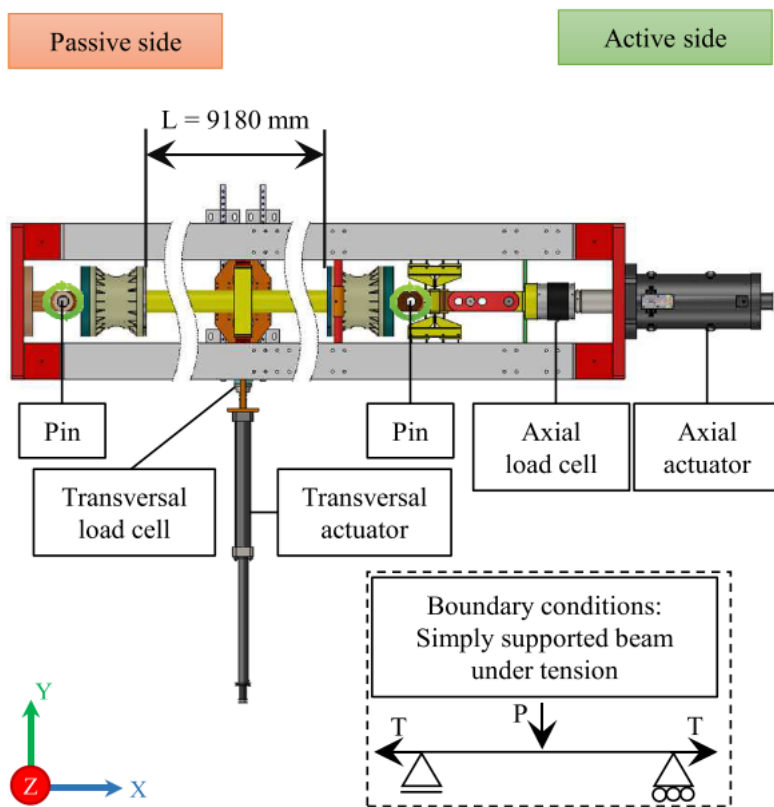


Figure 2.21: Setup for combined tension and bending test [128]

2.5.3. REMARKS ON TEST METHOD

While testing is considered fundamental and reliable, it comes with several limitations:

1. Each SPC is project-based. Its structural configuration differs from case to case. Tests need to be done specifically for a target SPC, thus they are costly and time-consuming. Besides, in the preliminary design phase, a cable sample is not available, making it hard to conduct tests.

2. The measurement of the local mechanical behaviour of the inner components in SPCs is scarce in the open literature, as SPCs are complicated multi-layer structures. Test methods are hard to provide insights into their internal mechanisms and how they propagate within structures; thus, internal behaviour is like a black box to engineers [140–143].

3. SPCs in real-world applications are subject to combined loadings, such as tension coupled with bending. Setting up facilities to replicate these complex conditions is exceedingly difficult [128].

However, tests are still necessary throughout the life cycle of an SPC. The test data can be used to guide the development of analytical or numerical methods, and serves as a validation tool for the developed model. As this dissertation aims to develop an effective modelling method for the local mechanical analysis of SPCs under combined loadings, the proposed method needs to be validated by test data. To be specific, tension test and bending test will be performed to validate the proposed method under tension and bending, respectively. These two loading scenarios are selected because they are the two most common loading cases in real life, as stated before; besides, the study of the combined tension and bending should be performed after the corresponding two pure loadings are analyzed. Two major points need to be paid attention to when performing corresponding test:

- The sample length is a crucial parameter in affecting the overall stiffness of SPCs. A proper length is relevant to the sample diameter and the pitch length of the inner components. In a tension test, the sample length should be at least five times the pitch length of the outer armour layer. For the bending case, the recommended length given by standards is at least longer than one pitch length of the outer armour layer; however, the sample lengths selected by experimenters are usually longer.

- The loading rate and temperature have been found to be crucial factors affecting the overall stiffness of SPCs. The loading process should be sufficiently slow to avoid dynamic amplification, and normally the test should be carried out under room temperature.

2.6. SUMMARY

AFTER introducing the cable configurations and the general design process, the gap within the field, i.e., local mechanical analysis, is exposed to readers. In order to fill up this gap, a modelling method in performing the local mechanical analysis is recommended to be based on analytical methods and numerical methods. The modelling method is required to be able to accurately predict the stiffness of the cable and the stress details of its components. The analytical method is a possible option to overcome the limitations in tests; however, due to the complexity of SPCs, many

assumptions are necessary, and accurately simulating internal mechanical behaviour is challenging. The numerical method is more recommended for further development due to its significant potential to capture the complex nonlinearity within SPCs if an appropriate modelling method is proposed to attain good calculation efficiency. Three actions need to be taken in order to propose such a modelling method:

- a). the setup of finite elements,
- b). the setup of contact,
- c). the establishment of boundary conditions.

Finally, in order to calibrate and validate the analysis tool, tests are required. It should be noticed that the sample length and the loading rate are crucial parameters in affecting the overall stiffness of SPCs. These two parameters should be confirmed according to the recommended values given by standards and the previous research.

Research scope

In the proposed model, stiffness measurements will be input into the global analysis model, while stress data will inform the fatigue analysis where the structure is under small deformation. Therefore, this dissertation excludes scenarios involving large deformations of SPCs. This manipulation is conventional and rational, supported by standards such as API and CIGRE. Consequently, for the global configuration of the structure, the majority of the SPCs experience only small deformations, affirming the viability and practical applicability of the proposed modelling method.

The local mechanical analysis of DPCs are performed under quasi-static loadings, which means the dynamic effects are not considered. Indeed, DPCs suffer from dynamic loadings during their operational life, and the dynamic effect has been found to affect the local mechanical analysis. However, incorporating the dynamic effect will make the analysis model even more complex, and preliminary research on the quasi-static analysis is mandatory before a further step into the dynamic field. Currently, in practical engineering, the local mechanical analysis of an SPC are usually carried out by imitating the structure under quasi-static loadings. The solution to cover the dynamic effect is by utilizing a safety coefficient. Similarly, the effect from temperature is also excluded from the current research, which can be further explored in the future study.

The loadings that will be considered in the proposed model include tension, bending and their combination as they are dominant in real life and in the fatigue life estimation. An SPC suffers many different loadings during its service, such as the aforementioned torsion. Besides, compression is also another type of axisymmetric loading that appears in practice. The touch-down point that touches the seabed is subjected to axial compression from the reverse end-cap and cyclic bending. This loading might cause a failure called birdcage for the helical wires, as well as the outer serving abrasion driven by the cable movement along the seabed. The proposed model can be further developed to tackle this issue. However, the topic is not discussed in this dissertation.

2.7. CHAPTER ARRANGEMENT

THE dissertation chapters are outlined in Figure 2.22. The methodology of the proposed model is detailed in Chapter 3. Validation of the model occurs in Chapter 4 for tension and Chapter 5 for bending. Subsequently, the model is demonstrated in Chapter 6. Finally, Chapter 7 concludes the work.

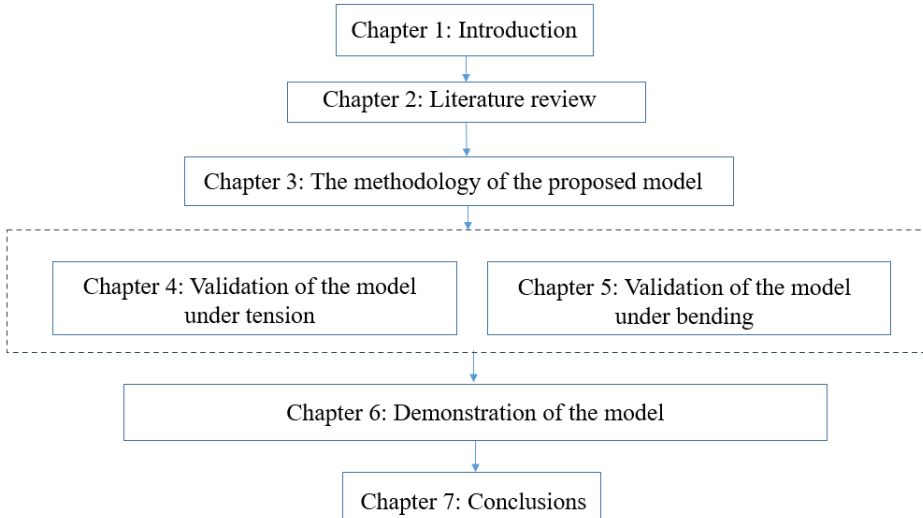


Figure 2.22: Graphical outline of this thesis, where the arrows indicate dependencies between chapters

REFERENCES

- [1] T. Worzyk. *Submarine power cables: design, installation, repair, environmental aspects*. Springer Science & Business Media, 2009.
- [2] M. Ikhennicheu, M. Lynch, S. Doole, F. Borisade, F. Wendt, M.-A. Schwarzkopf, D. Matha, R. Vicente, H. Tim, L. Ramirez, *et al.* “Review of the State of the Art of Dynamic Cable System Design”. In: *COREWIND: Brussels, Belgium* (2020).
- [3] Taihan Cable Solution Co., Ltd. *Power Generation*. 2022. URL: <https://www.taihan.com/en/business/product/productDetail?idx=20> (visited on 02/08/2024).
- [4] NEXANS. *SUBSEA CABLES | MV MEDIUM VOLTAGE POWER FIBRE OPTICS CABLES*. 2019. URL: <https://www.powerandcables.com/subsea-cables-joints-terminations/> (visited on 02/08/2024).
- [5] A. Devred, I. Backbier, D. Bessette, G. Bevilard, M. Gardner, M. Jewell, N. Mitchell, I. Pong, and A. Vostner. “Status of ITER conductor development and production”. In: *IEEE transactions on applied superconductivity* 22.3 (2012), pp. 4804909–4804909.
- [6] A. Devred, I. Backbier, D. Bessette, G. Bevilard, M. Gardner, C. Jong, F. Lillaz, N. Mitchell, G. Romano, and A. Vostner. “Challenges and status of ITER conductor production”. In: *Superconductor Science and Technology* 27.4 (2014), p. 044001.
- [7] H. Bajas, D. Durville, D. Ciazynski, and A. Devred. “Numerical simulation of the mechanical behavior of ITER cable-in-conduit conductors”. In: *IEEE Transactions on Applied Superconductivity* 20.3 (2010), pp. 1467–1470.
- [8] F. P. Nasution, S. Sævik, and J. K. Gjøsteen. “Study of fatigue strength of copper conductor considering irregularities surfaces by experimental testings and fe-analysis”. In: *International Conference on Offshore Mechanics and Arctic Engineering*. Vol. 44908. American Society of Mechanical Engineers. 2012, pp. 269–275.
- [9] F. P. Nasution, S. Sævik, and J. K. Gjøsteen. “Fatigue analysis of copper conductor for offshore wind turbines by experimental and FE method”. In: *Energy Procedia* 24 (2012), pp. 271–280.
- [10] F. P. Nasution, S. Sævik, and S. Berge. “Experimental and finite element analysis of fatigue strength for 300 mm² copper power conductor”. In: *Marine Structures* 39 (2014), pp. 225–254.

- [11] F. P. Nasution, S. Sævik, and J. K. Gjøsteen. “Finite element analysis of the fatigue strength of copper power conductors exposed to tension and bending loads”. In: *International journal of fatigue* 59 (2014), pp. 114–128.
- [12] S. K. Ganguli and V. Kohli. *Power cable technology*. CRC Press, 2016.
- [13] C. TB. *Offshore generation cable connections*. 2015. URL: https://www.researchgate.net/publication/338388640_CIGRE_TB_610_-_Offshore_generation_cable_connections/citations (visited on 03/16/2024).
- [14] T. Andritsch, A. Vaughan, and G. C. Stevens. “Novel insulation materials for high voltage cable systems”. In: *IEEE Electrical Insulation Magazine* 33.4 (2017), pp. 27–33.
- [15] I. Pleșa, P. V. Noțingher, C. Stancu, F. Wiesbrock, and S. Schlögl. “Polyethylene nanocomposites for power cable insulations”. In: *Polymers* 11.1 (2018), p. 24.
- [16] Z. Li and B. Du. “Polymeric insulation for high-voltage dc extruded cables: challenges and development directions”. In: *IEEE Electrical Insulation Magazine* 34.6 (2018), pp. 30–43.
- [17] N. Amyot, E. David, S. Lee, and I. Lee. “Influence of post-manufacturing residual mechanical stress and crosslinking by-products on dielectric strength of HV extruded cables”. In: *IEEE Transactions on dielectrics and electrical insulation* 9.3 (2002), pp. 458–466.
- [18] W. Wang, X. Yan, S. Li, L. Zhang, J. Ouyang, and X. Ni. “Failure of submarine cables used in high-voltage power transmission: Characteristics, mechanisms, key issues and prospects”. In: *IET Generation, Transmission & Distribution* 15.9 (2021), pp. 1387–1402.
- [19] M. Danikas, D. Papadopoulos, and S. Morsalin. “Propagation of Electrical Trees under the Influence of Mechanical Stresses: A Short Review.” In: *Engineering, Technology & Applied Science Research* 9.1 (2019).
- [20] Y. Xu, Y. Bai, P. Fang, S. Yuan, and C. Liu. “Structural analysis of fibreglass reinforced bonded flexible pipe subjected to tension”. In: *Ships and Offshore Structures* 14.7 (2019), pp. 777–787.
- [21] P. Fang, S. Yuan, P. Cheng, Y. Bai, and Y. Xu. “Mechanical responses of metallic strip flexible pipes subjected to pure torsion”. In: *Applied Ocean Research* 86 (2019), pp. 13–27.
- [22] P. Fang, Y. Xu, Y. Gao, L. Ali, and Y. Bai. “Mechanical responses of a fiberglass flexible pipe subject to tension & internal pressure”. In: *Thin-Walled Structures* 181 (2022), p. 110107.
- [23] Z. Yang, Q. Su, J. Yan, S. Wu, Y. Mao, Q. Lu, and H. Wang. “Study on the nonlinear mechanical behaviour of an umbilical under combined loads of tension and torsion”. In: *Ocean engineering* 238 (2021), p. 109742.
- [24] Q. Lu, J. Chen, Z. Yang, Y. Y. Chao, and Q. Yue. “Numerical and experimental analysis of umbilical cables under tension”. In: *Advanced Composites Letters* 26.2 (2017), p. 096369351702600205.

- [25] W. Nam, K. Chae, and Y. Lim. “Experimental and Theoretical Study on the Prediction of Axial Stiffness of Subsea Power Cables”. In: *Journal of Ocean Engineering and Technology* 36.4 (2022), pp. 243–250.
- [26] J. Mullins, D. Morin, A. Tyrberg, C. Sonesson, and J. Ekh. “Bitumen shear mechanics in a dynamic subsea electrical cable”. In: *International Conference on Offshore Mechanics and Arctic Engineering*. Vol. 56512. American Society of Mechanical Engineers. 2015, V05AT04A026.
- [27] M. Komperød, B. Konradsen, and B. Aspli. “Small-Scale Testing and Mathematical Modeling of Cable Elements’ Shear Forces Due to Dry Friction and Bitumen”. In: *ISOPE International Ocean and Polar Engineering Conference*. ISOPE. 2019, ISOPE-I.
- [28] DNVGL. *Subsea power cables for wind power plants*. 2020. URL: <https://www.dnv.com/energy/standards-guidelines/dnv-st-0359-subsea-power-cables-for-wind-power-plants.html> (visited on 08/31/2023).
- [29] M. Jeroense. “Recommendations for Mechanical Testing of Submarine Cables (and Their Accessories)”. In: *Accessories for HV and EHV Extruded Cables: Volume 2: Land and Submarine AC/DC Applications*. Ed. by P. Argaut. Cham: Springer International Publishing, 2023, pp. 351–424. ISBN: 978-3-030-80406-0. DOI: [10.1007/978-3-030-80406-0_5](https://doi.org/10.1007/978-3-030-80406-0_5). URL: https://doi.org/10.1007/978-3-030-80406-0_5.
- [30] “IEEE Guide for the Planning, Design, Installation, and Repair of Submarine Power Cable Systems”. In: *IEEE Std 1120-2004* (2005), pp. 1–45. DOI: [10.1109/IEEESTD.2005.95937](https://doi.org/10.1109/IEEESTD.2005.95937).
- [31] T. Dong, H. Brakelmann, and G. Anders. “Analysis method for the design of long submarine cables”. In: *Renewable and Sustainable Energy Reviews* 171 (2023), p. 113029.
- [32] J. C. Del-Pino-López and P. L. Cruz-Romero. “A 3D parametric thermal analysis of submarine three-core power cables”. In: *18th International Conference on Renewable Energies and Power Quality-ICREPQ'20 (2020)*, pp. 363–368. European Association for the Development of Renewable Energy, Environment ... 2020.
- [33] M. Hamdan, J. Pilgrim, and P. Lewin. “Analysis of thermo-mechanical stress in three core submarine power cables”. In: *IEEE Transactions on Dielectrics and Electrical Insulation* 27.4 (2020), pp. 1288–1296.
- [34] H. Brakelmann and J. Stammen. “Thermal analysis of submarine cable routes: LSM or FEM?” In: *2006 IEEE International Power and Energy Conference*. IEEE. 2006, pp. 560–565.
- [35] G. D. Scott, M. A. Pooley, and B. R. Cotts. “Numerical & Analytical Modeling of Electromagnetic Fields from Offshore Power Distribution Cables”. In: *IEEE Transactions on Magnetics* (2023).

- [36] P. R. Thies, L. Johanning, and G. H. Smith. "Assessing mechanical loading regimes and fatigue life of marine power cables in marine energy applications". In: *Proceedings of the Institution of Mechanical Engineers, Part O: Journal of Risk and Reliability* 226.1 (2012), pp. 18–32.
- [37] F. P. Nasution, S. Sævik, J. K. Gjøsteen, and S. Berge. "Experimental and finite element analysis of fatigue performance of copper power conductors". In: *International journal of fatigue* 47 (2013), pp. 244–258.
- [38] J. Buitrago, S. F. Swearingen, S. Ahmad, and C. F. Popelar. "Fatigue, creep and electrical performance of subsea power cable". In: *International Conference on Offshore Mechanics and Arctic Engineering*. Vol. 55355. American Society of Mechanical Engineers. 2013, V003T03A028.
- [39] M. Marta, S. Mueller-Schuetze, H. Ottersberg, D. Isus, L. Johanning, and P. R. Thies. "Development of dynamic submarine MV power cable design solutions for floating offshore renewable energy applications". In: (2015).
- [40] S.-H. Yang, J. W. Ringsberg, and E. Johnson. "Parametric study of the dynamic motions and mechanical characteristics of power cables for wave energy converters". In: *Journal of marine science and technology* 23 (2018), pp. 10–29.
- [41] A. Robertson, J. Jonkman, M. Masciola, H. Song, A. Goupee, A. Coulling, and C. Luan. *Definition of the semisubmersible floating system for phase II of OCA*. Tech. rep. National Renewable Energy Lab.(NREL), Golden, CO (United States), 2014.
- [42] J. Jonkman, S. Butterfield, W. Musial, and G. Scott. *Definition of a 5-MW reference wind turbine for offshore system development*. Tech. rep. National Renewable Energy Lab.(NREL), Golden, CO (United States), 2009.
- [43] I. Kraincanic and E. Kebabze. "Slip initiation and progression in helical armouring layers of unbonded flexible pipes and its effect on pipe bending behaviour". In: *The Journal of Strain Analysis for Engineering Design* 36.3 (2001), pp. 265–275.
- [44] E. Rodabaugh and H. George. "Effect of internal pressure on flexibility and stress-intensification factors of curved pipe or welding elbows". In: *Transactions of the American Society of Mechanical Engineers* 79.4 (1957), pp. 939–948.
- [45] J. McNamara, P. O'Brien, and S. Gilroy. "Nonlinear analysis of flexible risers using hybrid finite elements". In: (1988).
- [46] P. Delizisis, I. Dolianitis, D. Chatzipetros, V. Kanas, G. Georgallis, K. Tastavridis, A. Stamelos, and E. Angelis. "Full Scale Axial, Bending and Torsion Stiffness Tests of a Three Core HVAC Submarine Cable". In: *International Conference on Offshore Mechanics and Arctic Engineering*. Vol. 85147. American Society of Mechanical Engineers. 2021, V004T04A009.
- [47] H.-C. Chang and B.-F. Chen. "Mechanical behavior of submarine cable under coupled tension, torsion and compressive loads". In: *Ocean engineering* 189 (2019), p. 106272.

- [48] D. D. Tjahjanto, A. Tyrberg, and J. Mullins. “Bending mechanics of cable cores and fillers in a dynamic submarine cable”. In: *International Conference on Offshore Mechanics and Arctic Engineering*. Vol. 57694. American Society of Mechanical Engineers. 2017, V05AT04A038.
- [49] G. Kirchhoff. “Über das Gleichgewicht und die Bewegung eines unendlich dünnen Stabes”. In: *Journ. f. Mathematik* (1858), p. 291.
- [50] A. E. H. Love. *A treatise on the mathematical theory of elasticity*. University press, 1927.
- [51] J. Ericksen and C. Truesdell. “Exact theory of stress and strain in rods and shells”. In: *Archive for Rational Mechanics and Analysis* 1 (1957), pp. 295–323.
- [52] O. M. O’Reilly. “Kirchhoff’s Rod Theory”. In: *Modeling Nonlinear Problems in the Mechanics of Strings and Rods: The Role of the Balance Laws*. Cham: Springer International Publishing, 2017, pp. 187–268. ISBN: 978-3-319-50598-5. DOI: [10.1007/978-3-319-50598-5_5](https://doi.org/10.1007/978-3-319-50598-5_5). URL: https://doi.org/10.1007/978-3-319-50598-5_5.
- [53] O. M. O’Reilly. *Kinematics of rods*. 2020. URL: <https://rotations.berkeley.edu/kinematics-of-rods/> (visited on 08/31/2023).
- [54] E. H. Dill. “Kirchhoff’s theory of rods”. In: *Archive for History of Exact Sciences* (1992), pp. 1–23.
- [55] T. Schlick. “Modeling superhelical DNA: recent analytical and dynamic approaches”. In: *Current opinion in structural biology* 5.2 (1995), pp. 245–262.
- [56] S. Goyal. *A dynamic rod model to simulate* mechanics of cables and DNA*. University of Michigan, 2006.
- [57] S. Goyal, N. C. Perkins, and C. L. Lee. “Nonlinear dynamics and loop formation in Kirchhoff rods with implications to the mechanics of DNA and cables”. In: *Journal of Computational Physics* 209.1 (2005), pp. 371–389.
- [58] Y. Yang, I. Tobias, and W. K. Olson. “Finite element analysis of DNA supercoiling”. In: *The Journal of chemical physics* 98.2 (1993), pp. 1673–1686.
- [59] Z. Wang, M. Fratarcangeli, A. Ruimi, and A. Srinivasa. “Real time simulation of inextensible surgical thread using a Kirchhoff rod model with force output for haptic feedback applications”. In: *International Journal of Solids and Structures* 113 (2017), pp. 192–208.
- [60] L. Dong, Z. Qu, Q. Zhang, Y. Huang, and G. Liu. “A general model to predict torsion and curvature increments of tensile armors in unbonded flexible pipes”. In: *Marine Structures* 67 (2019), p. 102632.
- [61] L. Dong, Q. Zhang, Y. Huang, and G. Liu. “Slip and stress of tensile armors in unbonded flexible pipes close to end fitting considering an exponentially decaying curvature distribution”. In: *Marine Structures* 51 (2017), pp. 110–133.
- [62] R. Knapp. “Derivation of a new stiffness matrix for helically armoured cables considering tension and torsion”. In: *International Journal for Numerical Methods in Engineering* 14.4 (1979), pp. 515–529.

- [63] P. Fang, X. Jiang, H. Hopman, and Y. Bai. “Mechanical responses of submarine power cables subject to axisymmetric loadings”. In: *Ocean Engineering* 239 (2021), p. 109847.
- [64] L. Wang and Q. Yue. “A full layered numerical model for predicting hysteretic behavior of unbonded flexible pipes considering initial contact pressure”. In: *Applied Ocean Research* 111 (2021), p. 102626.
- [65] H. Lu, M. A. Vaz, and M. Caire. “A finite element model for unbonded flexible pipe under combined axisymmetric and bending loads”. In: *Marine Structures* 74 (2020), p. 102826.
- [66] L. Wang, N. Ye, and Q. Yue. “A novel helix contact model for predicting hysteretic behavior of unbonded flexible pipes”. In: *Ocean Engineering* 264 (2022), p. 112407.
- [67] C. Bournazel. “Calculation of stresses and slip in structural layers of unbonded flexible pipes”. In: (1987).
- [68] J. Feret and G. Momplot. “CAFLEX-a program for capacity analysis of flexible pipes. Theory manual”. In: *SINTEF Structural Engineering, Report STF71F91019* (1991).
- [69] S. Berge, A. Engseth, I. Fylling, *et al.* “FPS2000/Flexible Risers and Pipes: Handbook on Design and Operation of Flexible Pipes”. In: *Report STF70 A 92006* (1992).
- [70] S. Sævik. “On stresses and fatigue in flexible pipes”. In: (1992).
- [71] E. Kebabze. “Theoretical modelling of unbonded flexible pipe cross-sections.” PhD thesis. South Bank University, 2000.
- [72] S. Sævik. “A finite element model for predicting stresses and slip in flexible pipe armouring tendons”. In: *Computers & structures* 46.2 (1993), pp. 219–230.
- [73] T. V. Lukassen. *Constitutive behavior of tensile armor wires in unbonded flexible pipes*. Technical University of Denmark, 2019.
- [74] P. Estrier. “Updated method for the determination of the service life of flexible risers”. In: (1992).
- [75] Z. Tan, M. Case, and T. Sheldrake. “Higher order effects on bending of helical armor wire inside an unbonded flexible pipe”. In: *International Conference on Offshore Mechanics and Arctic Engineering*. Vol. 41979. 2005, pp. 447–455.
- [76] C. Larsen, S. Sævik, J. Qvist, D. Fergestad, and S. Lotveit. “Handbook on design and operation of flexible pipes”. In: *Joint Industry Project* (2014).
- [77] S. Sævik. “Theoretical and experimental studies of stresses in flexible pipes”. In: *Computers & structures* 89.23-24 (2011), pp. 2273–2291.
- [78] S. Sævik and H. Li. “Shear interaction and transverse buckling of tensile armours in flexible pipes”. In: *International Conference on Offshore Mechanics and Arctic Engineering*. Vol. 55362. American Society of Mechanical Engineers. 2013, V04AT04A013.

- [79] C. A. P. M. Gomes. “Finite element analysis of flexible pipes: Bending combined with tensile load”. In: (2017).
- [80] R. Johansen and K. Ekeberg. “Subsea Umbilicals-Joint Industry Project Aiming To Revise ISO 13628-5”. In: *Offshore Technology Conference*. OTC. 2005, OTC-17184.
- [81] R. Knapp, S. Das, and T. Shimabukuro. “Computer-aided design of cables for optimal performance”. In: *Sea Technology* 43.7 (2002), pp. 41–46.
- [82] K. Chae, W. Nam, and C. Shim. “Influence of coiling behavior on axial stress in steel wires of submarine power cables: A numerical study”. In: *Ocean Engineering* 288 (2023), p. 116014.
- [83] D.-H. Yoo, B.-S. Jang, and R.-H. Yun. “A simplified multi-layered finite element model for flexible pipes”. In: *Marine Structures* 63 (2019), pp. 117–137.
- [84] G. Owolabi *et al.* “Critical review of subsea structures in the Gulf of Guinea: “Finite element analysis to predict the behaviour of a multi-layer non-bonded flexible pipe under hydrate plug in a static application””. In: (2021).
- [85] S. Timoshenko, S. Woinowsky-Krieger, *et al.* *Theory of plates and shells*. Vol. 2. McGraw-hill New York, 1959.
- [86] M.-C. Hsieh, B.-F. Chen, Y. Wang, H.-C. Chang, W.-H. Liu, and H.-L. Hsu. “Determining optimal number of cores in a submarine power cable”. In: *International Journal of Naval Architecture and Ocean Engineering* 14 (2022), p. 100463.
- [87] K.-J. Bathe. *Finite element procedures*. Klaus-Jurgen Bathe, 2006.
- [88] J. N. Reddy. *Introduction to the finite element method*. McGraw-Hill Education, 2019.
- [89] F. Ménard and P. Cartraud. “A computationally efficient finite element model for the analysis of the non-linear bending behaviour of a dynamic submarine power cable”. In: *Marine Structures* 91 (2023), p. 103465.
- [90] J.-M. Leroy, Y. Poirrette, N. Brusselle Dupend, and F. Caleyron. “Assessing mechanical stresses in dynamic power cables for floating offshore wind farms”. In: *International Conference on Offshore Mechanics and Arctic Engineering*. Vol. 57786. American Society of Mechanical Engineers. 2017, V010T09A050.
- [91] F. Bussolati. “Modèle multi-échelle de la fatigue des lignes d’ancrage câblées pour l’éolien offshore flottant”. PhD thesis. Université Paris-Saclay (ComUE), 2019.
- [92] F. Ménard and P. Cartraud. “Solid and 3D beam finite element models for the nonlinear elastic analysis of helical strands within a computational homogenization framework”. In: *Computers & Structures* 257 (2021), p. 106675.
- [93] G. Skeie, N. Sødahl, O. Steinkjer, *et al.* “Efficient fatigue analysis of helix elements in umbilicals and flexible risers: Theory and applications”. In: *Journal of Applied Mathematics* 2012 (2012).

- [94] DNV-GL. “SESAM white paper—Helica, cross section analysis of compliant structures—flexibles, umbilicals and cables”. In: *Hövik, Norway* (2016).
- [95] M. Zhang, X. Chen, S. Fu, Y. Guo, and L. Ma. “Theoretical and numerical analysis of bending behavior of unbonded flexible risers”. In: *Marine structures* 44 (2015), pp. 311–325.
- [96] W. Ma, L. Su, S. Wang, Y. Yang, and W. Huang. “Influence of structural parameters of unbonded flexible pipes on bending performance”. In: *Ocean Engineering* 266 (2022), p. 113109.
- [97] U. S. Fernando, Z. Tan, T. Sheldrake, and R. Clements. “The stress analysis and residual stress evaluation of pressure armour layers in flexible pipes using 3D finite element models”. In: *International Conference on Offshore Mechanics and Arctic Engineering*. Vol. 37459. 2004, pp. 57–65.
- [98] X. Zhang, S. Wang, W. Ma, L. Su, and Y. Yang. “Study on the influence of bending curvature on the bending characteristics of unbonded flexible pipes”. In: *Ocean Engineering* 281 (2023), p. 114730.
- [99] J. Witz. “A case study in the cross-section analysis of flexible risers”. In: *Marine Structures* 9.9 (1996), pp. 885–904.
- [100] A. S. U. Manual. “Abaqus 6.11”. In: <http://130.149.89.2080> (2012), p. v6.
- [101] A. Tyrberg, D. Tjahjanto, and J. Hedlund. “Bend stiffness of submarine cables—An experimental and numerical investigation”. In: *Proceedings of the 10th International Conference on Insulated Power Cables*. 2019.
- [102] Y. Bai, T. Liu, W. Ruan, and W. Chen. “Mechanical behavior of metallic strip flexible pipe subjected to tension”. In: *Composite Structures* 170 (2017), pp. 1–10.
- [103] A. Bahtui, H. Bahai, and G. Alfano. “Numerical and analytical modeling of unbonded flexible risers”. In: (2009).
- [104] T. Dai, S. Sævik, and N. Ye. “Friction models for evaluating dynamic stresses in non-bonded flexible risers”. In: *Marine Structures* 55 (2017), pp. 137–161.
- [105] G. Wróbel and M. Szymiczek. “Influence of temperature on friction coefficient of low density polyethylene”. In: *Journal of Achievements in Materials and Manufacturing Engineering* 28.1 (2008), pp. 31–34.
- [106] E. Feyzullahoglu and Z. Saffak. “The tribological behaviour of different engineering plastics under dry friction conditions”. In: *Materials & Design* 29.1 (2008), pp. 205–211.
- [107] W. Pan, H. Li, H. Qu, L. Ling, and L. Wang. “Investigation of tangential contact damping of rough surfaces from the perspective of viscous damping mechanism”. In: *Journal of Tribology* 143.4 (2021), p. 041501.
- [108] X. Shi and A. A. Polycarpou. “Measurement and modeling of normal contact stiffness and contact damping at the meso scale”. In: *J. Vib. Acoust.* 127.1 (2005), pp. 52–60.
- [109] C. W. De Silva. *Vibration and shock handbook*. CRC press, 2005.

- [110] T. V. Lukassen, E. Gunnarsson, S. Krenk, K. Glejbøl, A. Lyckegaard, and C. Berggreen. “Tension-bending analysis of flexible pipe by a repeated unit cell finite element model”. In: *Marine Structures* 64 (2019), pp. 401–420.
- [111] T. V. Lukassen, S. Krenk, K. Glejbøl, and C. Berggreen. “Non-symmetric cyclic bending of helical wires in flexible pipes”. In: *Applied Ocean Research* 92 (2019), p. 101876.
- [112] J.-M. Leroy, T. e. Perdrizet, V. Le Corre, and P. Estrier. “Stress assessment in armour layers of flexible risers”. In: *International Conference on Offshore Mechanics and Arctic Engineering*. Vol. 49132. 2010, pp. 951–960.
- [113] T. Perdrizet, J. Leroy, N. Barbin, V. Le-Corre, D. Charliac, and P. Estrier. “Stresses in armour layers of flexible pipes: comparison of Abaqus models”. In: *SIMULIA Customer Conference*. 2011, pp. 500–512.
- [114] O. Sertã, R. Fumis, A. Connaire, J. Smyth, R. Tanaka, T. Barbosa, and C. Godinho. “Predictions of armour wire buckling for a flexible pipe under compression, bending and external pressure loading”. In: *International Conference on Offshore Mechanics and Arctic Engineering*. Vol. 44908. American Society of Mechanical Engineers. 2012, pp. 361–365.
- [115] S. Sævik and R. T. Igland. “Calibration of a flexible pipe tensile armour stress model based on fibre optic monitoring”. In: *International Conference on Offshore Mechanics and Arctic Engineering*. Vol. 36134. 2002, pp. 53–58.
- [116] N. Buannic and P. Cartraud. “Higher-order effective modeling of periodic heterogeneous beams. I. Asymptotic expansion method”. In: *International Journal of Solids and Structures* 38.40-41 (2001), pp. 7139–7161.
- [117] N. Buannic and P. Cartraud. “Higher-order effective modeling of periodic heterogeneous beams. II. Derivation of the proper boundary conditions for the interior asymptotic solution”. In: *International Journal of Solids and Structures* 38.40-41 (2001), pp. 7163–7180.
- [118] D. M. Smith, L. S. Cunningham, and L. Chen. “Efficient finite element modelling of helical strand cables utilising periodicity”. In: *International Journal of Mechanical Sciences* (2023), p. 108792.
- [119] M. Rahmati, H. Bahai, and G. Alfano. “An accurate and computationally efficient small-scale nonlinear FEA of flexible risers”. In: *Ocean Engineering* 121 (2016), pp. 382–391.
- [120] M. G. Geers, V. G. Kouznetsova, and W. Brekelmans. “Multi-scale computational homogenization: Trends and challenges”. In: *Journal of computational and applied mathematics* 234.7 (2010), pp. 2175–2182.
- [121] API. *API 17B: recommended practice for flexible pipe*. American Petroleum Institute, 2014.
- [122] Y. Guo and N. Ye. “Numerical and experimental study on full-scale test of typical offshore dynamic power cable”. In: *ISOPE International Ocean and Polar Engineering Conference*. ISOPE. 2020, ISOPE-I.

- [123] M. V. dos Santos Paiva, L. Silveira, H. Wang, C. B. Hebert, T. B. Coser, F. S. López, T. R. Strohaecker, and F. Bertoni. “Validation of Power Cable Local Stress Analysis”. In: *ISOPE International Ocean and Polar Engineering Conference*. ISOPE. 2016, ISOPE-I.
- [124] J. Witz and Z. Tan. “On the axial-torsional structural behaviour of flexible pipes, umbilicals and marine cables”. In: *Marine Structures* 5.2-3 (1992), pp. 205–227.
- [125] P. Fang, Y. Xu, S. Yuan, Y. Bai, and P. Cheng. “Investigation on mechanical properties of fibreglass reinforced flexible pipes under torsion”. In: *International Conference on Offshore Mechanics and Arctic Engineering*. Vol. 51272. American Society of Mechanical Engineers. 2018, V07BT06A028.
- [126] J. Bu, S. Wang, W. Liu, and X. Ding. “Theoretical prediction for the torsional stiffness of reinforced thermoplastic pipes (RTPs) based on the strain energy-work equivalence of anisotropic cylinders”. In: *Ocean Engineering* 261 (2022), p. 112037.
- [127] M. Vaz, L. Aguiar, S. Estefen, and M. Brack. “Experimental determination of axial, torsional and bending stiffness of umbilical cables”. In: *Proceedings of the 17th International Offshore & Arctic Engineering Conference (OMAE'98)*. Vol. 7. 1998.
- [128] T. B. Coser, T. R. Strohaecker, F. S. López, F. Bertoni, H. Wang, C. B. Hebert, L. Silveira, M. V. dos Santos Paiva, and P. Maioli. “Submarine power cable bending stiffness testing methodology”. In: *ISOPE International Ocean and Polar Engineering Conference*. ISOPE. 2016, ISOPE-I.
- [129] P. Maioli. “Bending stiffness of submarine cables”. In: *Proceedings of the 9th International Conference on Insulated Power Cables (Jicable'15)*. 2015.
- [130] M. Komperød, J. I. Juvik, G. Evenset, R. Slora, and L. Jordal. “Large-Scale Tests for Identifying the Nonlinear, Temperature-Sensitive, and Frequency-Sensitive Bending Stiffness of the NordLink Cable”. In: *International Conference on Offshore Mechanics and Arctic Engineering*. Vol. 57694. American Society of Mechanical Engineers. 2017, V05AT04A004.
- [131] H. Hu, J. Yan, S. Sævik, N. Ye, Q. Lu, and Y. Bu. “Nonlinear bending behavior of a multilayer copper conductor in a dynamic power cable”. In: *Ocean Engineering* 250 (2022), p. 110831.
- [132] J. Yan, H.-t. Hu, H.-l. Lu, Y.-c. Yin, Y.-f. Bu, and Q.-z. Lu. “Experimental study on the influence of cross-section type of marine cable conductors on the bending performance”. In: *China Ocean Engineering* 36.4 (2022), pp. 629–637.
- [133] B. Skallerud. “Damping Models and Structural Damping in a Nonbonded Pipe”. In: *FPS2000 report* (1991), pp. 2–2.
- [134] I. Takahashi, S. Masanobu, S. Kanada, K. Maeda, H. Manabe, T. Yamaguchi, and Y. Tanaka. “Bending tests and cross-sectional analyses of multilayered flexible pipe models”. In: *Journal of Marine Science and Technology* 25 (2020), pp. 397–410.

- [135] T. V. Lukassen, K. Glejbøl, A. Lyckegaard, and C. Berggreen. “Comparison between stress obtained by numerical analysis and in-situ measurements on a flexible pipe subjected to in-plane bending test”. In: *International Conference on Offshore Mechanics and Arctic Engineering*. Vol. 49965. American Society of Mechanical Engineers. 2016, V005T04A021.
- [136] S. Sævik and K. I. Ekeberg. “Non-linear stress analysis of complex umbilical cross-sections”. In: *International Conference on Offshore Mechanics and Arctic Engineering*. Vol. 36118. 2002, pp. 211–217.
- [137] C. RILEY *et al.* “HV CABLE QUALIFICATIONS TO IEC 62067-2006 AND ICEA S-108-720-2004”. In: *Jicable Conf.* 2011.
- [138] H. Lu, M. A. Vaz, M. Caire, and I. D. Hernández. “Full-scale experimental and numerical analyses of a flexible riser under combined tension-bending loading”. In: *Marine Structures* 86 (2022), p. 103275.
- [139] L. Jordal, R. Slora, E. Vermeer, and M. Komperod. “A Novel Bending Stiffness Rig for Identification of Subsea Cables’ and Umbilicals’ Sensitivity to Temperature Under Sinusoidal Curvature Oscillations”. In: *ISOPE International Ocean and Polar Engineering Conference*. ISOPE. 2017, ISOPE-I.
- [140] C. T. Poon, C. Mullins, L. Radziunas, E. O’Connell, A. Connolly, and S. Leen. “Finite Element Design Study of Dynamics in Submarine Power Cables for Offshore Renewable Wind Energy”. In: *International Conference on Offshore Mechanics and Arctic Engineering*. Vol. 86618. American Society of Mechanical Engineers. 2022, V001T01A023.
- [141] CATAPULT. *FLOATING OFFSHORE WIND CENTRE OF EXCELLENCE - DYNAMIC CABLE TECHNOLOGY QUALIFICATION FRAMEWORK AND CASE STUDIES*. 2022. URL: <https://ore.catapult.org.uk/wp-content/uploads/2022/10/Dynamic-Cable-Technology-Qualification-Oct-2022.pdf> (visited on 08/31/2023).
- [142] H.-T. Thai and S.-E. Kim. “Nonlinear static and dynamic analysis of cable structures”. In: *Finite elements in analysis and design* 47.3 (2011), pp. 237–246.
- [143] R. Nicholls-Lee, P. R. Thies, and L. Johannig. “Coupled modelling for dynamic submarine power cables: interface sensitivity analysis of global response and local structural engineering models”. In: (2021).

3

METHODOLOGY

In Chapter 2, the methods used for the local mechanical analysis of submarine power cables (SPCs) are reviewed, and the numerical method is recommended for the local mechanical analysis. The three challenges identified in Chapter 2 are:

- a). the establishment of finite elements,*
- b). the setup of contact,*
- c). the formulation of boundary conditions.*

These will be addressed in this chapter sequentially. An effective modelling method for the local mechanical analysis of SPCs at both the overall and component levels will be proposed.

This chapter is organized to address each challenge as follows: the setup of finite elements is discussed in Section 3.1, solutions to contact issues are presented in Section 3.2, and the establishment of boundary conditions is outlined in Section 3.3. Section 3.4 concludes the chapter.

Parts of this chapter are based on the following papers:

- [1] P. Fang, X. Li, X. Jiang, H. Hopman, and Y. Bai. "Bending study of submarine power cables based on a repeated unit cell model". In: *Engineering Structures* 293 (2023), p. 116606
- [2] P. Fang, X. Li, X. Jiang, H. Hopman, and Y. Bai. "Development of an effective modeling method for the mechanical analysis of three-core submarine power cables under tension". In: *Engineering Structures* 317 (2024), p. 118632. ISSN: 0141-0296

3.1. THE ESTABLISHMENT OF FINITE ELEMENTS

THE cross-section of an SPC is very complicated as it contains substantial members that need to be discrete by a huge amount of elements in FEM. Therefore, to speed up the calculation for the analysis, inspired by the work on helical ropes by Bussolati [1], a technique utilizing the combination of beam and shell elements will be used to simulate numerous helical wires and helical metals within SPCs. In this way, the number of elements in the model can be significantly reduced. The concept of the combination of helical components is already illustrated in Figure 2.12. As the contact issue is prominent in the analysis, shell elements are adopted to enable beam elements to capture contacts by coupling the nodes on the shell to their corresponding master nodes on a beam. Timoshenko beam elements and shell elements can be used for the beam and shell, respectively. Timoshenko beam theory offers a more accurate prediction of deformation and stress in beams than the simpler Euler-Bernoulli beam theory, making it a versatile and accurate tool for analyzing beams where shear deformation and rotary inertia are significant. The shell should have neither thickness nor stiffness but be able to capture the contact among interfaces.

The reference node on the beam has displacement \mathbf{U} and rotation ϕ degrees of freedom (DOF), while the nodes on the shell have three DOFs \mathbf{U} . The relations between the RP and the corresponding nodes on the same cross-section can be described below:

$$\begin{cases} \sum_n \mathbf{F}^i = \mathbf{F}^{RP} \\ \sum_n \mathbf{X}^i \times \mathbf{F}^i = \mathbf{M}^{RP} + \mathbf{X}^{RP} \times \mathbf{F}^{RP} \end{cases} \quad (3.1)$$

where \mathbf{F} and \mathbf{M} are the load and moment, while \mathbf{X} is the position of the corresponding point. i is the node sequence on the coupled cross-section, and n is the number of nodes. The coupling approach has been proved to provide a very good compromise between accuracy and computational efficiency [1, 2]. This will also be verified in Chapter 4 before it is applied for further analysis.

3.2. THE SETUP OF CONTACT

As mentioned in Chapter 2, the necessary factors related to contact behaviours are normal contact property, tangential contact property and the initial residual stress, in which the friction coefficient in the tangential direction and the equivalent external pressure in simulating the residual stress are most important and should be given. Both values are the intrinsic properties of a sample, and in the industry of flexible pipes, they are supposed to be given alongside the pipe construction data [3]. CIGRE [4] has pointed out a way to obtain the equivalent external pressure, i.e., calibrating it by the curvature-bending moment curve. In fact, Menard and Cartraud [5] calibrated both the friction coefficient and the equivalent external pressure by the curvature-bending moment curves from his bending test, considering the fact that the friction coefficients are also hard to test directly in practice.

To minimize the parameters that need to be calibrated through testing, a new method for addressing the contact issue is proposed, namely the introduction of contact damping into the cable system. Contact damping can reduce the relative motion among interfaces and slow down slippage. In the finite element method (FEM), damping can be added to a structure by incorporating damper elements such as dashpots, connectors, or springs [6]. However, these methods require additional elements within the structure, which increases the computational resources needed. Therefore, in the proposed model, a constant contact damping coefficient is applied to the interfaces of SPCs. The damping forces can be calculated with:

$$f_{vd} = \mu A v_{rel} \quad (3.2)$$

where A represents the nodal area, and v_{rel} is the rate of relative motion between the two surfaces. The damping coefficient μ should be provided as a constant with units of pressure divided by velocity. For example, in the International System of Units, it would be expressed as $\frac{N}{m^2} / \frac{m}{s}$. The proposed model is intended to handle a quasi-static system subjected to loads or changes that occur slowly enough for the rate of relative motion to remain stable throughout the process. Consequently, the damping force in the tangential direction is also nearly stable. This stability can be verified by monitoring the damping energy during the simulation process.

This method offers several advantages. First, it simplifies the process by equating the friction coefficient and initial residual stress through a single parameter: the damping coefficient. Second, unlike the method of applying equivalent external pressure, adding contact damping does not require an additional analysis step, thereby accelerating the overall calculation process and conserving computational resources. Third, the damping coefficient is easily adjustable within the SPC for specific contact interfaces, which is particularly convenient during the design process where sensitivity studies are often conducted. Finally, the introduction of damping also enhances the model's convergence.

3.3. THE FORMULATION OF BOUNDARY CONDITIONS

As introduced in Chapter 2, periodical B.C. for beam-like structures obtained from the homogenization method can be applied to SPCs. The homogenization method on the slender beam-like structures has rigorous mathematical derivation where multi-scale analysis, regarding a macroscale problem and a microscale problem, is utilized. The macroscale is, in fact, an anisotropic Navier–Euler–Bernoulli–Saint-Venant beam, while the microscale problem is based on a unit cell. Therefore, the macroscale problem and the microscale problem will be elaborated first in two subsections, followed by the derived periodical boundary conditions and the constructions of the boundary conditions for SPCs in the next two subsections.

3.3.1. MACROSCALE PROBLEM

For a slender beam-like structure, two small parameters are involved: 1) the ratio of the microscopic length to the macroscopic length, and 2) the inverse of the structure

slenderness (ratio of cable diameter to cable length). The parameters of microscopic length, macroscopic length and cable diameter are shown in Figure 3.1. The results are found the best when these two parameters are considered equal [7, 8], and they are denoted as ζ :

$$\zeta \simeq \frac{l}{L} \simeq \frac{d}{L} \quad (3.3)$$

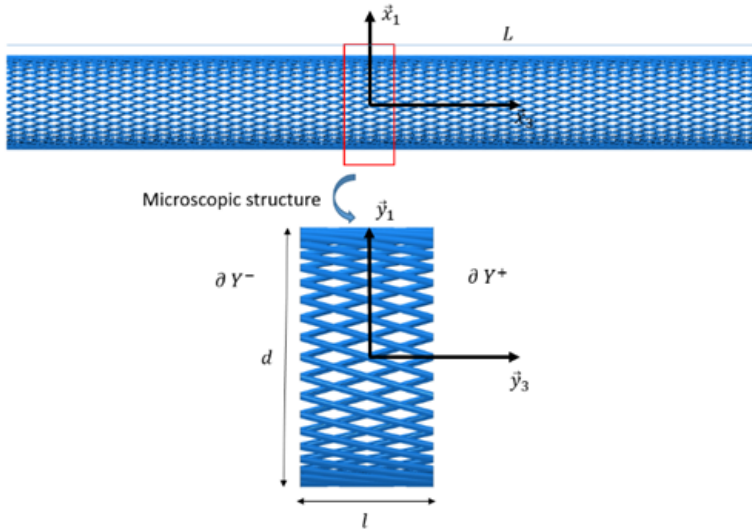


Figure 3.1: Presentation of a beam-like structure from macroscopic to microscopic

It is found that the most accurate effective properties are obtained when they simultaneously tend to zero [7]. As the two parameters are assumed to be equal, the asymptotic expansion method with one small parameter can be used to connect the two scales by $\mathbf{y} = \mathbf{x}/\zeta$. Where \mathbf{y} is the vector of the three variables in the micro scale and \mathbf{x} consists of three variables in the macro scale. By using standard asymptotic expansions, the solution to the three-dimensional elastic problem is given by Kolpakov [9]:

$$\mathbf{u}(\mathbf{x}) = u_{\alpha}^0(x_3)\mathbf{e}_{\alpha} + \zeta \mathbf{u}^1(x_3, \mathbf{y}) + \zeta^2 \mathbf{u}^2(x_3, \mathbf{y}) + \dots \quad (3.4)$$

where functions $\mathbf{u}^i(x_3, \mathbf{y})$ are periodic in variable y_3 with a period of Y_3 , which is the multiple of the length of the basic cell l shown in Figure 3.1. For the given example, a layer composed of numerous helices, the repetitive periodical length can be obtained by:

$$Y_3 = k \frac{p}{m} \quad (3.5)$$

where $k \in \mathbb{N}$, p is the pitch length, and m is the number of helices. The three-dimensional elasticity problem can be considered a macroscopic problem (in

powers of ε) that provides the overall beam response based on a microscopic problem posed on the basic cell. The unique solution to the macroscopic problem of the leading order is given by:

$$\mathbf{u}^1 = -y_\alpha \partial_3 u_\alpha^0(x_3) \mathbf{e}_3 + \hat{u}_i^1(x_3) \mathbf{e}_i + \varphi^1(x_3) (y_1 \mathbf{e}_2 - y_2 \mathbf{e}_1) \quad (3.6)$$

where φ and $\hat{u}_i^1(x_3)$ are the axis rotation around \mathbf{e}_3 and the translation, while ∂_3 denotes $\partial/\partial x_3$. The leading order solution constitutes an anisotropic Navier–Euler–Bernoulli–Saint-Venant beam where its axial displacement, transverse displacements and rotation are involved. The corresponding microscopic problem is then presented to solve the 3D elastic problem.

3.3.2. MICROSCALE PROBLEM

For the anisotropic beam, the macroscopic strain regarding the extension, curvatures and torsion can be described as:

$$\begin{cases} E^E(x_3) = \partial_3 \hat{u}_3^1(x_3) \\ E^{C_\alpha}(x_3) = \partial_{33} u_\alpha^0(x_3) \\ E^T(x_3) = \partial_3 \varphi^1(x_3) \end{cases} \quad (3.7)$$

where ∂_{33} denotes $\partial^2/\partial x_3^2$. For the microscopic problem, given by Cartraud and Messenger [10], the basic cell problems consist in finding the displacement \mathbf{u}^{per} , strain $\boldsymbol{\varepsilon}$ and stress $\boldsymbol{\sigma}$ such that:

$$\begin{cases} \mathbf{div}_y \boldsymbol{\sigma} = \mathbf{0} \\ \boldsymbol{\sigma} = \mathbf{a}(\mathbf{y}) : \mathbf{e} \\ e_{\alpha\beta} = e_{y_{\alpha\beta}}(\mathbf{u}^{per}), [\alpha, \beta] = [1, 2] \\ e_{13} = e_{y_{13}}(\mathbf{u}^{per}) - y_2 E^T / 2 \\ e_{23} = e_{y_{23}}(\mathbf{u}^{per}) + y_1 E^T / 2 \\ e_{33} = e_{y_{33}}(\mathbf{u}^{per}) + E^E - y_\alpha E^{C_\alpha} \\ \boldsymbol{\sigma} \cdot \mathbf{n} = \mathbf{0} \text{ on } \partial Y \\ \mathbf{u}^{per} \text{ per and } \boldsymbol{\sigma} \cdot \mathbf{n} \text{ anti-per} \end{cases} \quad (3.8)$$

where \mathbf{a} is the elastic moduli tensor, \mathbf{div}_y the divergence operator, \mathbf{e} the strain operator. 'per' means periodic in variable y_3 , while 'anti-per' means that $\boldsymbol{\sigma} \cdot \mathbf{n}$ are opposite on opposite sides ∂Y^+ and ∂Y^- in the beam axial direction. Due to the linearity of Equation 3.8, the solution of the displacement field \mathbf{u}^{per} and stress $\boldsymbol{\sigma}$ can be obtained and expressed as:

$$\begin{cases} \mathbf{u}^{per} = \boldsymbol{\chi}^E(\mathbf{y}) E^E(x_3) + \boldsymbol{\chi}^{C_\alpha}(\mathbf{y}) E^{C_\alpha}(x_3) + \boldsymbol{\chi}^T(\mathbf{y}) E^T(x_3) \\ \boldsymbol{\sigma} = \boldsymbol{\sigma}^E(\mathbf{y}) E^E(x_3) + \boldsymbol{\sigma}^{C_\alpha}(\mathbf{y}) E^{C_\alpha}(x_3) + \boldsymbol{\sigma}^T(\mathbf{y}) E^T(x_3) \end{cases} \quad (3.9)$$

Then the macroscopic axial force $N(x_3)$, the bending moments $M_\alpha(x_3)$ and the torsion moment $M_3(x_3)$ can be obtained by integrating the beam cross-section and averaging on the period length:

$$\left\{ \begin{array}{l} N(x_3) = \langle \sigma_{33} \rangle \\ M_\alpha(x_3) = \langle -y_\alpha \sigma_{33} \rangle \\ M_3(x_3) = \langle -y_2 \sigma_{13} + y_1 \sigma_{23} \rangle \\ \langle \bullet \rangle = \frac{1}{Y_3} \int_Y \bullet d y_1 d y_2 d y_3 \end{array} \right. \quad (3.10)$$

where Y_3 stands for the scaled length of period Y . From the above equations, the equilibrium equation for the homogenised structure can be obtained:

$$\left\{ \begin{array}{l} N \\ M_1 \\ M_2 \\ M_3 \end{array} \right\} = \mathbf{a}^{\text{hom}} \left\{ \begin{array}{l} E^E \\ E^{C_1} \\ E^{C_2} \\ E^T \end{array} \right\} \quad (3.11)$$

where \mathbf{a}^{hom} defines the homogenised stiffness matrix. For a particular structure, the matrix \mathbf{a}^{hom} of the unit cell is different from that of general problems, and thus, it needs to be derived for its own purpose. When different elements are required in the microscopic problem, the derivation of the matrix involves a cumbersome workload. Fortunately, there are sufficient ready element types in mature FEM packages, which can be utilized to solve the multi-scale problem by appropriately mapping the boundary conditions from the macroscopic scale to the microscopic scale. The following subsection will elaborately describe the implementation of the homogenization method regarding beam-like structures in FEM packages.

3.3.3. PERIODICAL BOUNDARY CONDITIONS

In a standard FEM solution, the stiffness matrix \mathbf{K} and force vector \mathbf{f} are described based on the strain-displacement matrix \mathbf{B} , material's constitutive matrix \mathbf{E} and unit strain field $\boldsymbol{\varepsilon}$ as:

$$\left\{ \begin{array}{l} \mathbf{K} = \int \mathbf{B}^T \mathbf{E} \mathbf{B} dV \\ \mathbf{f} = \int \mathbf{B}^T \mathbf{E} \boldsymbol{\varepsilon} dV \end{array} \right. \quad (3.12)$$

If the nodal displacement vector $\boldsymbol{\chi}$ corresponding to the unit strain field $\boldsymbol{\varepsilon}$ can be found such that $\boldsymbol{\varepsilon} = \mathbf{B}\boldsymbol{\chi}$, then the force vector \mathbf{f} can be rewritten as:

$$\mathbf{f} = \int \mathbf{B}^T \mathbf{E} \boldsymbol{\varepsilon} dV = \int \mathbf{B}^T \mathbf{E} \mathbf{B} \boldsymbol{\chi} dV = \int \mathbf{B}^T \mathbf{E} \mathbf{B} dV \cdot \boldsymbol{\chi} = \mathbf{K} \boldsymbol{\chi} \quad (3.13)$$

which means the nodal force vector can be calculated by multiplying stiffness matrix \mathbf{K} with the displacement field $\boldsymbol{\chi}$. In a FEM package, the force vector \mathbf{f} can be easily

obtained by applying appropriate nodal displacement χ in the right places. In this way, there is no need to derive the particular homogenised stiffness matrix \mathbf{a}^{hom} for a given problem, which makes the homogenization method more pragmatic. It greatly reduces the application threshold for implementation.

Back to the heterogeneous beam-like structure, according to the approach presented by Cartraud and Messager [10], the discretized field \mathbf{u} in the microscopic problem is determined from Eq. 3.8, yielding:

$$\begin{cases} u_1 = u_1^{\text{per}} + \frac{1}{2}y_3^2 E^{C_1} - y_2 y_3 E^T \\ u_2 = u_2^{\text{per}} + \frac{1}{2}y_3^2 E^{C_2} + y_1 y_3 E^T \\ u_3 = u_3^{\text{per}} + y_3 E^T - y_\alpha y_3 E^{C_\alpha} \end{cases} \quad (3.14)$$

The periodical boundary conditions on \mathbf{u}^{per} are dealt by connecting DOFs of opposite nodes on ∂Y^+ and ∂Y^- , as shown in Figure 3.1. The six DOFs between the opposite nodes have the following relation:

$$\begin{aligned} U_1^+ - U_1^- &= l(\bar{y}_3 E^{F_1} - y_2 E^T) \\ U_2^+ - U_2^- &= l(\bar{y}_3 E^{F_2} + y_1 E^T) \\ U_3^+ - U_3^- &= l(E^E - y_\alpha E^{F_\alpha}) \\ \theta_1^+ - \theta_1^- &= lE^{F_1} \\ \theta_2^+ - \theta_2^- &= lE^{F_2} \\ \theta_3^+ - \theta_3^- &= lE^T \end{aligned} \quad (3.15)$$

where U_i and θ_i are the translational and rotational DOFs, respectively.

The periodical boundary conditions can be inputted into finite element packages by constituting the correct relations of the corresponding nodes. An efficient approach to connect the microscopic problem to the macroscopic problem in Equation 3.15 can be realized by building a reference point (RP) C along the neutral axis of the structure, as shown in Figure 3.2. The opposite nodes on ∂Y^+ and ∂Y^- are on the same generatrix, as illustrated by nodes B and A. The node C_d is the dummy projected node that lies in the same cross-section as RP C . Equation 3.15 can be equivalent by using the following equations:

$$\begin{aligned} \mathbf{U}^B - \mathbf{U}^A - \mathbf{U}^{C_d} &= \mathbf{0} \\ \mathbf{U}^{C_d} &= \mathbf{U}^C + \mathbf{R}(\boldsymbol{\phi}^C) \overrightarrow{CC_d} - \overrightarrow{CC_d} \\ \boldsymbol{\phi}^{C_d} &= \boldsymbol{\phi}^C \end{aligned} \quad (3.16)$$

where \mathbf{U} is the displacement vector of the nodes, $\overrightarrow{CC_d}$ is the vector between node C and node C_d , $\boldsymbol{\phi}^C$ is the rotation vector of node C and $\mathbf{R}(\boldsymbol{\phi}^C)$ is the corresponding rotation matrix, which will be detailed in the following content.

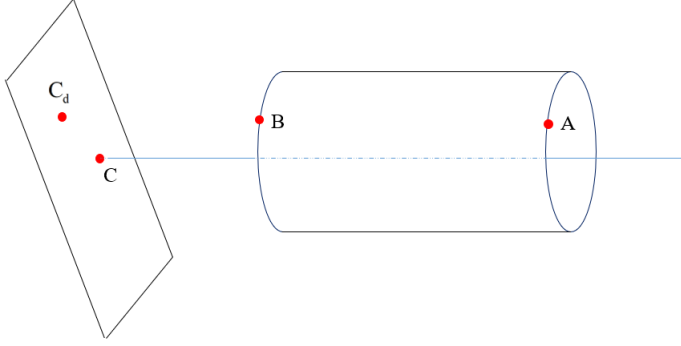


Figure 3.2: Correspondence between a pair of nodes B and A on the two end-cross sections and the dummy projected node C_d , which is constrained to the reference node C [11]

Eq. 3.16(1-2) are further reorganized and rewritten as:

$$\mathbf{U}^B - \mathbf{U}^A = \mathbf{U}^C + \mathbf{R}(\boldsymbol{\phi}^C)\overrightarrow{CB} - \overrightarrow{CB} \quad (3.17)$$

This can be further described by the vector form:

$$\overrightarrow{C'B'} = \mathbf{R}(\boldsymbol{\phi}^C)\overrightarrow{CB} + \overrightarrow{AA'}, \quad \boldsymbol{\phi}^C = [\phi_1^C \ \phi_2^C \ \phi_3^C] \quad (3.18)$$

where ϕ_1^C , ϕ_2^C and ϕ_3^C are the rotation angles of the master RP around the X, Y and Z axis, respectively. The original letters without a superscript denote the initial node, while the letters with the superscript represent the node after deformation. $\mathbf{R}(\boldsymbol{\phi}^C)$ is the rotation matrix at point C. The periodical boundary conditions were applied on flexible pipes before by Caleyron et al. [12] and Leroy et al. [13]. Given in their research, the kinematic relation among these three nodes A, B and C after deformation based on a rigid body rotation can be expressed by:

$$\overrightarrow{C'B'} = \mathbf{R}(\boldsymbol{\phi}^C)(\overrightarrow{CB} + \overrightarrow{AA'}), \quad \boldsymbol{\phi}^C = [\phi_1^C \ \phi_2^C \ \phi_3^C] \quad (3.19)$$

By comparing Eq. 3.19 and Eq. 3.18, the only difference is that whether or not $\overrightarrow{AA'}$ is multiplied by $\mathbf{R}(\boldsymbol{\phi}^C)$. In the case of small deformation, such difference can be ignored, and it can be regarded that these two equations can both constitute the periodical boundary conditions.

To have a better understanding of the physical meaning of the equations, an illustration is shown in Figure 3.3. The primary goal of this method is to establish a kinematic relationship between the nodes along the same generatrix, as illustrated by Node A and Node B. Since these two nodes lie on the same generatrix, the line they form is parallel to the neutral axis of the cable. They are paired together and then linked to Node C, located at the midpoint of the left cross section. Node B and Node C form a line that is perpendicular to the neutral axis. This constraint ensures

that the degrees of freedom (DOFs) of Node B are constrained, making Nodes A and the master Node C the controlling nodes. In this way the DOFs of nodes B are eliminated by the periodic constraint while nodes A and the master RP C remain as the controlling nodes. The following gives the construction of the kinematic equations among the three nodes in FEM packages.

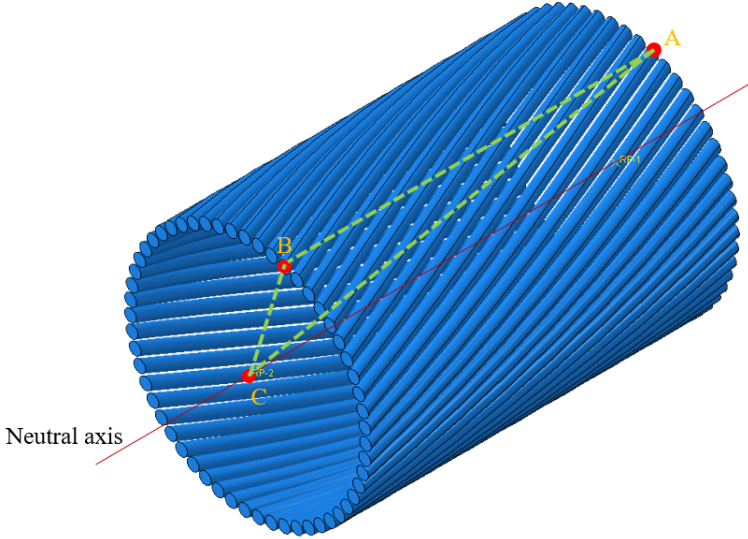


Figure 3.3: Nodes involved in periodicity conditions on the helical wire layer

The method to implement periodical boundary conditions provided by Rahmati et al. [14] needs to construct numerous dummy nodes projected by the nodes on ∂Y^+ and ∂Y^- in Figure 3.1. However, a more efficient way to accomplish this job is by directly constituting multi-point constraints (MPC) among Node A, B and C in Figure 3.3. In a FEM program, the matrices representing derivatives of the constraint function regarding the nodal DOFs need to be provided.

Now denoting the original coordinates of A, B and C as \mathbf{X}^A , \mathbf{X}^B and \mathbf{X}^C , respectively, then the coordinate of A', B' and C' can be described as $\mathbf{X}^A + \mathbf{U}^A$, $\mathbf{X}^B + \mathbf{U}^B$ and $\mathbf{X}^C + \mathbf{U}^C$, respectively. Here \mathbf{U} is the translational displacement vector of each node. Therefore, Eq. 3.18 can be rewritten as:

$$\mathbf{X}^B + \mathbf{U}^B - \mathbf{X}^C - \mathbf{U}^C = \mathbf{R}(\phi^C)(\mathbf{X}^B - \mathbf{X}^C) + \mathbf{X}^A + \mathbf{U}^A - \mathbf{X}^A \quad (3.20)$$

If the rotation DOFs are considered, then:

$$\phi^B - \phi^A - \phi^C = 0 \quad (3.21)$$

Equation 3.20 and Equation 3.21 can be reorganized as:

$$\mathbf{f}_1(\mathbf{U}^B, \mathbf{U}^A, \mathbf{U}^C) = \mathbf{X}^B + \mathbf{U}^B - \mathbf{X}^C - \mathbf{U}^C - \mathbf{R}(\phi^C)(\mathbf{X}^B - \mathbf{X}^C) - \mathbf{U}^A = 0 \quad (3.22)$$

$$f_2(\boldsymbol{\phi}^B, \boldsymbol{\phi}^A, \boldsymbol{\phi}^C) = \boldsymbol{\phi}^B - \boldsymbol{\phi}^A - \boldsymbol{\phi}^C = 0 \quad (3.23)$$

The derivation of the coefficient written in the MPC can be achieved by partial derivatives over the displacements of each node. It is clear that with respect to nodes A, B and C:

$$A^A = \left[\begin{array}{c|c} -\mathbf{R}(\boldsymbol{\phi}^C) & \mathbf{0} \\ \hline \mathbf{0} & -\mathbf{I} \end{array} \right] \quad (3.24)$$

$$A^B = \mathbf{I} \quad (3.25)$$

$$A^C = \left[\begin{array}{c|c} -\mathbf{I} & \mathbf{Q} \\ \hline \mathbf{0} & -\mathbf{I} \end{array} \right] \quad (3.26)$$

where $\mathbf{Q} = -\partial \mathbf{R}(\boldsymbol{\phi}^C)(\mathbf{X}^B - \mathbf{X}^C + \mathbf{U}^A) / \partial \boldsymbol{\phi}^C$. The three matrices are a 6×6 matrix when the rotational DOFs are incorporated into the model, for example, when beam or shell elements are utilized. Otherwise, when only translational DOFs are considered, the last three rows in the three matrix can be deleted. $\mathbf{R}(\boldsymbol{\phi}^C)$ has to be given in order to obtain A^A and A^C .

Rotations in 3D space can be specified using various representations, including Euler angles, axis-angle representation, or quaternions. Rotation matrices offer a concise and computationally efficient way to represent and perform rotations, particularly when multiple rotations need to be combined or interpolated. Normally, there are two ways to obtain the rotation matrix.

The components of the rotation vector $\boldsymbol{\phi} = [\phi_1 \ \phi_2 \ \phi_3]$ are stored as the degrees of freedom 4, 5, and 6 at any node where a rotation is required, consisting of a rotation magnitude $\phi = \sqrt{(\phi_1)^2 + (\phi_2)^2 + (\phi_3)^2}$ and a rotation axis or direction in space, $\mathbf{n} = \boldsymbol{\phi} / \phi$. Physically, the rotation vector $\boldsymbol{\phi}$ is interpreted as a rotation by ϕ radians around the axis \mathbf{n} . To conveniently describe this finite rotation mathematically, the rotation vector $\boldsymbol{\phi}$ needs to be converted into an orthogonal transformation or rotation matrix. For this purpose, the skew-symmetric matrix $\hat{\boldsymbol{\phi}}$ associated with $\boldsymbol{\phi}$ for all vectors \mathbf{v} is defined as:

$$\left\{ \begin{array}{l} \hat{\boldsymbol{\phi}} \cdot \boldsymbol{\phi} = \mathbf{0} \\ \hat{\boldsymbol{\phi}} \cdot \mathbf{v} = \boldsymbol{\phi} \times \mathbf{v} \end{array} \right. \quad (3.27)$$

where $\hat{\boldsymbol{\phi}}$ is a skew-symmetric two-dimensional tensor with the component matrix:

$$(\hat{\boldsymbol{\phi}})_{ij} = -\epsilon_{ijk} \phi_k = \begin{bmatrix} 0 & -\phi_3 & \phi_2 \\ \phi_3 & 0 & -\phi_1 \\ -\phi_2 & \phi_1 & 0 \end{bmatrix} \quad (3.28)$$

The permutation symbol ϵ_{ijk} is defined by:

$$\epsilon_{ijk} = \begin{cases} +1 & \text{if } (i, j, k) \in \{(1, 2, 3), (2, 3, 1), (3, 1, 2)\} \\ -1 & \text{if } (i, j, k) \in \{(1, 3, 2), (3, 2, 1), (2, 1, 3)\} \\ 0 & \text{for other cases} \end{cases} \quad (3.29)$$

One simple way to define the rotation matrix can be found in many sources:

$$\mathbf{R} = \cos \varphi \mathbf{I} + \sin \varphi \hat{\mathbf{n}} + (1 - \cos \varphi) \mathbf{nn}^T \quad (3.30)$$

The component form can be written using Kronecker's delta δ_{ij} for the unit matrix and the permutation symbol ϵ_{ijk} ,

$$R_{ij} = \cos \varphi \delta_{ij} - \sin \varphi \epsilon_{ijk} n_k + (1 - \cos \varphi) n_i n_j \quad (3.31)$$

$$\delta_{ijk} = \begin{cases} 1 & \text{if } i = j \\ 0 & \text{if } i \neq j \end{cases} \quad (3.32)$$

The other efficient and convenient way to treat finite rotations computationally, especially when there are compound rotations, is by utilizing quaternion parameters [15]. Quaternions are a mathematical concept widely used in 3D computer graphics, robotics, and physics to represent rotations and orientations. They are more numerically stable, having the advantages of avoiding gimbal lock issues and providing a concise and efficient representation of 3D rotations.

Quaternion can be expressed by the combination of a scalar $q_0 \in R$ and a vector field $\mathbf{q} \in R^3$:

$$\mathbf{q} = (q_0, \mathbf{q}) = q_0 + \mathbf{q} \quad (3.33)$$

where q_0 and \mathbf{q} are respectively defined as:

$$\begin{cases} q_0 = \cos(\phi/2) \\ \mathbf{q} = \sin(\phi/2) \mathbf{n} \end{cases} \quad (3.34)$$

In terms of the four quaternion parameters q_0 and \mathbf{q} the rotation matrix 3.30 takes the homogeneous quadratic form:

$$\mathbf{R} = (q_0^2 - \mathbf{q}^T \mathbf{q}) \mathbf{I} + 2q_0 \hat{\mathbf{q}} + 2\mathbf{q} \mathbf{q}^T \quad (3.35)$$

$\hat{\mathbf{q}}$ is the skew-symmetric matrix with axial vector \mathbf{q} . The corresponding component representation is:

$$R_{ij} = (q_0^2 - q_k q_k) \delta_{ij} - 2\epsilon_{ijk} q_0 q_k + 2q_i q_j \quad (3.36)$$

In full matrix form, the rotation representation is:

$$\mathbf{R} = \begin{bmatrix} r_0^2 + r_1^2 - r_2^2 - r_3^2 & 2(r_1 r_2 - r_0 r_3) & 2(r_1 r_3 + r_0 r_2) \\ 2(r_1 r_2 + r_0 r_3) & r_0^2 - r_1^2 + r_2^2 - r_3^2 & 2(r_2 r_3 - r_0 r_1) \\ 2(r_1 r_3 - r_0 r_2) & 2(r_2 r_3 + r_0 r_1) & r_0^2 - r_1^2 - r_2^2 + r_3^2 \end{bmatrix} \quad (3.37)$$

The coefficients in Eq. (3.24) and Eq. (3.26) can thus be obtained.

3.3.4. BOUNDARY CONDITIONS FOR SPCs

After the description of the principles of the periodic boundary conditions from the perspective of the homogenization method, the following gives all the boundary conditions for the proposed numerical model in detail.

As this model is proposed to deal with single-core SPCs, three-core SPCs, and other multi-core SPCs, the rules of selecting the model length regarding these different types of SPCs should be unified. In fact, the rule is already given in Eq. 2.18 in Chapter 2. For convenience, it has been rewritten below.

$$l = k \frac{p_i}{m_i} \quad (3.38)$$

where $k \in \mathbb{N}$, p is the pitch length, m is the number of helices, and the index i is the sequence of the current layer. For a single-core SPC, the helical components only exist in the armour layers, and the inner components are all straight. Therefore, the model length is only determined by the pitch lengths and the number of wires in the armour layers. However, when it comes to a multi-core SPC, the inner components are also helical and will also yield a model length based on Eq. 3.38. The final model length is decided by the least common multiple of the lengths of the armor layers and the inner helical components. Typically, the inner helical components dictate this value because their m , the number of helical components, is relatively small, and their pitch length is normally larger. For instance, $m = 3$ for the inner helical components in a three-core SPC. In any case, the calculated model length is shorter than the model with one pitch length of the inner components.

The solution to the periodical boundary conditions is similar to three-body movements [16] with specific internal constraints, which will cause rigid body displacements. Therefore, extra constraints on the structure are needed to eliminate the effect of the rigid body displacements. Unlike the approach employed by Tyrberg et al. [17], where a viscous damping coefficient is added to the model that requires the ratio of damping energy to total strain energy less than 5% at the end of the simulation, another B.C. is proposed in this dissertation to get rid of the damping effect from the rigid body movement. This B.C. is unified and can be conveniently applied on single-core SPCs and multi-core SPCs. More importantly, the setup of the B.C. is capable of dealing with not only individual loadings such as tension or bending but also combined loading cases conveniently. The unified B.C. for a single-core SPC and a three-core SPC is illustrated in Figure 3.4.

The outer PE cylinder on both sides is coupled with an RP in the middle of its corresponding cross-section. The other components on both sides are constricted by the periodical boundary conditions. The right RP is fixed, while the loadings are applied on the left RP. In this way, the rigid body movement is eliminated by the constraints on the outermost PE layer. The model is developed to deal with different loading cases, including tension T and bending angle θ_1 , as well as their combination. The loading strategy for each loading case will be stated in detail in the corresponding chapter. Besides, the B.C. for other multi-core SPCs can also be set up similarly. Note that the methodology presented here is universal and not confined to any specific

finite element (FE) code. Readers can construct an appropriate numerical model according to their preferences based on the principles of this methodology.

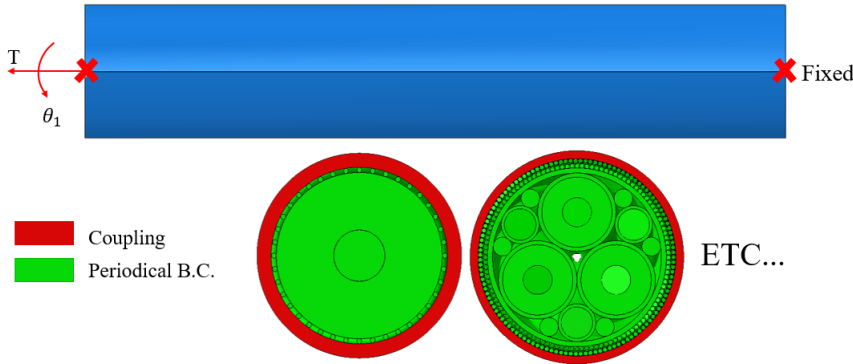


Figure 3.4: The illustration of the boundary conditions for SPCs under combined loadings

3.4. CONCLUSIONS

IN this chapter, an effective modelling method is proposed to address the challenges related to finite element setup, contact setup, and boundary conditions establishment. The method utilizes periodic boundary conditions on a repetitive unit cell (RUC), and for ease of reference in subsequent chapters, this proposed model will be termed the RUC model. The RUC model is versatile, suitable for analyzing single-core and multi-core SPCs under tension, bending, and their combinations. In the following chapters, the accuracy of the RUC model will be validated with test results; the efficiency of the RUC model will be verified by building a full-scale numerical model based on traditional boundary conditions. The details of the RUC model under all the loading cases are the same except for their boundary conditions.

Cable samples from the same production lot are prepared for the tension test and bending test. As the material properties are necessary before building up the RUC model and they are unknown, material test will be performed first. Then tension test will be performed to obtain the axial strain-force curve that will be used to validate the RUC model under tension. Curvature-bending moment curve will be obtained from the bending test, and it will be used to validate the RUC model under bending. The validation of these two loadings will be finished in Chapter 4 and Chapter 5, prior to demonstration of the RUC model for further application in Chapter 6.

REFERENCES

- [1] F. Bussolati. “Modèle multi-échelle de la fatigue des lignes d’ancrage câblées pour l’éolien offshore flottant”. PhD thesis. Université Paris-Saclay (ComUE), 2019.
- [2] F. Ménard and P. Cartraud. “Solid and 3D beam finite element models for the nonlinear elastic analysis of helical strands within a computational homogenization framework”. In: *Computers & Structures* 257 (2021), p. 106675.
- [3] I. Kraincanic and E. Kebabze. “Slip initiation and progression in helical armouring layers of unbonded flexible pipes and its effect on pipe bending behaviour”. In: *The Journal of Strain Analysis for Engineering Design* 36.3 (2001), pp. 265–275.
- [4] M. Jeroense. “Recommendations for Mechanical Testing of Submarine Cables (and Their Accessories)”. In: *Accessories for HV and EHV Extruded Cables: Volume 2: Land and Submarine AC/DC Applications*. Ed. by P. Argaut. Cham: Springer International Publishing, 2023, pp. 351–424. ISBN: 978-3-030-80406-0. DOI: [10.1007/978-3-030-80406-0_5](https://doi.org/10.1007/978-3-030-80406-0_5). URL: https://doi.org/10.1007/978-3-030-80406-0_5.
- [5] F. Ménard and P. Cartraud. “A computationally efficient finite element model for the analysis of the non-linear bending behaviour of a dynamic submarine power cable”. In: *Marine Structures* 91 (2023), p. 103465.
- [6] A. S. U. Manual. “Abaqus 6.11”. In: <http://130.149.89.2080> (2012), p. v6.
- [7] N. Buannic and P. Cartraud. “Higher-order effective modeling of periodic heterogeneous beams. I. Asymptotic expansion method”. In: *International Journal of Solids and Structures* 38.40-41 (2001), pp. 7139–7161.
- [8] N. Buannic and P. Cartraud. “Higher-order effective modeling of periodic heterogeneous beams. II. Derivation of the proper boundary conditions for the interior asymptotic solution”. In: *International Journal of Solids and Structures* 38.40-41 (2001), pp. 7163–7180.
- [9] A. Kolpakov. “Calculation of the characteristics of thin elastic rods with a periodic structure”. In: *Journal of Applied Mathematics and Mechanics* 55.3 (1991), pp. 358–365.
- [10] P. Cartraud and T. Messenger. “Computational homogenization of periodic beam-like structures”. In: *International Journal of Solids and Structures* 43.3-4 (2006), pp. 686–696.

- [11] M. Rahmati, H. Bahai, and G. Alfano. “An accurate and computationally efficient small-scale nonlinear FEA of flexible risers”. In: *Ocean Engineering* 121 (2016), pp. 382–391.
- [12] F. Caleyron, M. Guiton, J.-M. Leroy, T. Perdrizet, D. Charliac, P. Estrier, and L. Paumier. “A multi-purpose finite element model for flexible risers studies”. In: *International Conference on Offshore Mechanics and Arctic Engineering*. Vol. 45462. American Society of Mechanical Engineers. 2014, V06AT04A015.
- [13] J.-M. Leroy, T. e. Perdrizet, V. Le Corre, and P. Estrier. “Stress assessment in armour layers of flexible risers”. In: *International Conference on Offshore Mechanics and Arctic Engineering*. Vol. 49132. 2010, pp. 951–960.
- [14] M. Rahmati, G. Alfano, and H. Bahai. “Periodic and fixed boundary conditions for multi-scale finite element analysis of flexible risers”. In: *International Conference on Offshore Mechanics and Arctic Engineering*. Vol. 49965. American Society of Mechanical Engineers. 2016, V005T04A006.
- [15] S. Krenk. *Non-linear modeling and analysis of solids and structures*. Cambridge University Press, 2009.
- [16] S. H. Strogatz. *Nonlinear dynamics and chaos with student solutions manual: With applications to physics, biology, chemistry, and engineering*. CRC press, 2018.
- [17] D. D. Tjahjanto, A. Tyrberg, and J. Mullins. “Bending mechanics of cable cores and fillers in a dynamic submarine cable”. In: *International Conference on Offshore Mechanics and Arctic Engineering*. Vol. 57694. American Society of Mechanical Engineers. 2017, V05AT04A038.

4

VALIDATION OF THE RUC MODEL UNDER TENSION

The RUC model, based on the proposed modelling method in Chapter 3, requires validation through tests. This chapter focuses on validating the RUC model under tension using a three-core SPC sample. The axial strain-tension force curve obtained from the test serves as the primary tool for validation. This chapter addresses part of Sub-question 3: How can the accuracy and efficiency of the proposed modelling method be validated and verified?

This chapter is structured to cover several key areas: initially, the tension test of the three-core SPC is detailed in Section 4.1. This section presents the materials and geometries of the test samples before a tension test is performed. The details of the samples are prerequisite for the construction of the RUC model before it is validated. The introduction of the RUC model on the sample and the validation are discussed in Section 4.2. Subsequently, full-scale models for the three-core SPC under tension are introduced in Section 4.3. The chapter progresses to present the results and discussions in Section 4.4, culminating in Section 4.5, which concludes the chapter.

Parts of this chapter are based on the following papers:

- [1] P. Fang, X. Jiang, H. Hopman, and Y. Bai. "Mechanical responses of submarine power cables subject to axisymmetric loadings". In: *Ocean Engineering* 239 (2021), p. 109847
- [2] P. Fang, X. Li, X. Jiang, H. Hopman, and Y. Bai. "Development of an Effective Modelling Method for the Mechanical Analysis of Three-core Submarine Power Cables under Tension". In: *Engineering Structures*, 317, 118632

4.1. TESTS

THE core of this chapter is the validation of the RUC model under tension, which is accomplished after obtaining the data from the material test and the tension test regarding a three-core SPC. Figure 4.1 shows clearly how the tests work during the validation process. Material tests provide necessary material properties for the construction of the RUC models. Finally, the axial strain-tension force curve from the tension test regarding the three-core SPC will be used to validate the RUC model.

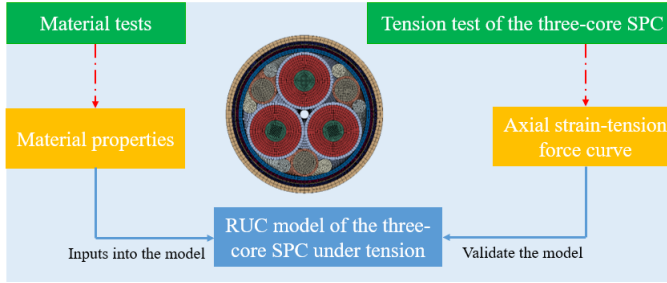


Figure 4.1: The calibration and validation flow chart under tension

4.1.1. MATERIAL TESTS

The test specimens in this paper are 35 kV alternative current dynamic power cables (DPC) produced by Oriental Cable (NBO), as shown in Figure 4.2. The three-core DPC and the stripped single-core SPC are both shown. The nomenclature of the main components within the cable is also given.

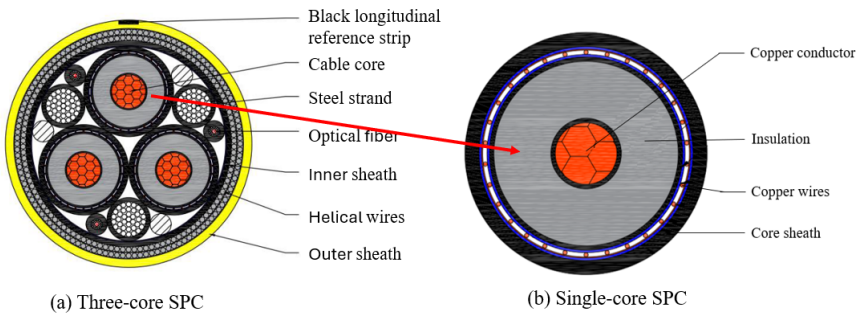


Figure 4.2: The cross sections of the SPCs

For commercial reasons, the detailed geometry and material parameters are not given, and the data in the following content are normalized. Polyethylene (PE) tends to change its behaviour after being extruded into cylinder shapes. There are three types of PE in the SPC sample: HDPE, XLPE and MDPE. Therefore, material tests are performed first to obtain the stress-strain relations of the PE. PE is considered

homogeneous, and thus the strain and stress represent all the components in the corresponding tensors.

According to ISO 527-2012 [1], PE cut from cable samples was made into dumb-bell shapes with a dimension in Figure 4.3. All three types of PE had five samples, as shown in Figure 4.4. The strains during the tension process were recorded by extensometers on an electronic universal test machine, as shown in Figure 4.5. The test machine has a measuring range of 2.5 kN, and the tension speed was controlled at 5 mm/min for all the samples.

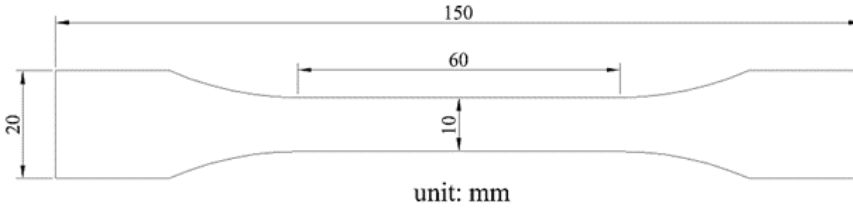


Figure 4.3: The detailed dimensions of HDPE, MDPE & XLPE



Figure 4.4: Dumbbell shape of HDPE (left), MDPE (middle) & XLPE (right)

After the test, the stress-strain relations can be obtained through the linear interpolation method and averaging process of the five samples of each material. The true stress and true strain are calculated according to:

$$\varepsilon_{True} = \ln(1 + \varepsilon_{Nominal}) \quad (4.1)$$

$$\sigma_{True} = \sigma_{Nominal}(1 + \varepsilon_{Nominal}) \quad (4.2)$$

To facilitate the manipulation in the numerical model, an expression for the true stress-strain relationship is generated via the Ramberg-Osgood equation [2]. The total strain is the sum of the elastic strain ε_e and the plastic strain ε_p , which results in:

$$\varepsilon_t = \varepsilon_e + \varepsilon_p = \frac{\sigma}{E} + \left(\frac{\sigma}{K}\right)^g \quad (4.3)$$



Figure 4.5: Tension test under an electronic universal testing machine

Where σ is the stress, K the nonlinear modulus, g the hardening exponent, E the Young's modulus calculated as the secant modulus when the true strain is between 0.05% and 0.25% based on the standard ISO527-2012 [1]. The generated Ramberg-Osgood curves of the three types of PE after normalization are shown in Figure 4.6. The corresponding strain-stress data will be inputted into the FE model to capture the plasticity behaviour of the materials.

4.1.2. TENSION TEST

The dimension of the test cable is given in Figure 4.7. The total length of the cable sample is 9 m. Two bend stiffeners are installed on both sides through which the loadings are applied, which makes the valid length of the sample 7 m. The bend stiffener is used to clamp the cable tightly so that it does not slip away from the loading device. During the tension test, one of the bend stiffeners is totally fixed, while the other one is able to rotate and is pulled through an axial force. The test configuration is shown in Figure 4.8.

To prepare the cable samples for testing, a preliminary tension of 70 kN was applied for approximately 10 minutes to straighten the cable, which was suspended between two end fittings. This initial elongation is not included in the test results. Subsequently, the load was gradually increased from 70 kN to 220 kN in 20 kN increments at a low speed to minimize dynamic effects. To establish a stable tension behaviour, this tension cycle—ranging from 70 kN to 220 kN and back to 70 kN—was repeated several times. An axial displacement sensor was installed directly on the cable end, rather than on the bend stiffener, to ensure accurate measurement and avoid any slippage. Additionally, to reduce the impact of gravity on the measurements, the cable was suspended using a wide rope. Data from the installed displacement and

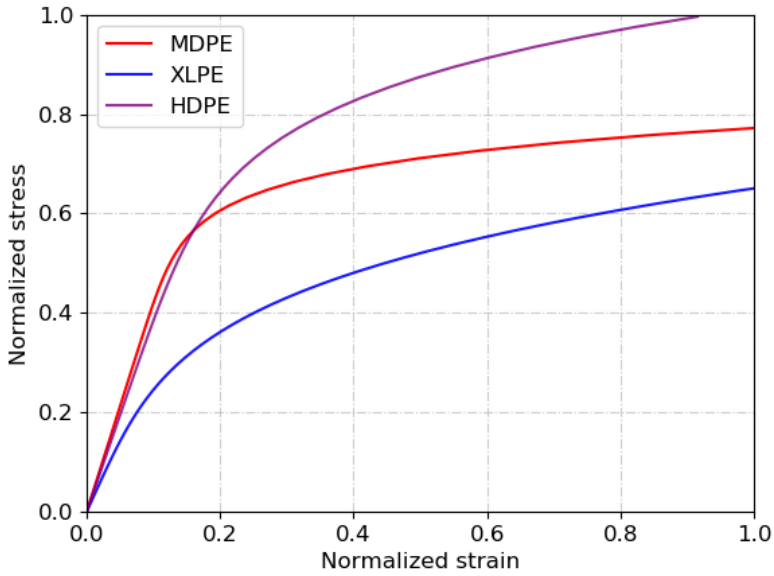


Figure 4.6: Normalized strain vs. stress curves for MDPE, XLPE & HDPE

loading sensors were used to determine the relationship between axial strain and axial force.

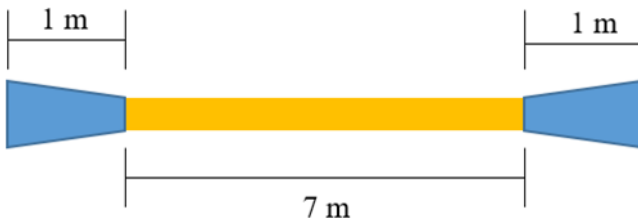


Figure 4.7: A sketch of the tension test



Figure 4.8: Tension test facility

4.2. VALIDATION OF THE RUC MODEL UNDER TENSION

IN this part, the axial strain-tension force curve is used to validate the RUC model of the three-core SPC under tension. Firstly, the construction of the three-core SPC is introduced, where the reliability of the beam-shell element will be verified under the tension case. Then, the validation of the RUC model against the test result is presented.

The model is constructed in the FEM software package ABAQUS/Standard 2022 [3]. ABAQUS is a powerful finite element analysis (FEA) software suite widely used in engineering and simulation.

As the geometries for the SPC samples are extremely complicated, some simplifications and assumptions are made before the simulation to reach a balance between accuracy and efficiency. The engineers who want to investigate more about specific layers can still add those details in their model based on current model technique.

1. The extremely thin layers compared with other layers are combined with the neighbouring layers, as they will introduce a large calculation cost, but their contribution can be ignored.
2. The copper conductors and steel strands in the cable product comprise numerous helical wires. However, they are simplified into a solid cylinder with an equivalent cross-section area. This assumption is satisfied when an SPC is under small deformation.
3. The initial deformation of the cross-section of the SPC sample is ignored, and the model is built according to the geometry information in the specification provided by the cable manufacturer.

The geometries of the three-core SPC model are presented in Figure 4.9. Its length is calculated according to Equation 3.38, and its boundary conditions are set according to those in Chapter 3. The RUC model for the three-core SPC is 792 mm.

All the contact interactions among each component are taken into account. Surface-to-surface discretization method is used to model the contact between surfaces where both the tangential behaviour and normal behaviour employ the penalty method. The friction coefficient provided by the cable manufacturer is 0.3. The normal contact is set as the default hard contact. Damping is not taken into account in the case of tension.

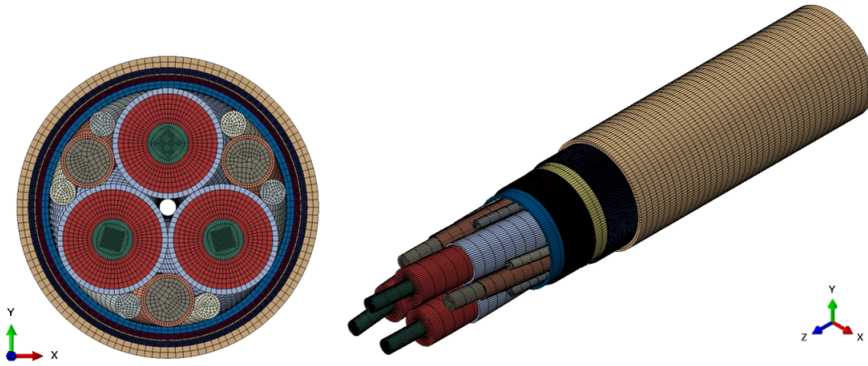


Figure 4.9: The RUC model of the three-core SPC

Before the validation, the soundness of the beam-shell elements needs to be verified. For the three-core SPC, since the inner components, as shown in Figure 4.9, are helix with periodical patterns, the influence of the helical configurations is also taken into account. After this consideration, the model length becomes larger, and there are many more helical wires in the three-core SPC, resulting in cumbersome and time-consuming calculations. Therefore, the technique of beam-shell elements given in Chapter 3 will be used.

beam-shell elements are used to simulate numerous helical wires and helical metals within the three-core SPC. It was mentioned that the coupling approach had been proven to provide a very good compromise between accuracy and computational efficiency [4, 5]. The model built with all solid elements is termed Case-1, while the other one built with beam-shell elements is termed Case-2. The boundary conditions of both models under tension have been given in Chapter 3 in Figure 3.4. The right side is totally fixed, and a tension force is applied to the left RP. The left reference point (RP) is allowed to rotate around the axial axis, like the situation in the tension test.

The mesh results of the three-core SPC in these two ways are shown in Figure 4.10 and Figure 4.11. The mesh densities in the axial direction for both models are the same. All the mesh details for the solid elements in both models are the same as well, except for the helical metals.

The information of both models is listed in Table 4.1 for reference. The number of elements and nodes decreases from 3,150,320 in Case-1 to 1,588,208 in Case-2. All models were run on the DelftBlue Linux supercomputer [6] with 16 cores. The calculation time of Case-1 is found to decrease from 70.3 hours to 3.7 hours, with around 19 times more efficient than Case-2. The soundness of the beam plus solid technique is verified by comparing the axial strain-tension force curve from both models, as shown in Figure 4.12. The curve predicted by the solid element is a straight line, while the one given by the beam-shell elements is a bit bendy, which is caused by the difference in the element property in both models. However, the difference regarding the stiffnesses from both models after curve fitting is 0,

illustrating the soundness of the simplification. Therefore, for the consideration of the model efficiency, the following analysis will rely on the model built with the technique of beam-shell.

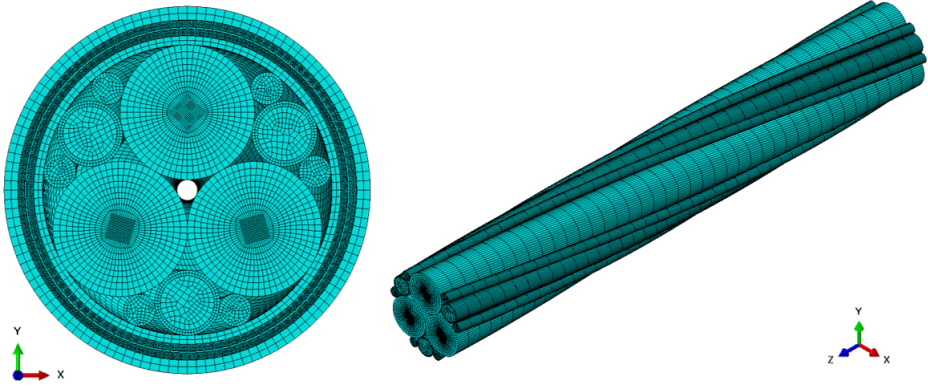


Figure 4.10: Mesh of the three-core SPC by using solid elements

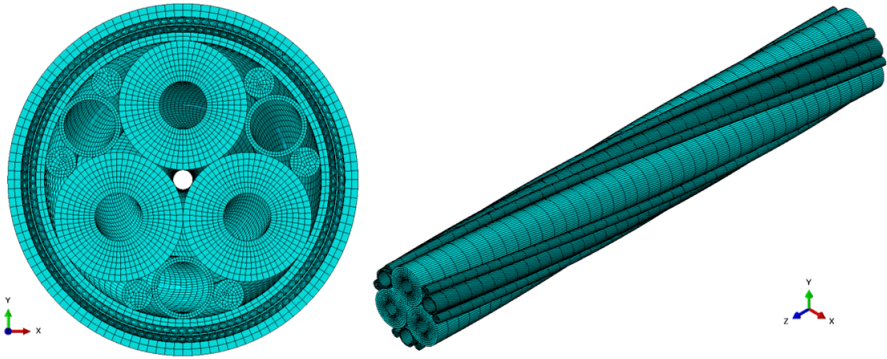


Figure 4.11: Mesh of the three-core SPC by using beam & surface helical wires

Subsequently, the simulation result by Case-2 is validated by the test result on the normalized strain-normalized tension force curve, as shown in Figure 4.12. It is found that the curves basically align with each other. The tension stiffness from the test is normalized to 1, and the stiffnesses from both cases are given in Table 4.1. In fact, the stiffnesses from Case-2 and test after curve fitting have an error of only 4.0%, illustrating the reliability of the RUC model.

Table 4.1: The information of the two types of RUC model under tension

	Case-1	Case-2
Element types	Solid	Solid & beam & surface
Number of elements	3,150,320	1,588,208
Number of nodes	6,276,347	2,905,591
Tension stiffness	0.96	0.96
Cost time	70.3 hours	3.7 hours

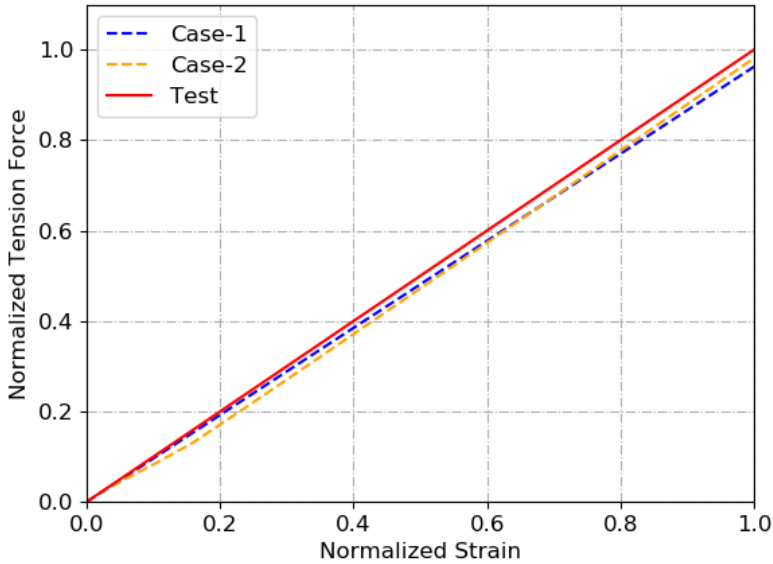


Figure 4.12: The axial strain-tension force curves from the two RUC models

4.3. FULL-SCALE MODEL

To verify the effectiveness of the RUC model over traditionally-built numerical models from the perspectives of accuracy and efficiency, a full-scale model is built for the comparison. The full-scale model here refers to the numerical model that is not based on periodical boundary conditions. The length of the full-scale model can not be reduced by taking advantage of the helical configurations of the components, which makes its length longer. The details are given below.

The mesh information of the full-scale model has been the same as that of the RUC model. The length selected here is 2376 mm, one pitch length of the inner components. As shown in Figure 4.13, both ends of the full-scale models are coupled to an RP, respectively. One of the RPs is totally fixed, whereas on the other RP, U1, U2, U4 as well as U5 are locked and tension is applied in the axial direction. The information of the full-scale model together with the RUC model for tension case are given in Table 4.2. Their results will be discussed together with the RUC model, as well as the test results in the next section.

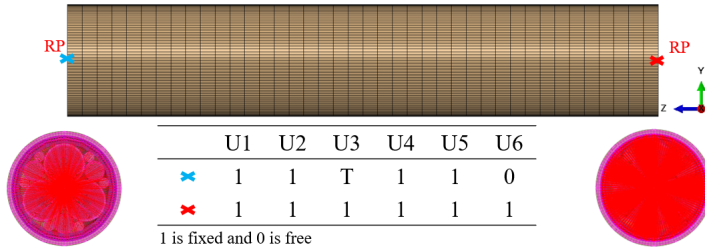


Figure 4.13: The boundary conditions of the full-scale model under tension

Table 4.2: The information of the RUC model and the full-scale model under tension

	Full-scale model	RUC model
Length	2376 mm	792 mm
Number of elements	4,745,288	1,588,208
Number of nodes	8,642,538	2,901,751
Tension stiffness	1.06	0.96
Cost time	22.4 hours	3.5 hours

4.4. RESULTS AND DISCUSSIONS

THE RUC model under tension has been validated by the test results. Then, the mechanical behaviour of the components can be studied based on this model from the overall and component levels.

4.4.1. CABLE OVERALL BEHAVIOUR

The axial strain-tension force curve from the full-scale model is put together with the RUC and the test results, as shown in Figure 4.14. The tension stiffness predicted by the full-scale model is larger than that of the test results, with an error of 6.0%, which might be caused by the boundary effect that can be eliminated much more if the full-scale model is prolonged longer. However, the longer the model is, the more calculation resources it will cost. The calculation time of the full-scale models and the RUC model are summarized in Table 4.2. It is found that the RUC model is almost 7 times faster than the full-scale model and its result agrees better with the test result, illustrating its effectiveness.

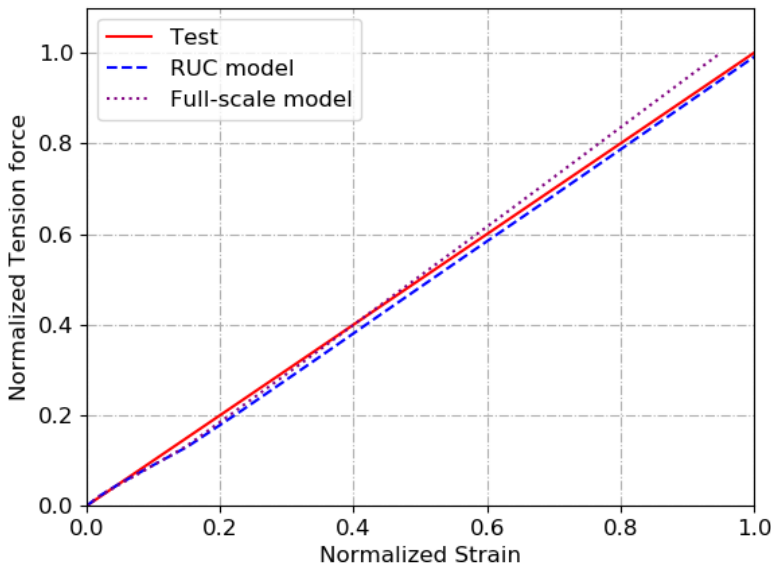


Figure 4.14: The strain-tension force curves from the RUC model and three full-scale models

The energy dissipation during the tension case is of interest, so five types of energy variation, frictional dissipation, viscous dissipation, plastic dissipation, internal energy and kinetic energy, throughout the simulation process from the RUC model are outputted and presented in Figure 4.15. First, it is found that the kinetic energy is near 0, illustrating that the dynamic effect can be safely ignored during the simulation. Second, the contribution from the frictional dissipation and viscous dissipation are not so large during the tension process, which demonstrates that slippage is not substantial in the system. Also, the plastic dissipation can be ignored. This will be further studied through the Mises stress distribution in the next subsection on the component level.

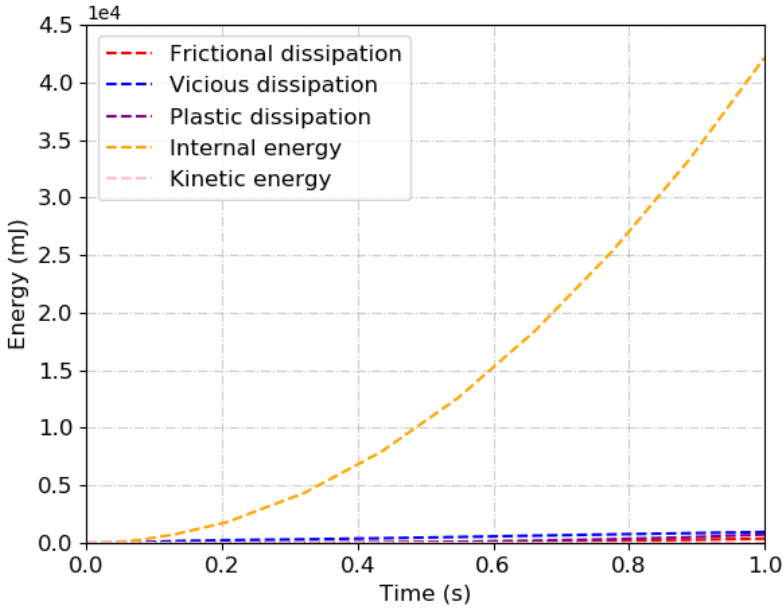


Figure 4.15: The variation of the plasticity dissipation and the internal energy throughout the tension based on RUC model

4.4.2. CABLE COMPONENT BEHAVIOUR

When zooming into the component level, firstly, the contact pressure on the inner sheath within the cable (shown in Figure 4.16) under tension is extracted and given in Figure 4.17. It is found that the maximum contact stresses are located at the contact areas between the inner sheath and the neighbouring internal components. To investigate how the contact pressure distributes around the cross-section of the inner sheath, a middle section is cut out, as shown in Figure 4.17b. Then the contact pressure of the inner sheath at this cross-section when $t = 0.5\text{s}$ and $t = 1\text{s}$ is outputted and shown in Figure 4.18.

It can be found that the maximum contact pressure appears at the contact point between the inner sheath and the inner components, while the areas with no contact do not have any pressure. The maximum contact pressure appears at the contact point between the inner sheath and the three cores, namely Point B, Point F and Point J, corresponding to the nodes in Figure 4.19. The values on the three points are basically the same in the tension case.

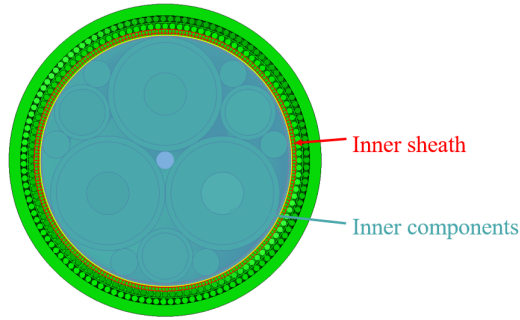


Figure 4.16: The nomenclature of the inner sheath and inner components

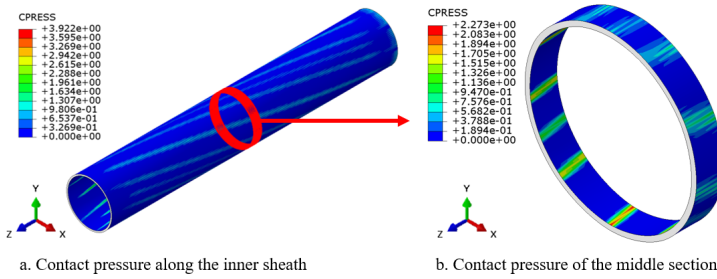


Figure 4.17: The contact pressure of the inner sheath within the cable under tension when $t = 1s$

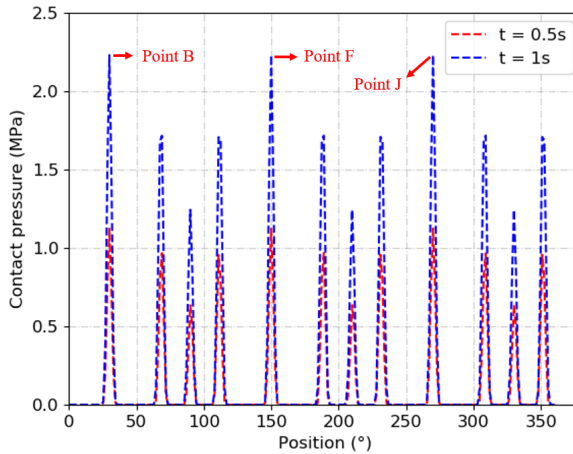


Figure 4.18: Contact pressure of the inner sheath under tension

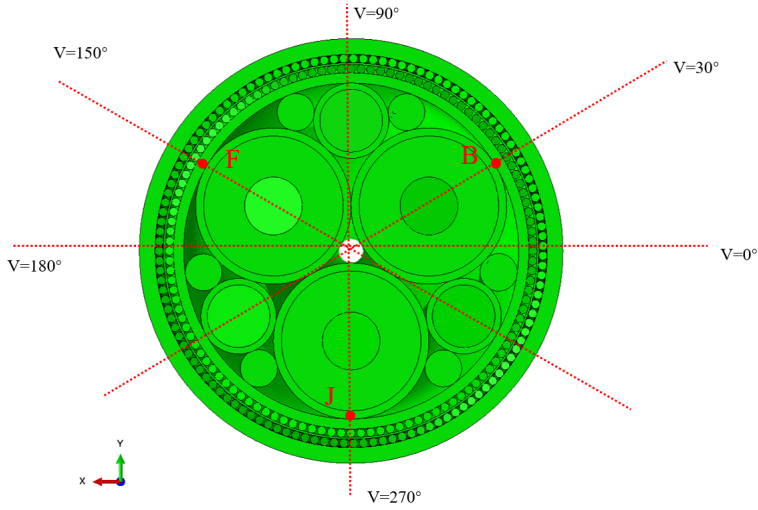


Figure 4.19: Illustration of the nodes in the middle cross-section of the three-core SPC

One also needs to check the stress distribution of the components for the tension case, as shown in Figure 4.20a. It can be found that the metals in the SPC, including the steel strand, helical wires and conductors, have the largest stresses. As Young's modulus of the material steel is much higher than that of the material copper, the stress of the former is also much higher than that of the latter. All the metals are within their elastic phase. Most PE materials are also within their elastic phase, with only a few localized areas along the boundary entering into plasticity. This observation holds true under conditions where the applied stress does not exceed a certain value, beyond which the material may experience more significant plastic deformation. It is observed from Figure 4.20b that the insulation layers have quite small stress, which increases the safety of the overall SPC as the insulation layer should be protected in real life to get rid of water tree or electrical tree [7, 8] that are highly related to high-stress distribution.

The stress distributions of the metals along the axial direction need to be extracted for further analysis. First, the nomination of the three steel strands and three copper conductors are illustrated in Figure 4.22. As there are numerous helical wires in two armour layers and the axial stresses of these wires are distributed unevenly due to the uneven pressure, only four wires in each layer are taken out for illustration purposes. Their starting positions correspond to $V = 0^\circ$, $V = 90^\circ$, $V = 180^\circ$ and $V = 270^\circ$ in Figure 4.19. The axial stress distributions of these metals are then shown in Figure 4.21.

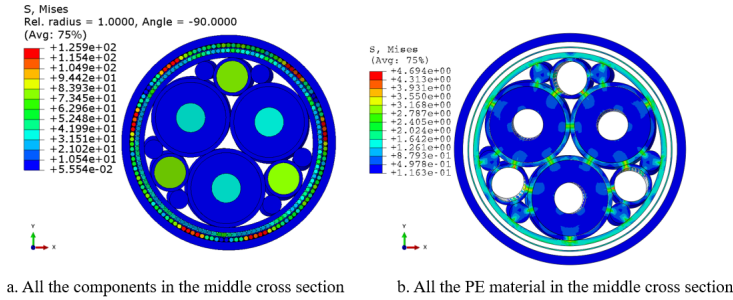


Figure 4.20: The Mises stress distribution of the cable under tension when $t = 1s$

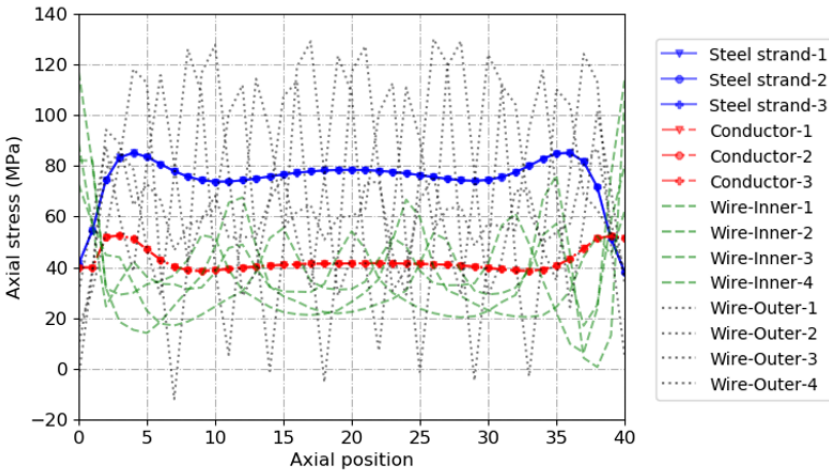


Figure 4.21: Axial stress of the metals when $t = 1s$ in the tension case

From Figure 4.21, it is found that the helical wires in both armour layers have more stress than the inner metals. The inner metals only have tension without any compression stress. The axial stresses of the three steel strands along the axial position are basically the same, thus the curves of the three steel strands are overlapped. This is the same for the conductors. The stresses near the boundaries are abnormal due to the boundary effect. If one wants to get rid of this effect, then it is suggested to double the length of the RUC model and only output the results in the middle. However, this will cause a huge increase in the calculation; thus, whether it is necessary to take this step depends on the requirement of practical engineering and the calculation resources. The steel strands have nearly two times the stress as the conductors, which reduces the possibility of fatigue for conductors by avoiding excessive stress. Besides, it can be observed that the axial stress borne by the outer armour layer is much larger than that by the inner armour layer.

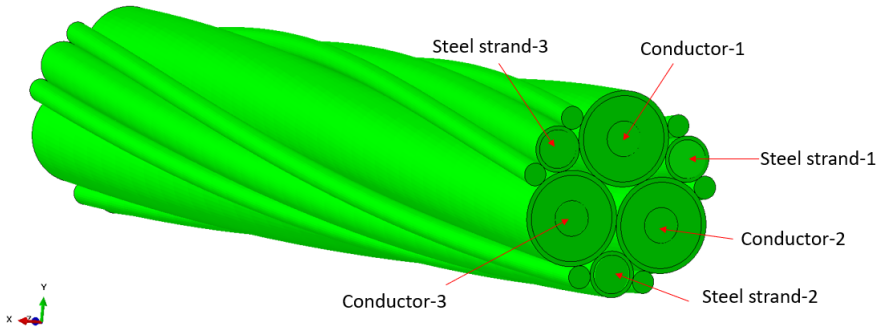


Figure 4.22: Illustration of all the inner metals

4.5. CONCLUSIONS

IN this chapter, a tension test regarding the three-core SPC is presented. The obtained tension stiffness is used to validate the RUC model under tension. The RUC model is 4.0% smaller than the test results regarding the tension stiffness, while the full-scale model is 6% larger than the test results. Besides, the RUC model is around 7 times more efficient than the traditionally-built full-scale model. Therefore, the RUC model holds the potential for conducting tension studies on SPCs with a good balance between accuracy and efficiency. Then, the local mechanical behaviours of the three-core SPC under tension are studied in detail through the RUC model in this chapter at the overall and component levels. The key findings of this section can be summarized as follows:

- 1). **Stick-slip Absence:** In cases of SPCs under tension, there is no significant stick-slip problem, aligning with the RUC model's findings where both friction and viscous dissipation are negligible.
- 2). **Material behaviour:** Under the conditions of small deformation during tension simulations, plastic deformation can be disregarded, and the materials can be considered to exhibit linear elasticity. This assumption does not significantly impact the simulation outcomes.
- 3). **Pressure Distribution:** The internal arrangement of helical components leads to uneven pressure distribution on the inner sheath, resulting in uneven stress across the wires of the armour layers. This highlights the inaccuracies that can arise from assuming evenly distributed pressure in analytical methods.
- 4). **Stress Distribution:** Metals, particularly helical wires, have the majority of the stress, with wires in the outer armour layer experiencing greater stress than those in the inner layer.

Subsequently, the RUC model under bending will be validated in the next chapter.

REFERENCES

- [1] B. Standard and B. ISO. “Plastics—Determination of tensile properties—”. In: *Part 1* (1996), pp. 527–521.
- [2] W. Ramberg and W. Osgood. “Description of stress-strain curves by three parameters. NACA, Tech”. In: *No902* (1943).
- [3] G. Abaqus. “Abaqus 6.11”. In: *Dassault Systemes Simulia Corporation, Providence, RI, USA 3* (2011).
- [4] F. Bussolati. “Modèle multi-échelle de la fatigue des lignes d’ancrage câblées pour l’éolien offshore flottant”. PhD thesis. Université Paris-Saclay (ComUE), 2019.
- [5] F. Ménard and P. Cartraud. “Solid and 3D beam finite element models for the nonlinear elastic analysis of helical strands within a computational homogenization framework”. In: *Computers & Structures* 257 (2021), p. 106675.
- [6] DELFTBLUE. *DELFT HIGH PERFORMANCE COMPUTING CENTRE (DHPC), DelftBlue Supercomputer (Phase 1)*. 2022. URL: <https://www.tudelft.nl/dhpc/ark/delftbluephase1> (visited on 09/28/2023).
- [7] W. Wang, X. Yan, S. Li, L. Zhang, J. Ouyang, and X. Ni. “Failure of submarine cables used in high-voltage power transmission: Characteristics, mechanisms, key issues and prospects”. In: *IET Generation, Transmission & Distribution* 15.9 (2021), pp. 1387–1402.
- [8] M. Danikas, D. Papadopoulos, and S. Morsalin. “Propagation of Electrical Trees under the Influence of Mechanical Stresses: A Short Review.” In: *Engineering, Technology & Applied Science Research* 9.1 (2019).

5

VALIDATION OF THE RUC MODEL UNDER BENDING

The focus of this chapter is the validation of the RUC model under bending. A series of tests, including material tests and mechanical tests, are presented to validate the RUC model. Two types of SPC samples, single-core and three-core, are prepared for bending tests to obtain their curvature–bending moment relations.

After validating the RUC models under bending, full-scale models for both single-core and three-core SPCs are studied to better understand their mechanical behaviours and demonstrate the advantages of the RUC model. The mechanical analysis of the three-core SPC will then be performed using the RUC model. This chapter addresses part of sub-question 3: How can the accuracy and efficiency of the proposed modelling method be validated and verified?

This chapter is structured to first present the bending tests of the studied cable samples in Section 5.1. Validation of the RUC model follows in Section 5.2. Subsequently, full-scale models are constructed in Section 5.3, and results and discussions are outlined in Section 5.4. Finally, Section 5.5 concludes the chapter.

Parts of this chapter are based on the following papers:

- [1] P. Fang, X. Li, X. Jiang, H. Hopman, and Y. Bai. “Bending study of submarine power cables based on a repeated unit cell model”. In: *Engineering Structures* 293 (2023), p. 116606
- [2] P. Fang, X. Li, X. Jiang, H. Hopman, and Y. Bai. “Development of an Effective Modelling Method for the Mechanical Analysis of Submarine Power Cables under Bending”. In: *Computer Methods in Applied Mechanics and Engineering* (Under review)

5.1. TESTS

THE core of this chapter is the validation of the RUC model under bending, accomplished after obtaining the data from the material test, the bending test regarding single-core SPCs and a three-core SPC. Figure 5.1 shows clearly how the tests work during the calibration and validation process. Material tests, performed in Chapter 4, provide necessary material properties for the construction of the RUC models. The curvature-bending moment curves from the single-core SPC test aim to calibrate the damping coefficient that will be input into the RUC model of the three-core SPC. Finally, the curvature-bending moment curve from the bending test regarding the three-core SPC will be used to validate the RUC model.

Bending tests regarding the single-core SPC and the three-core SPC are given in the following two subsections, respectively. The configurations of test facilities and the test process are described in detail. Curvature-bending moment curves of the two types of SPCs are the core outputs from the tests.

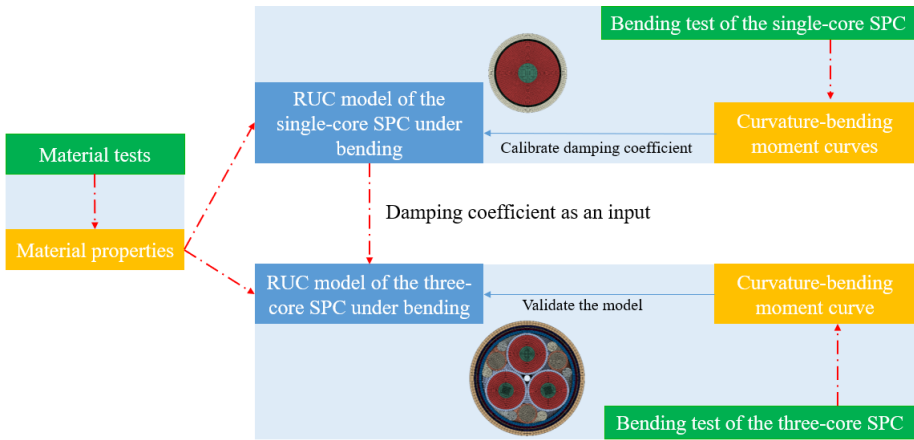


Figure 5.1: The calibration and validation flow chart

5.1.1. BENDING TESTS OF THE SINGLE-CORE SPC

The traditional techniques for the bending test of a slender structure can be three-point bending or four-point bending, as described in Chapter 2. A four-point bending test is adopted here for four cable samples, three of which are shown in Figure 5.2 (a). The vertical displacements at three spots should be recorded to obtain the curvature. Three displacement laser sensors are installed below them, as shown in Figure 5.2 (b), and then the displacements of these three points could be captured for calculating the curvature. Since the curvature in the middle section is near constant, the three points form a standard circle, based on which the curvature can be calculated.

The total length of each cable sample is 600 mm. The size of the samples in the length direction is shown in Figure 5.2 (c). They were then placed on a four-point

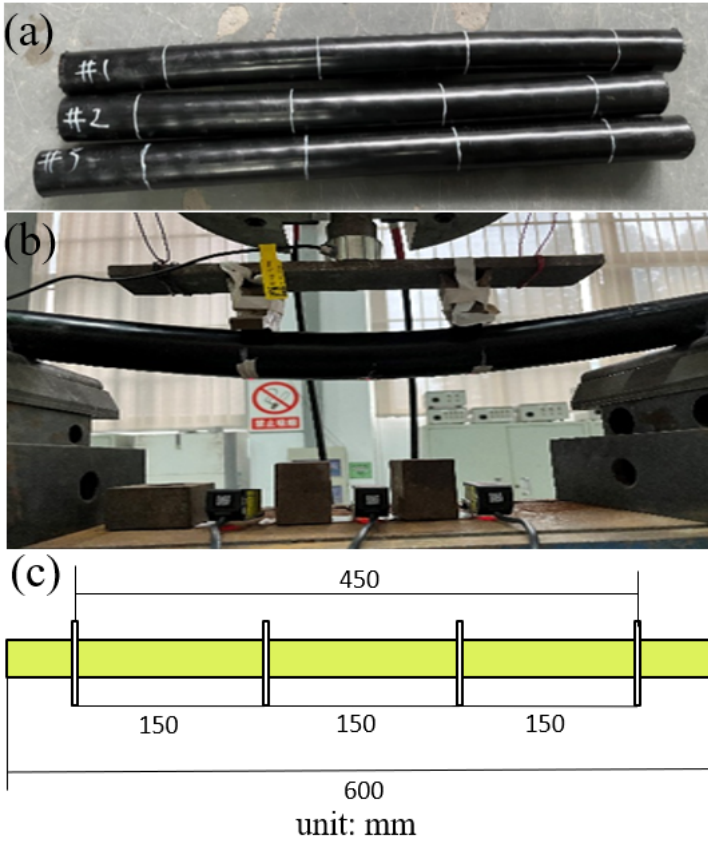


Figure 5.2: The cable samples (a), the four-point bending test (b) and the dimensions (c)

bending test facility with two supports to hold the cables and two loading rings to apply the bending on them, as shown in Figure 5.2 (b). The bending results are given and discussed in Section 5.2.

5.1.2. BENDING TEST OF THE THREE-CORE SPC

Figure 5.3 (a) shows the three-core SPC sample that was used in the bending test. It has a length of 9 m. The size of the samples in the length direction is shown in Figure 5.3 (b). The sample was bent manually several times before the bending test to make the inner components contact as much as possible. They were then placed horizontally on a four-point bending test facility to avoid the influence of gravity. The facility has two supports to hold the cables and two loading rings to apply the bending on them. Three displacement sensors were installed on the loading rings and the middle of the cable to record the displacements of the corresponding three nodes illustrated in Figure 5.3 (a). Meanwhile, the loadings applied by the two loading rings were also recorded. The curvature of the cable and the moment applied to it can then be calculated. The loading rings can bend the cable in one direction and then bend it back to its original place, therefore, in this way, the curvature of the cable increases first and decreases back to zero at last.

5

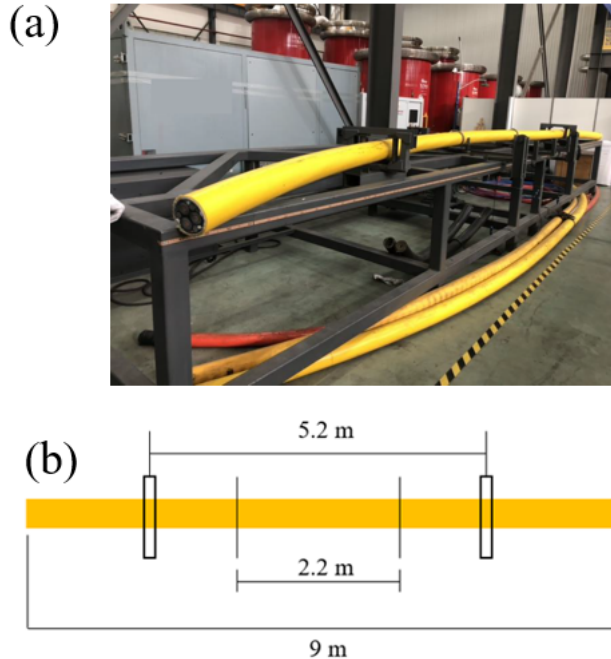


Figure 5.3: Test of three-core SPC (a) and the dimension of the specimen (b)

5.2. VALIDATION OF RUC MODEL UNDER BENDING

As mentioned in Chapter 3, the influence of the initial residual stress within the SPC can be dealt with by applying damping among the contact interfaces. However, the damping coefficient is unknown and needs to be calibrated through test results. In this part, the curvature-bending moment curves from the single-core SPC test are set as the calibration benchmark, and then the value of the calibrated damping coefficient is inputted into the three-core SPC model, which outputs the curvature-bending moment curve that is validated by the test data from the three-core SPC test. The calibration and validation flow chart is already shown in Figure 5.1. The constructions of the RUC model of the single-core SPC and the three-core SPC are presented first.

5.2.1. CONSTRUCTION OF THE TWO TYPES OF SPCs

The construction of the three-core SPC has been introduced in 4. The geometries of the single-core SPC model are presented in Figure 5.4. Their lengths are calculated according to Equation 3.38, and their boundary conditions are set according to those in Chapter 3. The RUC model for the single-core SPC is 40 mm, while the one for the three-core SPC is 792 mm.

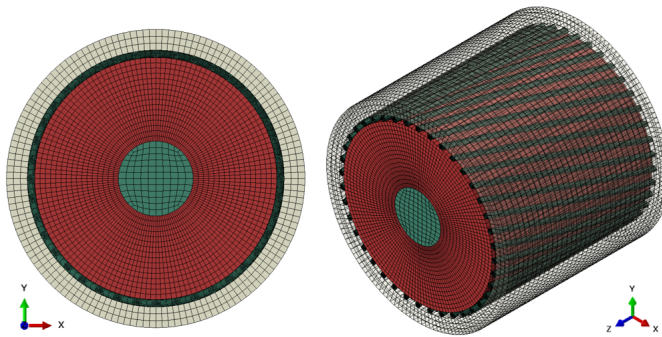


Figure 5.4: The RUC model of the single-core SPC

All the contact interactions among each component are taken into account. Surface-to-surface discretization method is used to model the contact between surfaces where both the tangential behaviour and normal behaviour employ the penalty method. The friction coefficient provided by the cable manufacturer is 0.3. The normal contact is set as the default hard contact. Contact damping coefficient is set upon all the contact surfaces, and the value will be calibrated by the curvature-bending moment curves from the bending test regarding the single-core SPCs.

Before the calibration, the soundness of the beam-shell elements under the bending case also needs to be verified first without damping introduced yet. The model built with all solid elements is termed Case-1, while the other one built with beam-shell elements is termed Case-2. The mesh results of the three-core SPC in these two ways

are already shown in Figure 4.10 and Figure 4.11. The boundary conditions of both models under bending have been given in Chapter 3 in Figure 3.4.

The calculation time of Case-2 is found to decrease from 90.6 hours to 5.3 hours, with around 17 times more efficient than Case-1. The reliability of the beam plus solid technique is verified by comparing the curvature-bending moment curve from both models, as shown in Figure 5.5. Notice, the curves are normalized according to the maximum curvature and the maximum bending moment the three-core SPC has in the test, which will be presented in the following context. The information of both models is listed in Table 5.1 for reference. The overall curvature-bending moment from both models is quite near, with an error of 2.0%. Therefore, for the consideration of the model efficiency, the following analysis will rely on Case-2.

Table 5.1: The information of the two types of RUC model

	Case-1	Case-2
Element types	Solid	Solid & beam & surface
Number of elements	3,150,320	1,588,208
Number of nodes	6,276,347	2,905,591
Cost time	90.6 hours	5.3 hours

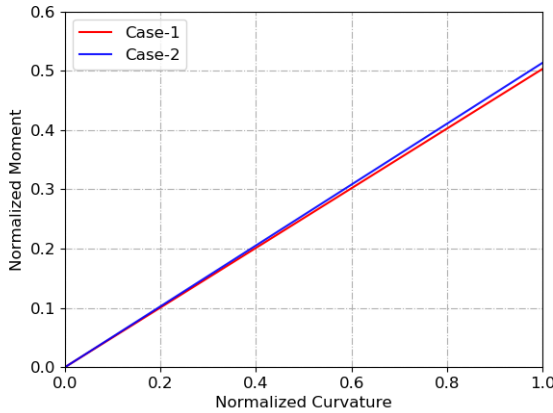


Figure 5.5: The curvature-moment curves from the two RUC models for the three-core SPC

5.2.2. CALIBRATION OF THE DAMPING COEFFICIENT

The curvature-bending moment curves of the single-core SPCs from the test are presented in Figure 5.6(a). Notice, the curves are normalized according to the maximum curvature and the maximum bending moment the three-core SPC has in the test. The maximum curvature applied in the single-core test is nearly ten times larger than that in the three-core bending test. Some of the materials in the single-core SPC sample will enter their plasticity if the curvature is larger than a specific value, and the conductor will not keep as an entirety; therefore, the curve gradually shows more nonlinear variation. This deformation has violated the assumption of simplifying the copper conductor into a solid cylinder. As the curvature considered in the three-core bending test is less than 1, there is no need to consider the deformation when the curvature is larger than 1. Only the curves corresponding to a curvature less than 1 are extracted and averaged for the single-core SPC as well.

The curve after the average and fitting process is presented in Figure 5.6(b) for the purpose of calibration. It is observed that the curve is composed of two lines, although the first line is not so obvious in the image. This curve also demonstrates that there is the stick-slip issue within the single-core SPC. After slippage, the bending stiffness, i.e., the slope of the curve, becomes smaller. It is worth mentioning at this juncture the bending moment contributed by the single-core SPC is only near 0.6% of the overall three-core SPC when curvature = 1, demonstrating that the three cores are not the main contribution to the overall bending behaviour in the three-core SPC. Therefore, for an efficient calculation of the three-core SPC model, the armour wires in the single-core SPC can be merged into the neighbouring layer. This simplification has a minor influence on the overall behaviour but saves many calculation resources.

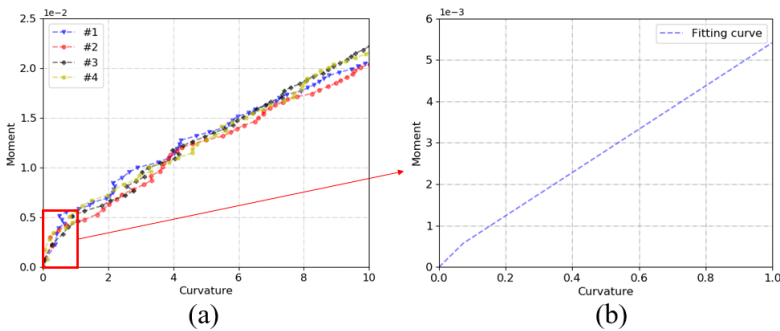


Figure 5.6: The test results of the single-core SPC (a) and the curve after average and fitting (b)

A sensitivity study on the damping coefficient is performed on the single-core SPC. The damping coefficient is kept the same throughout the simulation process. Four cases are studied with values varying from 0 to 3 with an increment of 1. The simulation results, together with the test result, are shown in Figure 5.7. The curvature-bending moment curves after damping incorporated into the model are basically composed of two lines corresponding to the stick and slip phases. The

stiffness before the slip appears is termed stick stiffness, while the one after the slip is termed slip stiffness. With the increase of the damping coefficient, the stick curve becomes longer, which means the slippage appears later; the bending moment predicted by the model becomes larger, while the slip stiffness does not change significantly. The materials within the single-core SPC under such curvature range are basically within their elastic phase. The simulation curve best fits the test result when the damping coefficient equals 1. Therefore, this calibrated value will be inputted into the three-core SPC for validation.

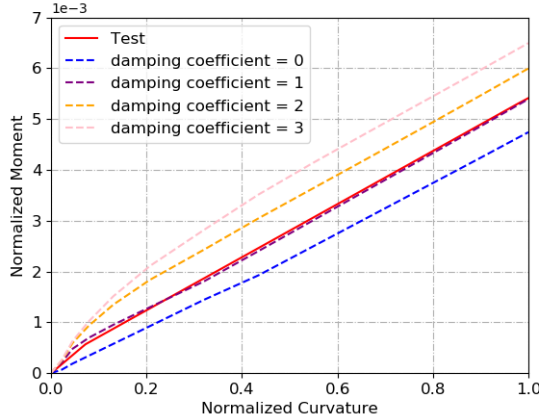


Figure 5.7: The influence of damping coefficient on the curvature-bending moment curves of the single-core SPC

5.2.3. VALIDATION OF THE RUC MODEL UNDER BENDING

Subsequently, the calibrated damping coefficient is inputted into the RUC model for the three-core SPC. A cyclic bending is applied on the RUC model where the variation of bending angle θ is illustrated in Figure 5.8. The time in this figure is for the convenience of the elaboration of the following content where 't' appears frequently and corresponds to the time here in this image. A sensitivity study of the damping coefficient on the bending behaviour is performed. The damping coefficient changes as 0, 0.5, 1 and 2. The curvature-bending moment curves from the four cases are presented in Figure 5.9. When the damping coefficient equals 0, again it is found that no stick-slip curve is predicted. This is because the components immediately slip away from each other within the SPC. The classical hysteresis curve can be obtained after inputting the damping coefficient into the RUC model. When the damping coefficient equals 1, i.e., the value calibrated from the single-core SPC bending test, the simulation result agrees the best with the test result.

When the damping coefficient equals 1, the curvature-bending moment curves from the simulation and the test are shown in Figure 5.10. There are two sections of stick stiffness and two sections of slip stiffness from the test curve. They are named stick

stiffness-1, stick stiffness-2, slip stiffness-1 and slip stiffness-2, respectively. The fitting curves of these stiffnesses are shown in Figure 5.10, and their values are given in Table 5.2. In the test results, it is observed that there is a difference between stick stiffness-1 and stick stiffness-2, which is also the same situation for the two slip stiffnesses. This might be caused by the operation during the test and the complication of the cable cross section. The cable sample will become stabler after several cyclic bending, and their stiffnesses will tend to stable values. The slip stiffnesses in the loading process and unloading process from the RUC model, however, tend to be close to each other. The stiffnesses during the unloading process from the test are more reliable because the cable sample became stabler after the first loading process; therefore, it is found that the stick stiffness and slip stiffness during the unloading process from the test and the RUC model agree with each other quite well, with an error of 2.2% and 5.1%, respectively. The values of the stiffness from both methods after the fitting process are listed in Table 5.2.

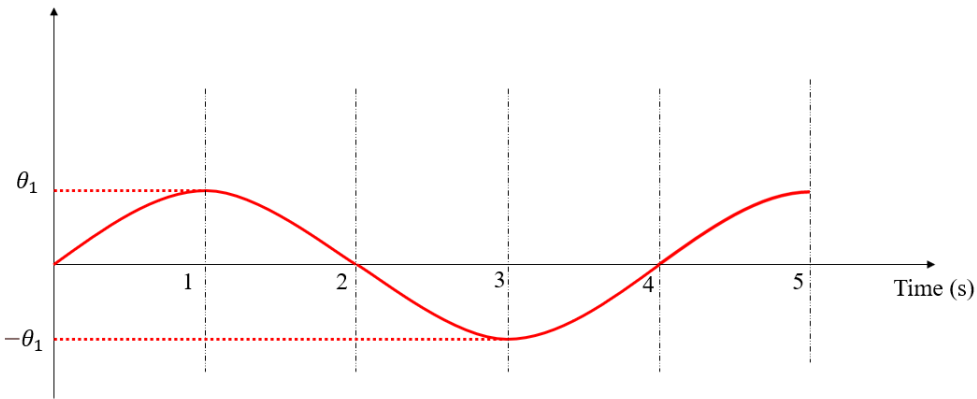


Figure 5.8: Loading strategy for cyclic bending of the three-core SPC

Table 5.2: The stiffness from the test and RUC model

	Test	RUC model	Error
Stick stiffness-loading	8.41	7.01	16.6%
Slip stiffness-loading	0.55	0.74	25.7%
Stick stiffness-unloading	6.86	6.71	2.2%
Slip stiffness-unloading	0.79	0.75	5.1%

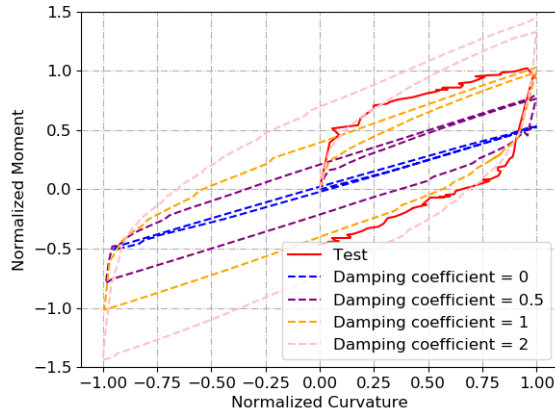


Figure 5.9: The sensitivity study of the damping coefficient on the three-core SPC

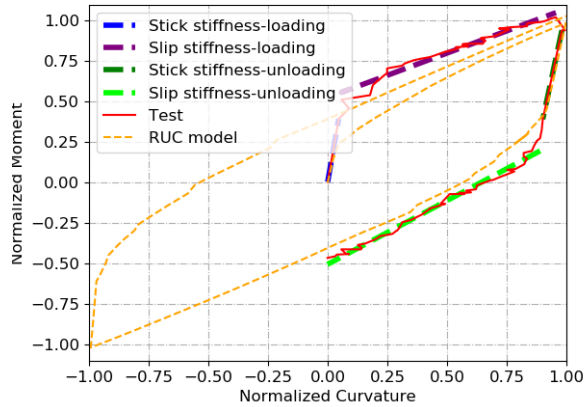


Figure 5.10: Curvature-bending moment for the three-core SPC from RUC model

5.3. FULL-SCALE MODELS

IN order to verify the efficiency of the RUC models, full-scale models of the single-core SPC and the three-core SPC are built. The full-scale models here refer to the numerical models not based on periodical boundary conditions. The lengths of the full-scale models can not be reduced by taking advantage of the helical configurations of the components, which makes their lengths longer. Their details are given below.

5.3.1. CONSTRUCTION OF THE FULL-SCALE MODELS

It is extremely difficult to simulate the bending process by building the model exactly like that in the test, i.e., the four-point test condition, as this will cost too much calculation resources and thus not realistic under current computation capability. Therefore, the full-scale models have to be simplified in a way that balances accuracy and calculation efficiency. However, there is scarce guidance on how to set up the appropriate boundary conditions for the pure-bending section of a four-point bending test sample, and so is the case for the specific rules on the requirement of the model length. Here the boundary conditions under two extreme conditions are tested, i.e., one with all the components on both sides coupled with the corresponding RPs, termed B.C.-1, and the other one with only the PE materials coupled with the corresponding RPs, named as B.C.-2. They are shown in Figure 5.11. The first one corresponds to the situation where all the components on both sides are restricted, while the second one enables the movement of the metals within the cable more freely without any boundary constraints but only with the constraints from the neighbouring layers. Two opposite bending angles are applied on the RPs to simulate the pure-bending section. The full-scale model of the single-core SPC has a length of 400 mm, equaling one pitch length of the helical wires and also meeting the requirement given by Paumier [1], who claimed that the model length is supposed to be 5 times longer than its diameter in a flexible pipe. The full-scale model of the three-core SPC has a length of 2376 mm, which equals one pitch length of the component with the maximum pitch length in the structure.

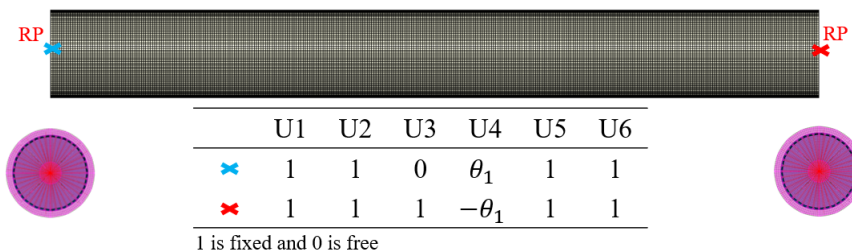


Figure 5.11: The boundary conditions for the full-scale model

5.3.2. DISCUSSIONS

The curvature-bending moment curves from the two full-scale models, as well as the fitting curve from the test regarding the single-core SPC, are presented in Figure 5.12. Unlike the test curve, the simulation curves from both models are composed of only one straight line, which does not represent the stick-slip phenomenon. It is also found that the moments from both simulation curves are lower than those from the test curve. The reason is that the initial residual stress has not been considered in current models. A similar phenomenon will be found in the following simulation results on the three-core SPC as well. To deal with this issue, the initial residual stress also needs to be taken into account.

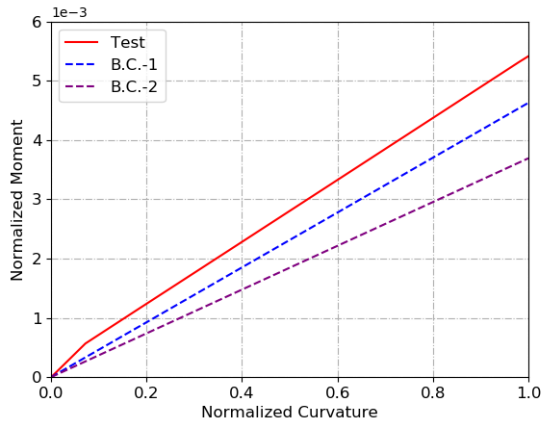


Figure 5.12: The test results and the simulation results under two boundary conditions of the single-core SPC

The curvature-bending moment curves from the two full-scale models and the curve from the test regarding the three-core SPC are presented in Figure 5.13. The process of the SPC's reversing back is not simulated by the full-scale model considering the calculation cost. The same as the situation in the single-core case, in the three-core case, it is observed that, unlike the test curve, the simulation curves from both models are composed of only one straight line. The stiffnesses from both models are less than the stick stiffness from the test result. This is also because current models do not consider the initial residual stress within the SPC. Thus the components immediately slip after loaded, and the stick-slip issue does not appear. The friction force is determined by the friction coefficient and the normal stress of a contact interface. The lack of normal stress in current models enables the slippage instantly when a bending is applied. Therefore, for a more realistic representation of the mechanical behaviour of the SPC under bending, the full models also show that initial residual stress has to be taken into account in a reasonable way.

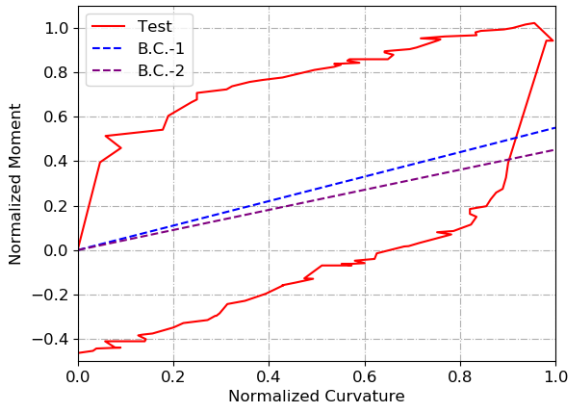


Figure 5.13: The curvature-moment curves from the models under two different boundary conditions

5.4. RESULTS AND DISCUSSIONS

THE RUC model has been validated by the test results. Then the mechanical behaviour of the components can be studied based on this model, from the overall level and component level. The focus is on the three-core SPC as it is the final form after all the components, including the single-core SPCs, are assembled.

5.4.1. CABLE OVERALL BEHAVIOUR

Figure 5.14 presents the curvature-bending moment curves from the experiment, the RUC model and two full-scale models with the same damping coefficient calibrated by the single-core SPC test. These two full models have the same boundary conditions as those of B.C.-1 and B.C.-2 in Section 5.3.1. The calculation times of the two models are summarized in Table 5.3. The cost time regarding the RUC model is recorded when it stops at $t = 1$ s, and the cost time is 5.3 hours. The full-scale models stop before $t = 1$ s, yet their cost time has already reached 70 hours.

Due to the differences regarding the boundary conditions between the full-scale models and the RUC model, their curves still have differences even when the length of the full-scale model is prolonged to 2376 mm. It is found that the curve from the RUC model is sandwiched between the curves from Full-scale model-1 and Full-scale model-2, regarding both their stick stiffnesses and slip stiffnesses. This can be well explained by their boundary differences. All the components on both sides in Full-scale model-1 are coupled, which is an extreme situation as both cross sections are constrained. However, in Full-scale model-2, only the PE components are coupled, and the contributions from the metals are only propagated to the coupled RP through the contact within the interfaces. As compared to the full-scale models, the RUC model predicts the stiffnesses closer to the test results overall as the RUC model is

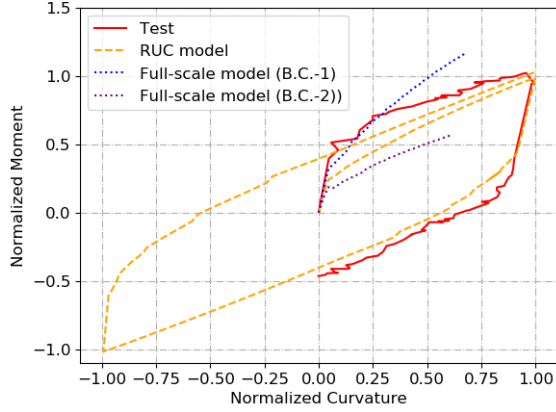


Figure 5.14: Overall behaviours from all the methods

Table 5.3: The information of the RUC model and the full-scale model

	Full-scale model (B.C.-1)	Full-scale model (B.C.-2)	RUC model
Length	2376 mm	2376 mm	792 mm
Number of elements	4,745,288	4,745,288	1,588,208
Number of nodes	8,642,538	8,642,538	2,901,751
Cost time	70 hours	70 hours	5.3 hours

proposed to deal with a structure with infinite length where the boundary effects can be neglected. Therefore, the RUC model performs better than the full-scale models in terms of both efficiency and accuracy. The following analysis will rely on the RUC model.

The appearance of the stick-slip point in the curvature-bending moment and the stick-slip phenomenon strongly involve the energy dissipation in the structure; therefore, the energy variation during the simulation process is of interest. Five types of energy variation, frictional dissipation, viscous dissipation, plastic dissipation, internal energy and kinetic energy, throughout the simulation process from the RUC model, are outputted and presented in Figure 5.15(a). First, the kinetic energy during the process is extremely small, illustrating that the dynamic effect can be ignored. The second large energy is the plasticity dissipation energy, which gradually increases after several cyclic bendings in the RUC model but is still quite small. This also explains why the curve corresponding to 0-1s does not coincide with the curve corresponding to 4-5 s in Figure 5.10. The internal and plastic dissipation energy within the SPC vary throughout the process; thus, the curvature-bending moment curve is not always the same after a bending cycle, which should be paid attention to in practice. Although the frictional dissipation becomes more obvious than the plastic dissipation, it is not the dominant factor to cause the loss of energy in the model. Rather, the viscous dissipation due to the contact damping is found to be much larger than the other energy types, illustrating its major influence on the mechanical behaviour of the SPC. This is exactly why the overall mechanical behaviour is obviously affected by the damping coefficient in Figure 5.9. Moreover, it is observed from Figure 5.15(b) that damping in the tangential direction plays a significant role, whereas damping dissipation in the normal direction can be disregarded. This is because the damping coefficient in the normal direction extremely small in our model. A sensitivity study on the friction coefficient is also performed, given below.

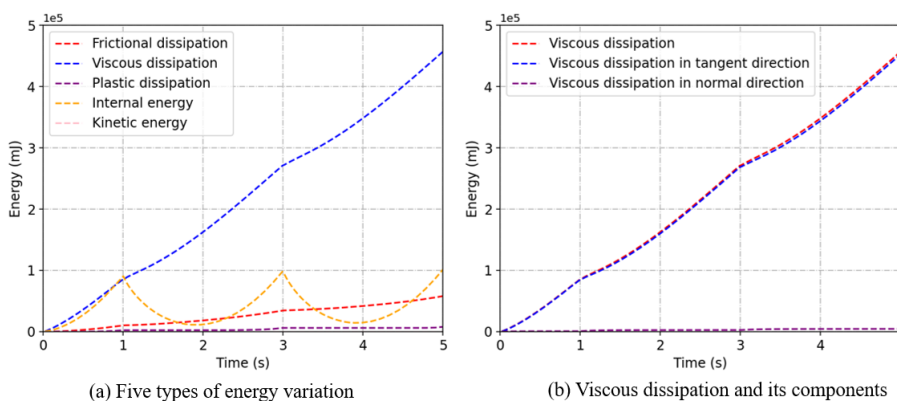


Figure 5.15: The energy variation within the model throughout the bending based on RUC model

Their corresponding curvature-bending moment curves of five RUC models under different friction coefficients are presented in Figure 5.16. It is found that all of the curves basically overlap. This can also be explained by the energy variation in Figure 5.15. The friction dissipation in the model under these situations is not the main factor in affecting the overall mechanical behaviour, instead, the viscous dissipation caused by the damping is the dominant factor. Even if the friction coefficient changes from 0 to 0.4, the stick stiffness basically has no change; the slip stiffness only has an error of 6.7%, as summarized in Table 5.4. In order to check how stresses are distributed within the cable, and how the inner components behave, an analysis on the component level is given below.

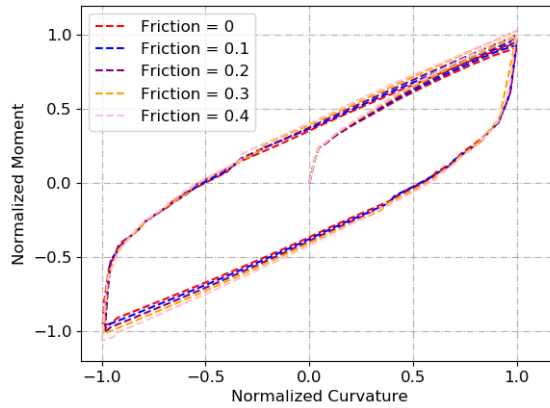


Figure 5.16: Curvature-bending moment curves of models with different friction coefficients

Table 5.4: The predicted bending stiffnesses of the models with different friction coefficient

	Stick stiffness-loading	Slip stiffness-loading
Friction = 0	7.01	0.70
Friction = 0.1	7.01	0.72
Friction = 0.2	7.01	0.73
Friction = 0.3	7.01	0.74
Friction = 0.4	7.01	0.75

5.4.2. CABLE COMPONENT BEHAVIOUR

As the inner components are arranged in the inner sheath helically with gaps, the pressure does not distribute uniformly along the sheath after bending is applied. As shown in Figure 5.17, when $t = 1s$, CPRESS, i.e., the contact pressure, has a specific pattern according to the helical shapes of the inner components. To investigate how the contact pressure distributes around the cross-section of the inner sheath, a middle section is cut out, as shown in Figure 4.19(b). Then the contact pressure of the inner sheath at this cross-section when $t = 1s$, $t = 2s$ and $t = 3s$ is outputted and shown in Figure 5.18.

First, a few important contact points need to be defined for the convenience of the elaboration. As shown in Figure 4.19, point B, point F and point J are the contact points between the three cores and the inner sheath. Their positions around the cross-section are presented clearly. Now from Figure 5.18, it can be found that the maximum contact pressure appears at the contact point between the inner sheath and the inner components, while the areas with no contact do not have any pressure. When $t = 1s$ and $2s$, the maximum contact pressures are located at point B, point F and point J. However, when $t = 3s$, the SPC has been bent into the reverse direction, the locations of the three peak locations are no longer the same. The uneven contact pressure throughout the bending process will also cause uneven stress on the components, which will be investigated below.

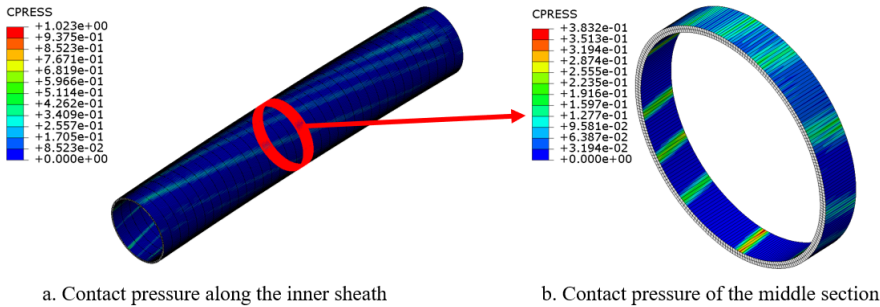


Figure 5.17: Contact pressure of the inner sheath when $t = 1s$

When $t = 1s$, a bending moment has been applied on the SPC that achieves the highest curvature. The stress distribution among the components is one of the design parameters that cable designers care about. Figure 5.19 presents the stress distributions of the cross-section of the whole cable and all the PE layers. It can be found that the metals in the SPC, including the steel strand, helical wires and conductors, have much of the stresses. As Young's modulus of the material steel is much higher than that of the material copper, the stress of the former is also much higher than that of the latter. In addition, the stresses of the inner steel strands are also higher than those of the helical wires in the armour layers. These steel strands are put into the SPC to have those harsh loadings together with the armour layers. As fatigue has also been reported for the armour layer, this special design reduces the

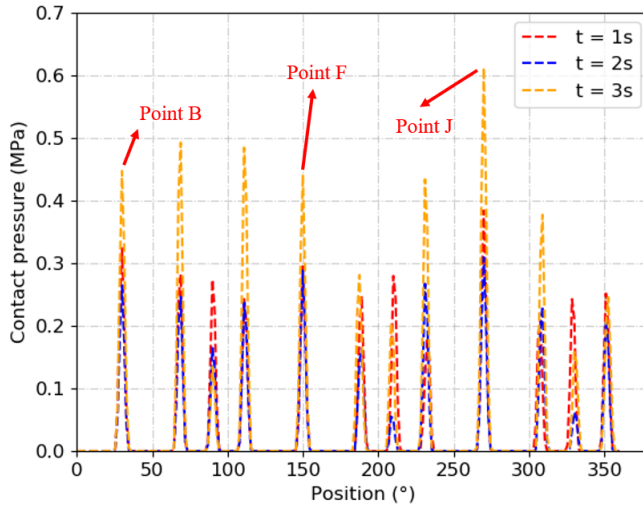
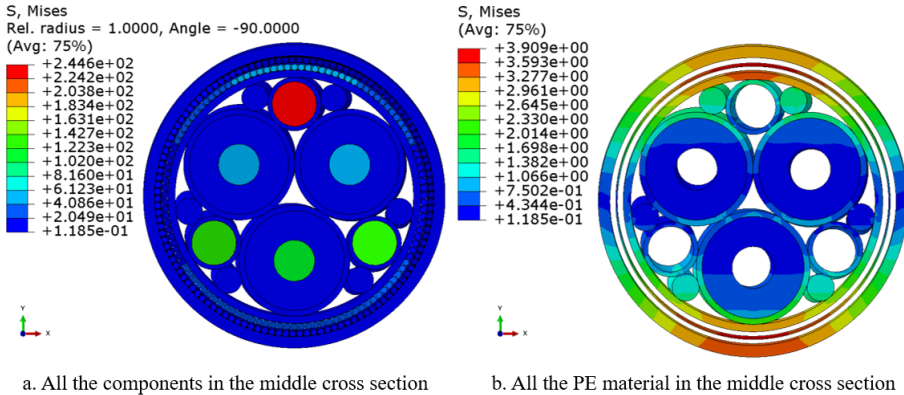


Figure 5.18: contact pressure along the cross section

stresses in the helical wires and then increases the performance of the SPC. From Figure 5.19(b), the maximum stress the PE materials withstand is only 3.91 MPa, with most part of the PE materials staying in their elasticity phase, which justifies the assumption that PE materials can be regarded as elastic in almost all of the previous studies [2, 3]. As the metals have fatigue risk in practice, their stresses along the cable are of interest and are extracted for a detailed analysis.



a. All the components in the middle cross section

b. All the PE material in the middle cross section

Figure 5.19: The stress distribution of the SPC when $t = 1s$

The axial stresses of the metals when $t = 1s$, i.e., the time when the highest curvature is applied, are plotted in Figure 5.20. The nomination of the three steel strands and three copper conductors are illustrated in Figure 4.22. As there are

numerous helical wires in two armour layers, and the axial stresses of these wires are distributed unevenly due to the uneven pressure, only four wires in each layer are taken out for illustration purposes. Their starting positions correspond to $V = 0^\circ$, $V = 90^\circ$, $V = 180^\circ$ and $V = 270^\circ$ in Figure 4.19.

From Figure 5.20, it can be observed that the axial stresses of the inner metals are not disordered like those of the helical wires. The steel strands obviously have more stress than other metals. Steel strand-3 has only tension stress as it is located on the upper part of the cable, which is tensioned after the bending when $t = 1$ s. However, the other two steel strands have not only tension stress but also compression stress. A similar phenomenon is also observed regarding the conductors. Even though the stresses of the helical wires are disordered, one thing that can be observed is that the outer armour layer has less stress than the inner armour layer. In addition, the helical wires in the armour layers still have much potential, for their stresses are still quite small compared to those from the steel strands and conductors. This can be improved by modifying the configurations of these helical wires. Noteworthy, the stresses of most parts of the metals are within their yield strength, which is realized by the helical design that allows the slippage among components.

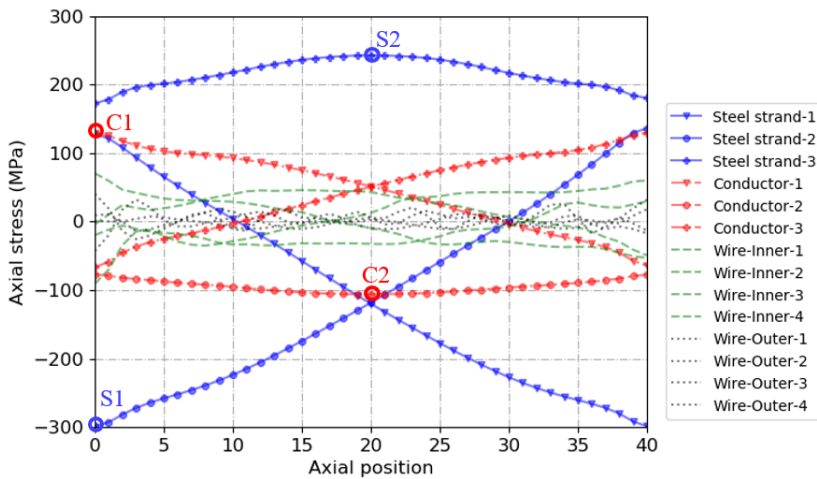


Figure 5.20: Axial stress of the metals when $t = 1$ s

The points on helical strands and copper conductors that have the highest tension and compression stresses are of special interest. They are named as S1, S2, C1 and C2 for the steel strands and copper conductors, as the points illustrated in Figure 5.20. Then the stress variations of the four points along with loading time are presented in Figure 5.21. Similar variation patterns are found for the four points. Take S1 as an example, when the SPC is bent in one direction, the stress of this point increases until $t = 1$ s. Then the SPC is bent back to the original location, and the stress decreases to 0 until $t = 2$ s. Afterwards, the SPC is still bent in the opposite direction and the stress becomes negative, illustrating this point is under compression, and so on.

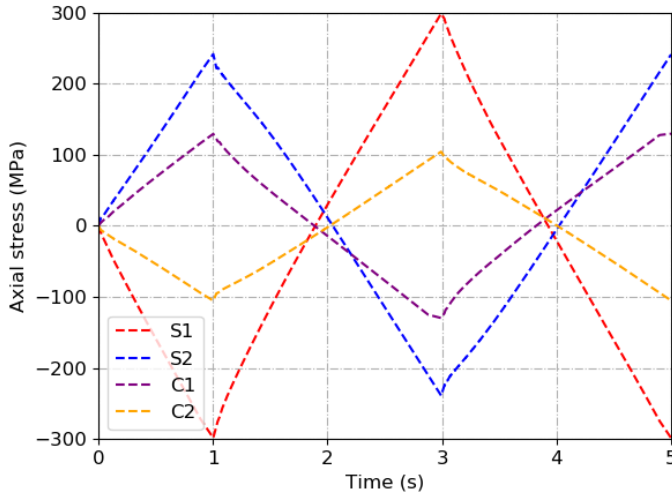


Figure 5.21: The stress variation of the four feature points

As the inner components are designed into helix, these structures are able to relax themselves by allowing slippage among the interfaces. To have a better understanding of the slip mechanism, it is of interest to detect the slip phenomenon among the cable components. For this purpose, the relative displacements between the inner metals and the inner sheath are calculated based on the outputs from the RUC model, which is compared with the results from the simplified loxodromic curve Equation 2.16. The results are shown in 5.22. It is found that the prediction from the RUC model agrees well with the loxodromic curve. The steel strands have larger relative displacement than cores because they are farther away from the SPC's middle axis, enabling them to slip away more easily. The slips become the smallest around the positions near extrados and intrados, aligning with the analytical derivation in Chapter 2.

The relative movements between the two wire layers and their neighbouring layer are also calculated based on the results from RUC model, together with the loxodromic curves presented in Figure 5.23. The simulation results again agree well with the loxodromic curves. In this case, the winding angles of Wire-I and Wire-II are opposite; therefore, their slips are opposite as well. Besides, Wire-II, the wires farther away from the middle axis of the SPC, slip more than Wire-I does.

5.5. CONCLUSIONS

IN this chapter, the validation process of the RUC model under bending is detailed, alongside the introduction of all necessary tests used for constructing, calibrating, and validating the RUC model. Following validation, full-scale models with two different boundary conditions are built for further analysis. It is discovered that

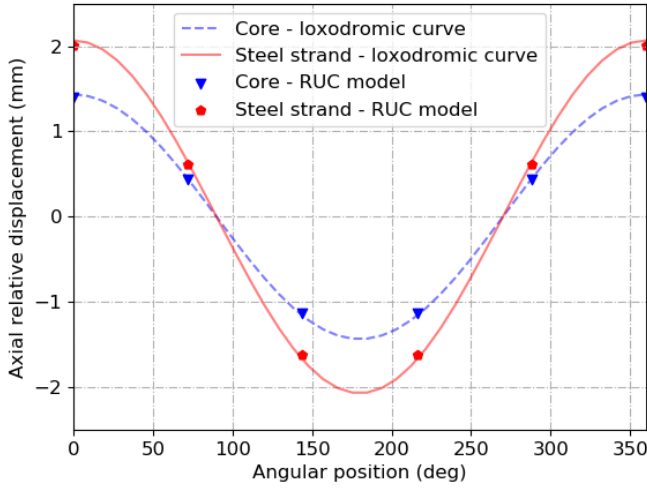


Figure 5.22: The slips of the inner metals along the circular positions

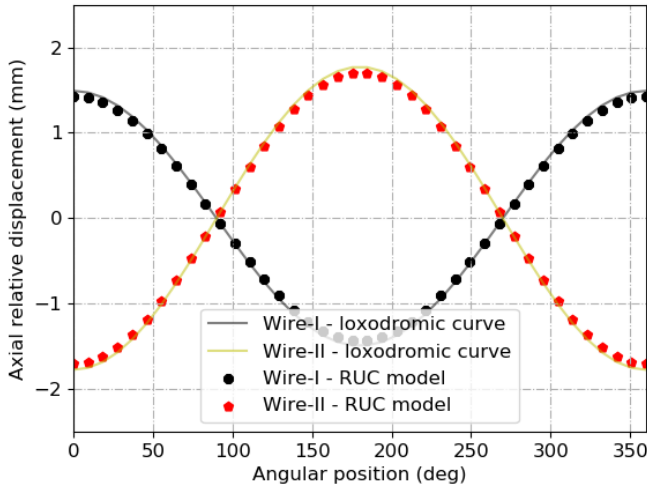


Figure 5.23: The slips of wires along the circular positions

the RUC model significantly outperforms the full-scale models in both accuracy and efficiency, being at least 14 times more efficient. Subsequently, the mechanical behaviours of the three-core SPC under bending are thoroughly investigated using the RUC model, examining both the overall and component levels. The findings demonstrate the RUC model's potential for conducting bending studies on SPCs effectively, balancing accuracy and efficiency. The key findings of this chapter can be summarized as follows:

1) Initial residual stress significantly influences the timing of slip appearance and the corresponding bending moment, necessitating careful calibration using the test curve.

2) The friction coefficient has minimal impact on the overall bending behaviour once damping is incorporated into the model; therefore, this parameter need not be specified by cable manufacturers.

3) The metal components within the SPC sample primarily have the stress load, with inner steel strands experiencing the highest stress, followed by copper conductors, and then armour layers.

4) Stress distribution across the armour layers is uneven and without a specific pattern, attributed to variable contact pressure during the bending process. The inner armour layer endures more stress than the outer layer. Additionally, there is untapped potential in both armour layers that could be leveraged during design.

5) Helical components slip according to the loxodromic curve, with the components on the extrados and intrados experiencing minimal slippage.

Following the successful validation of the RUC model under tension and bending in Chapter 4 and Chapter 5, respectively, the model will be employed to address combined loading scenarios in the subsequent chapter.

REFERENCES

- [1] L. Paumier, D. Averbuch, and A. Felix-Henry. “Flexible pipe curved collapse resistance calculation”. In: *International Conference on Offshore Mechanics and Arctic Engineering*. Vol. 43437. 2009, pp. 55–61.
- [2] F. Ménard and P. Cartraud. “A computationally efficient finite element model for the analysis of the non-linear bending behaviour of a dynamic submarine power cable”. In: *Marine Structures* 91 (2023), p. 103465.
- [3] H. Wang, C. B. Hebert, G. Barbato, L. Silveira, M. V. dos Santos Paiva, T. B. Coser, F. S. López, T. R. Strohaecker, and F. Bertoni. “Submarine Power Cable Design Validation through Model Testing”. In: *ISOPE International Ocean and Polar Engineering Conference*. ISOPE. 2016, ISOPE-I.

6

DEMONSTRATION OF THE RUC MODEL

In this chapter, the validated RUC model is employed to demonstrate its capabilities by examining combined loadings and the impact of inner components. This chapter addresses Sub-question 4: How to demonstrate the modelling method for further application?

The chapter is structured as follows: Initially, the demonstration of the RUC model under combined tension and bending is detailed in Section 6.1. This includes the construction of the model and studies at both the overall and component levels. Subsequently, parametric studies are conducted in Section 6.2, where the contributions of the inner components to the overall stiffness and the effects of the pitch length of these components and the helical wires are explored. Finally, Section 6.3 concludes the chapter.

Parts of this chapter are based on the following papers:

[1] P. Fang, X. Li, X. Jiang, H. Hopman, and Y. Bai. “Local Mechanical Analysis of a Three-core Submarine Power Cables under Combined loadings”. In: Marine Structures (Under review)

6.1. COMBINED TENSION AND BENDING

THE construction of the RUC model regarding the three-core SPC under bending is presented in Section 6.1.1. Afterwards, the mechanical behaviours of the SPC are studied from the cable overall level in Section 6.1.2 and the component level in Section 6.1.3, respectively.

6.1.1. CONSTRUCTION OF THE RUC MODEL

All the details of the model, including its material, geometry and mesh, are the same as the RUC model in Chapter 4 and Chapter 5, except its loading strategy. As the simulated situation is combined tension and bending, a tension force is gradually increased until $t = 1$ s and remained unchanged ever since. Then a cyclic bending is applied after $t = 1$ s on the SPC to simulate the combined tension and bending, as shown in Figure 6.1. Again, the time in this figure is for the convenience of explanation in the following content. In the study, to compare with the pure bending, i.e., $T = 0$, the other two combined loading cases are presented, i.e., $T = 0.5$ and $T = 1$. $T = 1$ means the tension value applied is the same as the tension value in Chapter 5, and $T = 0.5$ is half of the applied force.

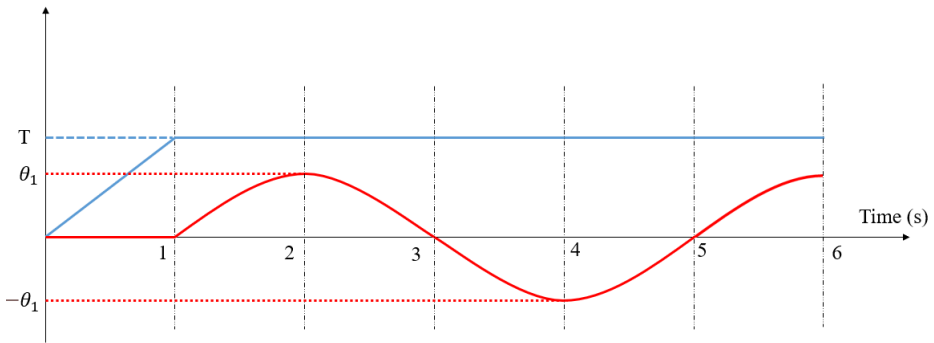


Figure 6.1: The loading strategy of the three-core SPC under combined loadings

6.1.2. CABLE OVERALL BEHAVIOUR

After the simulation, the curvature-bending moment curves of the three cases are presented in Figure 6.2. It can be observed that the applied tension force enlarges the overall hysteric curves. The larger the tension force, the later the stick-slip point appears and the larger the bending moment under the highest curvature. The stick stiffnesses from the three models are found basically overlapped, stating that the tension force does not affect the stick stiffness too much. However, there is an increasing trend of slip stiffness. The stick stiffness and the slip stiffness during the loading process are summarized in Table 6.1.

The five types of energy variation, i.e., Frictional dissipation, viscous dissipation, plastic dissipation, internal energy and kinetic energy throughout the simulation

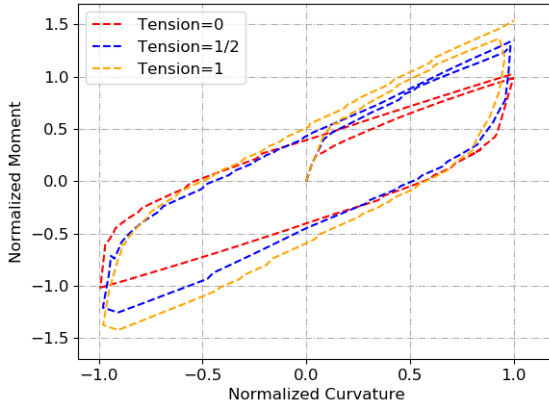


Figure 6.2: Curvature-bending moment curves of three models under combined loadings

Table 6.1: The predicted bending stiffnesses of the models under combined tension and bending

	Stick stiffness-loading	Slip stiffness-loading
T = 0	7.01	0.74
T = 0.5	7.09	0.93
T = 1	7.15	0.97

process for the two cases are outputted and presented in Figure 6.3 and Figure 6.4, respectively. Again, the kinetic energy in both figures is extremely small, quite near to 0 during the whole process, illustrating that the dynamic effect can be basically ignored. Unlike in the pure bending case, frictional dissipation starts to play a larger role when the SPC is under combined loading. By comparing these two figures, it can be observed that the higher the tension, the larger the frictional dissipation takes up in the energy system. This is because the applied tension introduces pressure among the contact interfaces, and the larger the tension force, the higher the contact pressure. When the SPC starts to bend after $t = 1$ s, the frictional dissipation induced by the contact pressure starts to increase. Another phenomenon that can be observed from the two figures is that the plastic dissipation becomes much higher than that in the pure tension case or pure bending case. Which material is the dominant contribution to plasticity will be discussed in detail in the next section through the Mises stress distribution on the component level.

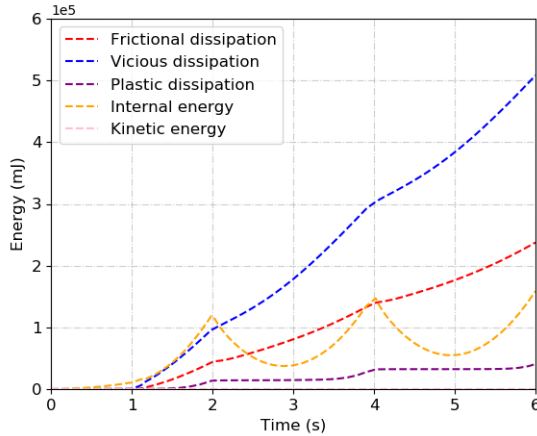


Figure 6.3: The variation of the relevant energy throughout the loading when $T = 0.5$

6.1.3. CABLE COMPONENT BEHAVIOUR

To keep the dissertation concise, only one of the two combined loading cases is studied further, namely the one when $T = 1$. The analysis process for the other one is the same. When zooming into the component level, firstly, same as the bending analysis, the contact pressure on the inner sheath within the cable under tension is also extracted and given in Figure 6.5. The contact stress distribution is also similar to that in the bending case where the maximum contact stresses are located at the contact areas between the inner sheath and the neighbouring internal components. To investigate how the contact pressure distributes around the cross-section of the inner sheath, a middle section is cut out, as shown in Figure 6.5b. Then the contact

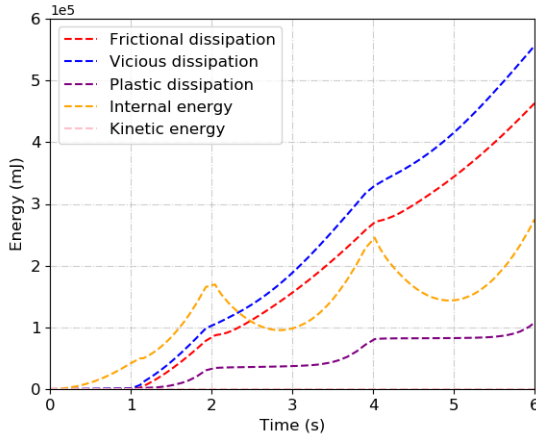


Figure 6.4: The variation of the relevant energy throughout the loading when $T = 1$

pressure of the inner sheath at this cross-section when $t = 1s$, $t = 2s$ and $t = 3s$ is outputted and shown in Figure 6.6.

It can be found that the maximum contact pressure appears at the contact point between the inner sheath and the inner components, while the areas without contact do not have any pressure. The maximum contact pressure appears at the contact point between the inner sheath and the three cores, namely Point B, Point F and Point J, corresponding to the nodes in Figure 4.19. When $t = 1s$, the contact stresses on these three points are the same because now the SPC is under pure tension. However, when $t = 2s$ and $t = 3s$, the contact stresses on the three points are no longer the same. Besides, the contact stresses on the cross-section after bending in the combined loading case are larger than those in the pure bending case, since the contribution from the tension is superimposed.

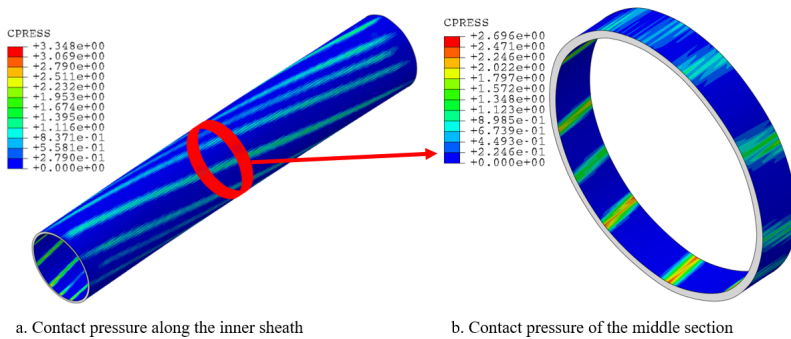


Figure 6.5: The contact pressure of the inner sheath within the cable under combined bending and tension when $t = 2s$

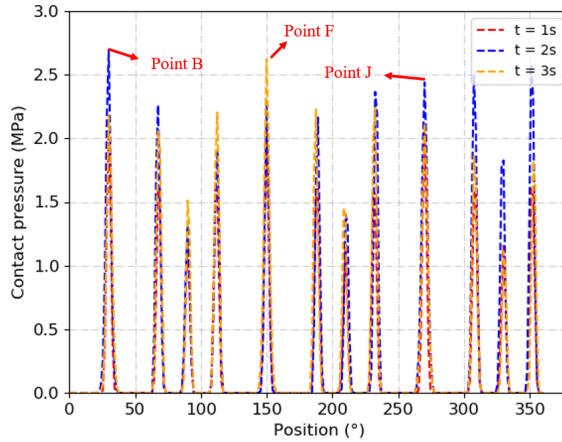


Figure 6.6: Contact pressure of the inner sheath under combined bending and tension

When $t = 2s$, a bending moment has been applied on the SPC that achieves the highest curvature. The stress distribution among the components is one of the design parameters that cable designers care about. Figure 6.7 presents the stress distributions of the cross-section of the whole cable and all the PE layers. It can be found that the metals in the SPC, including the steel strand, helical wires and conductors, have much of the stresses. As Young's modulus of the material steel is much higher than that of the material copper, the stress of the former is also much higher than that of the latter. In addition, the stresses of the inner steel strands are also higher than those of the helical wires in the armour layers. From Figure 6.7(b), the maximum stress the PE materials withstand is only 5.30 MPa, with most part of the PE materials staying in their elasticity phase. Therefore, it can be inferred that the metals within the SPC contribute much of the plasticity dissipation in Figure 6.4. Therefore, their stress details are paid attention to in the following content.

When $t = 2s$, the axial stresses of the metals along the model are presented in Figure 6.8. It is found that stresses in this figure move up towards the positive axis more than those in the pure bending case due to the contribution of the axial stress from the tension. The boundary nodes of the steel strands and conductors have already entered into their yield strength, 300 MPa for the former and 130 MPa for the latter. However, the wires in armour layers are still under their yield strength. The wires in the armour layers hold much potential to protect the inner metals, especially the conductors, by utilizing more of their resistance. For a better view of the stress variations on the inner metals, two feature nodes, C1 and C2, on the conductors, as well as two feature nodes, S1 and S2, on the steel strands, are picked. Their locations correspond to the illustration in Figure 6.8. Then, the axial stress variations of the four nodes along with time are presented in Figure 6.9.

In the tension step, the stresses on the four nodes are gradually increasing until $t = 1s$. Then, the variation patterns of Nodes C1 and S1 are opposite those of Nodes C2 and S2. Take S1 as an example; when the SPC is bent in one direction, the stress at

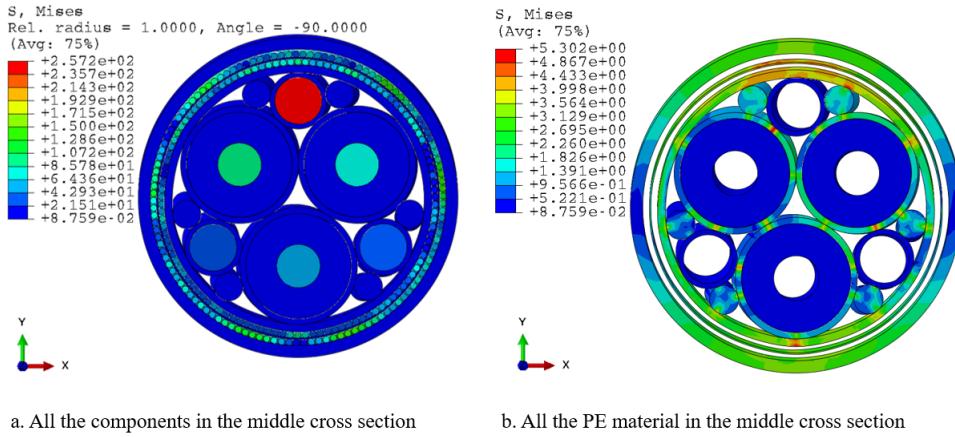


Figure 6.7: The stress distribution of the SPC under combined tension and bending when $t = 2s$

this point decreases. When the SPC is bent back to the original location, the stress is increasing back. The metals on these nodes are found to easily enter into their yield strength, even before the highest curvature attains. Therefore, in practical engineering, these nodes should be paid attention to for the safety consideration of the SPC.

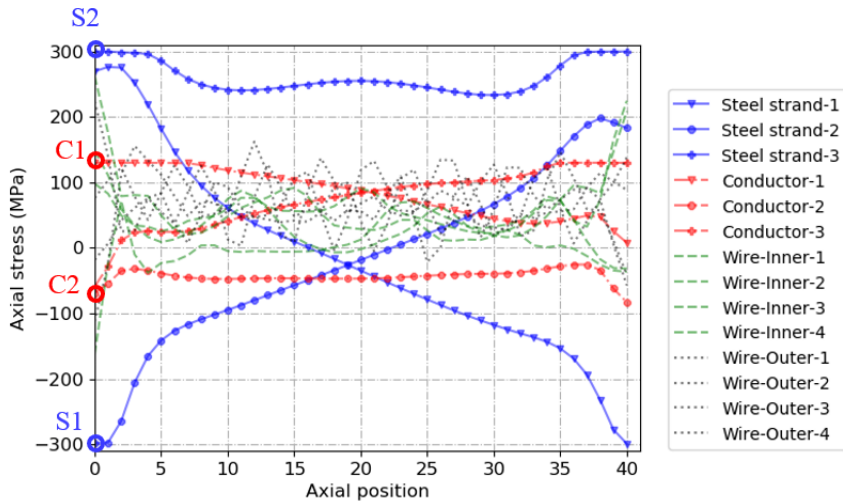


Figure 6.8: The stresses of the metals along the axial position under combined bending and $T = 1$ when $t = 2s$

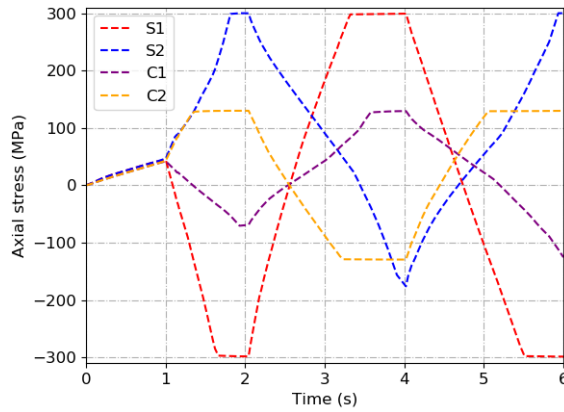


Figure 6.9: The stress variation of the four feature points when $T = 1$

6.2. PARAMETRIC STUDIES

THE inner components make the SPC different from traditional flexible structures. They should be paid more attention to during a design. In order to quantify their influence on the local mechanical behaviour of the SPC, a few parametric studies are performed in this section. The details of the model are identical to those of the previously mentioned three-core SPC, except where otherwise specified. First, the inner components are all removed so that the contribution from them can be inferred. Second, the helical pitch of the inner components is modified, and the influence of this is studied. Third, as the armour layers are added to the cable for better mechanical performance, it deserves a closer study, especially about its pitch length.

6.2.1. THE LOCAL MECHANICAL BEHAVIOURS OF THE SPC WITHOUT INNER COMPONENTS

A traditional flexible pipe is hollow for transporting oil and gas; thus, no inner components exist in the middle. An SPC is responsible for transporting electricity and thus contains necessary components such as copper conductors. How much the inner components contribute to the overall mechanical behaviour will be of interest to the cable designers; therefore, this subsection studies the SPC whose inner components are all removed, as shown in Figure 6.10. Its stiffnesses under tension, bending, and their combination are fitted and put together with those of the original SPC model, as shown in Table 6.10.

It is found that under all three loading cases, the stiffnesses have diminished, no matter whether it is the tension stiffness or bending stiffness, illustrating the significant contribution from the inner components. Especially prominently, the tension stiffness decreased by 89.6% as compared with the original model. Indeed, the stress distribution of the inner metals and the helical wires have been demonstrated

in Figure 4.21, Figure 5.20 and Figure 6.8 already, and it is found the stress of the inner metals are too large to be ignored. The large cross-section of the inner metals finally leads to a not insignificant force. This result also demonstrates the substantial difference between an SPC and a flexible pipe.

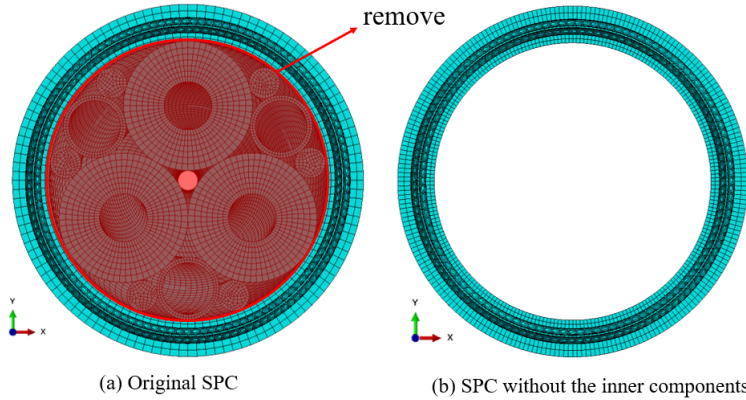


Figure 6.10: The original model and the model with no inner components

Table 6.2: The stiffnesses of SPCs without the inner components

	Tension	Bending		Combined tension and bending	
	Tension stiffness	Stick stiffness	Slip stiffness	Stick stiffness	Slip stiffness
Original model	0.96	7.01	0.74	7.15	0.97
No inner components	0.10	3.78	0.34	3.86	0.38

6.2.2. THE LOCAL MECHANICAL BEHAVIOURS OF THE SPC WITH DIFFERENT PITCH LENGTHS REGARDING THE INNER COMPONENTS

The inner components in an SPC are normally designed into helical shapes such that the converged stresses can be relaxed by allowing enough slippage among the contact interfaces. The relaxation extent is strongly related to the pitch length of these components. To investigate how this factor affects the overall behaviour, the pitch length of the inner components is modified in this subsection and the models under tension, bending and their combination are studied. The pitch length is changed to 2/3 and 1/3 of its original length. The stiffnesses under three loading cases from the original model and the two models are summarized in Table 6.3.

It can be observed that when the pitch length becomes smaller, all the stiffnesses become smaller. We can say the SPC will gradually become more flexible if we shorten the inner pitch length. This result aligns with our intuition. When the pitch length becomes smaller, the inner components wind around the cable by a larger winding angle, which makes the contribution in the axial direction of the cable

smaller. The stress component in the axial direction significantly affects the tension and bending behaviour. This is why we observed a more flexible trend in the data in this table. It also tells us that the pitch of the inner components can not be ignored during the design process if a more accurate calculation result is needed, no matter from an overall perspective or a component perspective.

Table 6.3: The stiffnesses of SPCs with different pitch length

	Tension	Bending		Combined tension and bending	
	Tension stiffness	Stick stiffness	Slip stiffness	Stick stiffness	Slip stiffness
Original	0.96	7.01	0.74	7.15	0.97
2/3*Pitch	0.74	3.48	0.71	4.97	0.95
1/3*Pitch	0.29	1.50	0.57	1.77	0.64

6.2.3. THE LOCAL MECHANICAL BEHAVIOURS OF THE SPC WITH DIFFERENT PITCH LENGTHS REGARDING THE HELICAL WIRES

Another important factor in determining the flexibility and strength of an SPC is the pitch length of the helical wires. Unlike the inner components, where the electric field and thermal field need to be considered carefully during the design, the helical wires are mainly added for mechanical purposes. Therefore, their structure configuration can be adjusted more flexibly without much consideration of the electric field or thermal field, although the amount of metal wires needs to be taken notice of because it will affect the ultimate manufacturing cost. The pitch length of the helical wires is modified to 2 times and 4 times their original pitch lengths. The stiffnesses of these models under different loadings are summarized in Table 6.4.

The trend in this table does not change linearly; however, it is obvious that the smaller the pitch length is, the more flexible the SPC is under all the loadings, the same as the conclusion for the inner components. The pitch length has been quite a dominant factor in determining the local mechanical behaviours of SPCs, no matter the pitch length of the inner components or the helical wires. They need to be decided by an interactive process during the design, finally leading to a configuration that satisfies the requirements of a specific engineering project.

Table 6.4: The stiffnesses of SPCs with different pitch length regarding the helical wires

	Tension	Bending		Combined tension and bending	
	Tension stiffness	Stick stiffness	Slip stiffness	Stick stiffness	Slip stiffness
Original	0.96	7.01	0.74	7.15	0.97
2*pitch	1.22	8.08	0.89	8.51	0.99
4*pitch	1.29	10.02	0.98	14.80	1.27

6.3. CONCLUSIONS

IN this chapter, the RUC model has been applied to demonstrate its functionality under combined tension and bending, building on its validation in previous chapters. The mechanical behaviours of the three-core SPC are examined at both the overall cable and component levels. The findings discussed herein are pivotal for industry design, especially given the practical challenges of replicating combined loading scenarios through physical testing.

Key findings include:

1). Under combined tension and bending, tension significantly affects the mechanical behaviours of the SPC. Notably, slip stiffness increases by 31.1% when the tension force is increased from 0 to 220 kN, whereas stick stiffness is less affected.

2). With substantial applied loads, plasticity dissipation becomes significant. When tension force is increased to 220 kN, the plasticity dissipation takes up 25.5% of the internal energy. Frictional dissipation also plays a more crucial role in the RUC model as tension increases.

3). The yield of metals within the cable is a crucial factor in plasticity dissipation. Cable engineers should closely monitor the inner metals, which may enter plasticity under high loads, while the wires in both armour layers still retain considerable potential.

4). The inner components significantly influence the overall behaviour of the SPC under various loadings. Remarkably, tension stiffness decreases by 89.6% when inner components are removed.

5). The pitch length is a dominant factor affecting the local mechanical behaviours of SPCs under tension, bending, and their combination. Generally, shorter pitch lengths enhance the flexibility of the SPC.

7

CONCLUSIONS AND DISCUSSIONS

In this dissertation, an effective modelling method is proposed for the local mechanical analysis of Submarine Power Cables (SPCs) under tension, bending, and their combination. This method aims to enhance understanding of the local mechanical behaviours of SPCs at both the overall and component levels. A numerical model, based on the proposed modelling method, has successfully addressed all research questions outlined in Chapter 1. The findings and conclusions of this research are detailed in Section 7.1, with limitations of the modelling method and recommendations for future research discussed in Section 7.2. Practical guidelines for implementing the proposed RUC model are provided in Section 7.3.

7.1. CONCLUSIONS

THE objective of this project is developing an effective modelling method for the local mechanical analysis of Submarine Power Cables (SPCs) that provides both more accurate input parameters for the global analysis as well as detailed component data to be used in the fatigue life prediction.

This is further explored through several sub-questions, each contributing to the comprehensive development and validation of the method.

1. How are SPCs structured?
2. What are the methods used by industry for the local mechanical analysis of SPCs?
3. What are the requirements for the new modelling method to be effective in generating the required information?
4. What is the best modelling principle to be used as a starting point for the development of the new modelling method?

Chapter 2 presents the detailed configuration and design process for SPCs, providing an overview of current methods used to perform the local mechanical analysis. The requirements and the outputs of the modelling methods are also identified. The local mechanical analysis output outcomes at both the overall and component levels. The former offers essential parameters, such as stiffness, into the global analysis step. The latter, on the other hand, delivers detailed component details, such as stress variations, into the fatigue analysis step. Both aspects are crucial during the design stage. In Chapter 2, the design process for SPCs is detailed, with particular attention to Dynamic Power Cables (DPCs) that are subject to repetitive loadings leading to fatigue failure. This chapter identifies the local mechanical analysis of SPCs as a research gap.

Two analysis methods to perform the local mechanical analysis of SPCs are discussed: analytical and numerical. Analytical methods are noted for their efficiency but often fall short in complex structures like SPCs, particularly in detailing internal interactions such as contact, resulting in inaccurate component detail estimations.

Numerical methods, in contrast, are adept at handling complex structures with extensive contact areas and have been extensively applied to flexible structures. They can accommodate geometric and material nonlinearities as well as stick-slip phenomena, making them well-suited for accurately performing the local mechanical analysis of SPCs at the component level.

Although numerical methods have been utilized for decades in analysing flexible pipes, their direct application to SPCs is not straightforward due to the evolving configurations of SPCs and their distinct structural differences. A significant challenge is the presence of substantial helical components within SPCs, which introduce a couple of issues that could compromise the accuracy and efficiency of a model. For instance, if finite element types are not selected carefully, the number of meshed elements required for these helical components can become excessively large. Additionally, without proper handling of contact properties, the slip phenomenon may not be predicted properly. Moreover, traditionally-built full-scale models require a

sufficiently long length to minimise boundary effects as much as possible; however, this approach increases the model size and extends computation times substantially.

To address these issues, three key challenges must be overcome when developing an effective numerical model for SPCs:

a). the setup of finite elements,

Beam and surface elements are combined to reduce the number of finite elements in the SPC model while maintaining high accuracy.

b). the setup of contact,

Contact damping is proposed to deal with the effect of the initial residual stresses within the cable.

c). the establishment of boundary conditions.

The boundary conditions are based on periodic boundary conditions and are updated to accommodate both single-core and multi-core SPCs under pure tension, pure bending, and their combination.

Finally, test can provide insights into the overall cable stiffness under specific loading conditions, such as pure tension or bending. Test data is also used to validate the accuracy of a developed modelling method.

5. How can a modelling method be specifically developed for the local mechanical analysis of SPCs?

In order to develop the modelling method, Chapter 3 presents solutions to address the three identified challenges sequentially. For the helical metals within SPCs, the combination of beam and surface elements is recommended, which significantly reduces the number of mesh elements required and facilitates the calculation of complex structures. The presence of initial residual stresses within the interfaces complicates the contact issue. To manage this, damping among contact surfaces is introduced, enabling the simulation of the stick-slip phenomenon effectively. Regarding boundary conditions, the unique configuration of an SPC, characterized by a large number of periodically patterned helical structures, allows for the application of periodic boundary conditions. These boundary conditions are formulated using the homogenization method for a beam-like structure, with the micro-problem focusing on a unit cell. This approach not only reduces the model's length but also minimizes boundary effects as much as possible. The boundary conditions are refined to accommodate various SPC configurations, including single-core, three-core, and other multi-core SPCs, under both individual and combined loading conditions. The model, developed through this approach and based on periodic boundary conditions on a representative unit cell (RUC), is thus termed the RUC model.

6. How can the accuracy of the proposed modelling method be validated?

The validation of the proposed RUC model under tension is detailed in Chapter 4. A series of tests, including material property tests and tension tests on three-core SPCs, were conducted. These tests generated the axial strain-tension force curve used to validate the RUC model. The RUC model demonstrated superior accuracy in

replicating the tension stiffness compared to traditionally-built full-scale models and proved to be approximately seven times more efficient in computation. Moreover, the local mechanical analysis of the three-core SPC under tension were performed at both the overall and component levels.

The efficacy of the RUC model under bending is similarly validated in Chapter 5. Curvature-bending moment curves from bending tests on single-core SPCs were used to calibrate the equivalent damping coefficient, which was then applied to the three-core SPC in the RUC model. Validation was achieved by comparing the model's output to curvature-bending moment curves from bending tests on the three-core SPC. The RUC model's results were consistently more accurate than those from two full-scale models with differing boundary conditions. In terms of computational efficiency, the RUC model is able to finish in a only a few hours, at least thirteen times faster than the full-scale models that have been simplified. This chapter also performs the local mechanical analysis of the three-core SPC under bending at both the overall and component levels.

4. How to demonstrate the modelling method for further application?

After validating the RUC model under pure tension and bending through test data in Chapters 4 and 5, respectively, Chapter 6 extends the investigation to the local mechanical analysis of the three-core SPC under combined tension and bending. The model setup—comprising materials, geometries, and mesh—remains consistent with Chapter 4, with modifications only to the loading strategies. To simulate combined loading, tension is applied before cyclic bending. The simulation results are analysed both at the overall cable level and component level, demonstrating the RUC model's capability to study the SPC under combined loading conditions. Furthermore, the influence from inner components and pitch lengths of helical components are studied to gain deeper insights into cables.

For the studied SPC sample in this dissertation, a few findings are summarized. Despite metals being the primary contributors to the SPC's overall stiffness, stress distribution between the inner metals and helical wires varies under different loading scenarios. Under tension, the helical wires experience greater stress compared to the inner metals; however, under bending, the inner metals sustain most of the stress, a trend that persists under combined loading. These findings underscore the importance of component arrangement in cable design, considering varied load types. Chapter 6 illustrates the significant contribution of the inner components to the overall stiffness, affirming their pivotal role in distinguishing SPCs from traditional flexible pipes. Additionally, the influence of pitch lengths on the overall stiffness is explored; longer pitches increase stiffness, providing cable designers with a method to tailor SPC flexibility according to engineering requirements.

7.2. LIMITATIONS AND RECOMMENDATIONS

ANCILLARY equipment such as bend stiffeners and buoyancy modules are installed on DPCs in their global configuration to ensure safety and minimal deformation during service, as illustrated in Figure 7.1. The proposed method addresses SPCs under the assumption of constant curvature when bending is involved. This assumption is conventional in practical engineering and is considered acceptable for most sections of a DPC, according to standards and brochures. However, special attention must be given to the hang-off point and the touch-down point, where the constant curvature assumption is invalid due to curvature variations along these sections. For a more accurate analysis of the SPC near these areas, a local model with appropriate boundary conditions considering varying curvature should be developed.

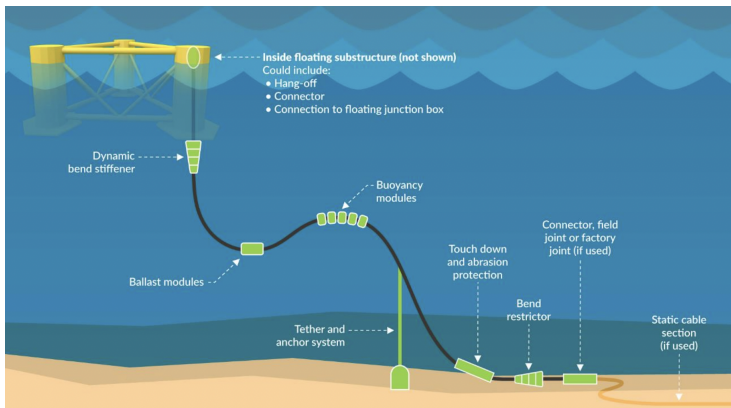


Figure 7.1: Ancillary equipment on the dynamic cable [1]

The RUC model, employing periodic boundary conditions derived from the homogenization method based on multi-scale analysis, is optimized for situations where SPCs undergo small deformations. At the macro scale, it corresponds to a Navier–Euler–Bernoulli–Saint-Venant beam, while at the micro scale, it is based on a unit cell with assumed small deformation. This makes the RUC model most effective when the SPC remains within its linear deformation phase, as primarily considered in this dissertation. The accuracy of the RUC model under larger deformations remains to be validated with additional test data and is suggested as a focus for future research.

The local mechanical analysis of DPCs have traditionally been performed under quasi-static loadings, neglecting the impact of dynamic effects that occur during their operational life. It is crucial to acknowledge that dynamic loadings significantly influence the accuracy of local mechanical analysis, as evidenced by existing research [2, 3]. While the proposed RUC model incorporates a dynamic algorithm, allowing for the simulation of dynamic effects by adjusting the loading rate to mirror real-world engineering conditions, the validity of the simulation results must be rigorously confirmed. This can be achieved through the comparison between simulation results

and more test data. Enhancing the model's credibility necessitates this critical step, thereby ensuring its applicative reliability in engineering contexts.

When moving further into the analysis method, a few more recommendations can be given. For example, the treatment of initial residual stress within multi-layer flexible structures remains a complex issue. In this dissertation, introducing an equivalent contact damping coefficient among contact interfaces simulates the macroscopic effects of residual stress effectively enough to align with practical experimental outcomes. However, a deeper scientific understanding of how initial residual stress impacts deformation requires more detailed studies at the contact interfaces.

Furthermore, while the use of beam and surface elements to perform the local mechanical analysis of the SPC has proven effective, incorporating thermal effects poses additional challenges. The operational life of SPCs involves temperature fluctuations that affect material properties and, consequently, mechanical behaviours. Although literature such as CIGRE [4] and IEC [5] recommends temperature-variant bending tests, these tests are costly and time-consuming. Therefore, the compatibility of beam and surface elements with thermal transfer mechanisms needs verification before temperature can be effectively included in the RUC model.

Additionally, the RUC model's simulation of combined tension and bending without corresponding test validation highlights a gap. Although challenging, performing such a test is crucial as this loading condition is prevalent in practice. This gap also extends to torsion tests, which are essential yet difficult due to the complexities of torsion test facilities. Despite the absence of direct research on SPCs under torsion, insights from flexible structures suggest potential areas for study using the RUC model. Future research should aim to validate the RUC model under torsion through practical tests, ideally obtaining torsion angle-torque curves.

7

7.3. GUIDELINES FOR EMPLOYING THE RUC MODEL

THE local mechanical analysis is a critical step in the fatigue analysis of Dynamic Power Cables (DPCs), as detailed in Chapter 2. The stiffnesses from the RUC model are inputs into the global model for global analysis; the detailed component details, such as stress variations, are input into the fatigue analysis step. Although the dissertation cuts into the storyline based on fatigue analysis, the proposed RUC model should not be confined only to this area. Two examples of more application scenarios are given. First, in the design of SPCs, cross-sectional optimization is essential to achieve a design that not only fulfils project specifications but also optimizes costs. Leveraging the accuracy and efficiency of the RUC model facilitates an iterative analysis process, thereby substantially reducing the project duration. Second, the electrical tree and water tree are strongly related to the mechanical behaviour of the insulation [6, 7]. The stress value from the RUC model is also able to help estimate whether the insulation is in a safe condition. Therefore, practitioners can flexibly choose to use this model and extend the application scenarios according to their actual needs. Other applications, such as vortex-induced vibration prediction [8], which require stiffness data from the RUC model, also await exploration in the future.

To aid cable engineers in using the RUC model based on the proposed modelling method, guidelines are provided. Essential inputs are summarized in Table 7.1. Cable manufacturers must supply material properties such as Young's modulus/stress-strain relation, Poisson's ratio, and yield strength of metals. Particularly for PE materials whose properties may alter after manufacturing, it is advisable to derive the stress-strain curve from a cut piece of an assembled cable for a more accurate estimation. If testing is not feasible, material properties from open publications [9–11] or previous engineering experiences may be used as references.

Additionally, cable manufacturers should provide detailed component geometries, including component sizes, pitch lengths of helical structures, the number of helical wires in the armour layers, and the initial residual stress. Since direct testing of initial residual stress is challenging, one method, as suggested by CIGRE [4], involves calibrating an equivalent external pressure using curvature-bending moment curves from bending tests.

This dissertation introduces a convenient alternative: a contact damping coefficient in the tangential direction, calibrated at $2.5 \frac{Ns}{mm^3}$, to simulate the effect of initial residual stresses, making the friction coefficient less crucial in affecting local mechanical analysis. Recommended values of the friction coefficient for the model range from 0.2-0.3.

The RUC model predominantly uses a combination of beam and surface elements to simulate helical metals, which significantly enhances calculation efficiency. However, this approach does not yield detailed stress information in the radial direction of the helical metals. If users require these details, simulating helical metals with solid elements is recommended, although this significantly increases computational demands. Users must carefully weigh the importance of efficiency and accuracy when they decide to use solid elements.

The code for implementing periodical boundary conditions, and for developing beam-shell elements in ABAQUS are made freely available to download at <https://pan-fang.github.io/Codes/>.

Table 7.1: Input parameters for the local mechanical analysis in the RUC model

Input parameters	Details
Material properties	Young's Modulus/Stress-strain relation, Poisson's ratio, Yield strength
Component geometry	Number of components, Size of components, Pitch length component radius, equivalent damping coefficient, etc.
Global loads	Time series of tension & curvature or classes of tension & curvature variations

REFERENCES

- [1] WFO. *Floating Offshore Wind Dynamic Cables: Overview of Design and Risks*. 2024. URL: <https://wfo-global.org/wp-content/uploads/2024/02/WFO-Cables-and-FOSS-White-Paper.pdf> (visited on 05/31/2024).
- [2] M. Komperød, J. I. Juvik, G. Evenset, R. Slora, and L. Jordal. “Large-Scale Tests for Identifying the Nonlinear, Temperature-Sensitive, and Frequency-Sensitive Bending Stiffness of the NordLink Cable”. In: *International Conference on Offshore Mechanics and Arctic Engineering*. Vol. 57694. American Society of Mechanical Engineers. 2017, V05AT04A004.
- [3] J. Fang and G. Lyons. “Structural damping behaviour of unbonded flexible risers”. In: *Marine structures* 5.2-3 (1992), pp. 165–192.
- [4] M. Jeroense. “Recommendations for Mechanical Testing of Submarine Cables (and Their Accessories)”. In: *Accessories for HV and EHV Extruded Cables: Volume 2: Land and Submarine AC/DC Applications*. Ed. by P. Argaut. Cham: Springer International Publishing, 2023, pp. 351–424. ISBN: 978-3-030-80406-0. DOI: [10.1007/978-3-030-80406-0_5](https://doi.org/10.1007/978-3-030-80406-0_5). URL: https://doi.org/10.1007/978-3-030-80406-0_5.
- [5] C. RILEY *et al.* “HV CABLE QUALIFICATIONS TO IEC 62067-2006 AND ICEA S-108-720-2004”. In: *Jicable Conf.* 2011.
- [6] W. Wang, X. Yan, S. Li, L. Zhang, J. Ouyang, and X. Ni. “Failure of submarine cables used in high-voltage power transmission: Characteristics, mechanisms, key issues and prospects”. In: *IET Generation, Transmission & Distribution* 15.9 (2021), pp. 1387–1402.
- [7] M. Danikas, D. Papadopoulos, and S. Morsalin. “Propagation of Electrical Trees under the Influence of Mechanical Stresses: A Short Review.” In: *Engineering, Technology & Applied Science Research* 9.1 (2019).
- [8] J.-n. Song, L. Lu, B. Teng, H.-i. Park, G.-q. Tang, and H. Wu. “Laboratory tests of vortex-induced vibrations of a long flexible riser pipe subjected to uniform flow”. In: *Ocean engineering* 38.11-12 (2011), pp. 1308–1322.
- [9] D. D. Tjahjanto, A. Tyrberg, and J. Mullins. “Bending mechanics of cable cores and fillers in a dynamic submarine cable”. In: *International Conference on Offshore Mechanics and Arctic Engineering*. Vol. 57694. American Society of Mechanical Engineers. 2017, V05AT04A038.
- [10] J.-M. Leroy, Y. Poirrette, N. Brusselle Dupend, and F. Caleyron. “Assessing mechanical stresses in dynamic power cables for floating offshore wind farms”. In: *International Conference on Offshore Mechanics and Arctic Engineering*. Vol. 57786. American Society of Mechanical Engineers. 2017, V010T09A050.

- [11] F. Ménard and P. Cartraud. “A computationally efficient finite element model for the analysis of the non-linear bending behaviour of a dynamic submarine power cable”. In: *Marine Structures* 91 (2023), p. 103465.

ACKNOWLEDGEMENTS

I would like to express my thanks to my promoter, Prof. Hans Hopman, for your great support and kindness during the long journey. The monthly meetings with you have benefited me so much, especially the last year when we had so much discussion about the overall structure of the PhD project. What has impressed me the most is your emphasis on how to truly contribute to the engineering and scientific worlds. You can not push me forward more to consistently pondering a clear and logical storyline for my PhD project so that the outsiders can immediately realize the issue within this field and the practitioners can quickly grasp the effective information they can use directly. I still remember the first time we met in China where you interviewed a bunch of masters who want to do their PhD in TU Delft. "How are you going to find the real gap within your research field and how can you make sure it is there indeed?" You asked me this question. I was in a daze for a moment and then mumbled to myself, "How weird this question is." I can not remember how I replied to you then, but during my PhD life when I racked my brains trying to find evidence supporting my storyline, I do realize how important this question is.

I also want to express my appreciation to my daily supervisor Dr. Xiaoli Jiang, for your great contributions and guidance on my research. Without your help, it is impossible to finish the difficult task. Thanks for allowing me to make mistakes and fall into pitfalls during the first two years. I thought you might blame me for choosing directions that did not work out as expected, but you gave me enough time and guided me through all the challenges based on your substantial experience and knowledge. You pushed me to acquire constantly on the basic skills for a PhD, such as presentation skills and writing skills. I can not thank you more for your effort in building connections with European cable companies and relevant institutions as far as you can. These experiences are going to be indispensable for my future career development.

Many thanks go to Prof. Yong Bai, who has been my supervisor throughout these years. On one hand, you wanted me to continue as your PhD student at Zhejiang University. On the other hand, you recommended me to do a PhD abroad without any hesitation when you got that opportunity for me. During my first year as a master's student, when my first conference paper was rejected, you called me and comforted me like a father, saying, "Be patient. It's not a big deal. You still need more time to grow." These were what you told me. I tried to be patient and still my mind, though I was not successful until the last two years of my PhD. In the Netherlands, I still enjoy being connected with you. Every time I come back to China, I also like to pay a visit to you. I believe you were an optimistic young man who was fighting for a bright future when you were my age, just like a couple of young men I met in the Netherlands. I enjoy being with them, and I believe I would want to be friends with you if we were of the same age.

Dear Dr. Xiao Li, thanks for sharing your knowledge with me on all the simulations and thanks for helping me reshape the structure of my PhD dissertation. You gave me lots of useful and insightful advice that pushed forward the project. The most appreciated is that you encouraged me to try the repetitive unit cell method. Without you, I would have relied on my old skills and have had no courage to make this risky attempt. It's like you were always there to support me during the reproduction process. The most beneficial outcome of this attempt is that I complain no more about difficulties and I got the courage to try many new stuffs in my future research. You must remember at the end of my PhD I updated our model by further incorporating a few new techniques, which cost me more time and resulted in a delay. You probably do not know that I would not do these alone if it was not for the first successful attempt with your support. By following your suggestion on the research, I might be able to get my PhD degree sooner. However, I hope, one night many years later when I read my dissertation, I am still satisfied with the content and go to bed happily after I close it. I will thank you so much.

Thanks to the China Scholarship Council, the financial support for living abroad is greatly appreciated. I will never forget my root and my goal. Being a member of Association of Chinese Student and Scholars in the Netherlands (ACSSNL), I was fortunate to have a few chances to visit the Chinese embassy in the Kingdom of the Netherlands and have discussions with the teachers in the Education Department. Thanks for your care and support during my overseas life. Take this chance, I would also like to thank ACSSNL where I met many outstanding people in many different areas. Yu Chen, Yuxin Chen, Xiaowen Liu, Yiyang Li, Xinhui Wang, Yichi Mo, Tianchang Ji, Xiao Du and An Pan. I will always remember the activities we organized together and the happy time I spent with you all.

Also many thanks go to all the colleagues in our 3ME building, especially the lovely guys on the second, third and fourth floors. I like hanging out, chatting and partying with you. My officemates Ahmed Hadi, Breno Alves Beirigo, Jesper Zwaginga and Qinqin Zeng, we exchanged our opinions on our cultures from different perspectives, even though sometimes politics are involved (Haha). Dear Adrien Nicolet, Cigdem Karademir, Abhishek Dhyani, Nikolaos Kougiatsos, Konstantinos Zoumpourlos, Zongchen Li, Jie Cai, Wei Jun Wong, Rongxin Song, Xin Xiong, Yimeng Zhang, Mingxin Li, Xiuhan Chen, Qianyi Chen, and Ping He, thank you all! Many thanks to our secretaries Patty, Anouk, Pauline, and Monique for always being kind and helpful during my PhD journey. Thanks Evelien, for helping my revising the Dutch version of my summary.

After the stupid Covid-19, I got chances to meet many new friends. Zhaochong Cai, you are undoubtedly one of the most important ones. We quickly got acquaint with each other, probably because we are both from Jiangxi and we studied in the same university before. Maybe it's because we share many hobbies. I will never forget how Binbin Zhang and we climbed those snow mountains in Europe. The splendid pictures we saw in the mountains always enter my mind. They have become one of the energy sources in my life. In Delft Blaw bouldering gym, I met many interesting friends. Yujuan Gui, Qi Shen, Nianlei Zhang, Weichen Xu, Joan, Binge, Hongjie, thanks for those wonderful bouldering times. Being familiar with one's own body is an exciting thing. I like the feeling of touch on a rock with my figures, especially true rocks in the wild.

I also like the feeling from my feet when my snowboard transverses a snow slope. Thanks, Binbin for inviting me to have a try in skiing. I never loved a sport so much and wanted to put much effort into improving my skills. Provided it was not my research, I probably want to develop a career related to skiing. After all, I am so good at it. I want to thank all the friends I met on the skiing journey: Qi An, Xue Yao, Hanqing Liu, Chao Song, Sifeng He, Tianli Song, Terrance, Sherry, Leo, Yichen Yang, Biao Chen, Xiaowei, Chen Liu, etc. Special thanks to Xiaowei who snowboarded a lot with me when I was so crazy in improving my snowboarding skills. I enjoyed the time with you in Snowworld and the skiing journey in France. You are not only an excellent student, but also a nice friend very good at listening.

Very personal and special thanks go to our library group, named TUD lib. rolling kings. This group was first initiated with only three people who usually studied in TUD library. After more time spent in the library, more people joined. By the time I am writing Acknowledgements, there are already 11 people. We shared many wonderful memories and passed through many hard times together. I like enjoying lunch with you, complaining about our supervisors and sharing gossip, etc. Thanks, Yunzhong Zhou for starting the group. We had many great times not only in the library but also in Germany. Thanks for complaining about nothing when we hiked in a wood till very late at night and found nowhere to camp. I really like that camping area, especially the moment listening to the rain drop on the top of our camp during the night and seeing the beautiful shining lake when I first opened my eyes in the morning. Thanks for spending a memorable spring festival with me in Germany and tolerating my driving to a speed near 200 km/hour on the highway in our rented poor car. Thanks for providing me with tons of useful information on everything, etc. Thank all the members of the group: Zhaochong Cai, Yunzhong Zhou, Xue Yao, Yitao Huang, Xiuli Wang, Xin Ren, Yuexin Huang, Weijun Wong, Di Yan and Dr. Wang who studies aerospace.

感谢东方电缆、中天电缆、亨通电缆和杭州电缆。Thanks Ningbo Oriental Cable, ZTT, Hengtong and Hangzhou Cable. Without your products and help, I have no test data to guide the development and finish the validation of my model. I sincerely hope your markets will expand all over the world.

亲爱的爸爸方年林、妈妈饶慧萍，感谢你们。你们既希望我留在你们身边，又愿意让我放手去做自己想做的事。我小时候你们问我长大想干嘛？我回答说：“要成为一名科学家”。我只是随便编一个显得高大上的职业让你们觉得开心，省得不停地拷问我。没想到最后我真的成了一名科研打工人。感谢你们尽你们的能力把最好的给我。谢谢外公、外婆和亲爱的家人们，每次回家看到你们的笑脸都让我感觉很开心。希望你们健康快乐！

*Pan Fang
Delft, April 2024*

CURRICULUM VITÆ

Pan FANG

25-10-1994 Born in Jingde Zhen, China.

EDUCATION

2011–2015 Undergraduate, Civil Engineering
Nanchang Institute of Technology

2016–2019 Master, Ocean Engineering
Zhejiang University

2019 PhD, Mechanical, Maritime & Materials
Technische Universiteit Delft

Thesis: Development of an Effective Modelling Method for the
Local Mechanical Analysis of Submarine Power Cables

Promotor: Prof. dr. Hans Hopman

Copromotor: Dr. Xiaoli Jiang

LIST OF PUBLICATIONS

11. P. Fang, X. Li, X. Jiang, H. Hopman, and Y. Bai. "Development of an effective modeling method for the mechanical analysis of three-core submarine power cables under tension". In: *Engineering Structures* 317 (2024), p. 118632. ISSN: 0141-0296
10. P. Fang, X. Li, X. Jiang, H. Hopman, and Y. Bai. "Bending study of submarine power cables based on a repeated unit cell model". In: *Engineering Structures* 293 (2023), p. 116606
9. P. Fang, Y. Xu, Y. Gao, L. Ali, and Y. Bai. "Mechanical responses of a fiberglass flexible pipe subject to tension & internal pressure". In: *Thin-Walled Structures* 181 (2022), p. 110107
8. P. Fang, X. Jiang, H. Hopman, and Y. Bai. "Mechanical responses of submarine power cables subject to axisymmetric loadings". In: *Ocean Engineering* 239 (2021), p. 109847
7. P. Fang, X. Li, X. Jiang, H. Hopman, and Y. Bai. "Development of an Effective Modelling Method for the Mechanical Analysis of Submarine Power Cables under Bending". In: *Computer Methods in Applied Mechanics and Engineering* (Under review)
6. P. Fang, X. Li, X. Jiang, H. Hopman, and Y. Bai. "Local Mechanical Analysis of a Three-core Submarine Power Cable under Combined Loadings". In: *Marine Structures* (Under review)
5. P. Fang, X. Li, X. Jiang, H. Hopman, and Y. Bai. "A review of the analysis tools in the local mechanical study of submarine power cables". In: *Marine Structures* (Under review)
4. P. Fang, X. Li, X. Jiang, H. Hopman, and Y. Bai. "Bending Analysis of Submarine Power Cables under multi-physical effects". In: (To be submitted)
3. P. Fang, X. Li, X. Jiang, H. Hopman, and Y. Bai. "Computational homogenization method for the bending analysis of submarine power cables". In: *Journal of Physics: Conference Series*. Vol. 2647. 2. IOP Publishing. 2024, p. 022010
2. P. Fang, X. Li, X. Jiang, H. Hopman, and Y. Bai. "Study of the Effects of Cross Section Shape on the Structural Behaviour of Helical Wires on a Bent Flexible Structure". In: *The 33rd International Ocean and Polar Engineering Conference*. OnePetro. 2023
1. P. Fang, X. Jiang, H. Hopman, and Y. Bai. "A review of mechanical analysis of submarine power cables". In: *Maritime Technology and Engineering 5 Volume 2* (2021), pp. 559–568

TRAIL THESIS SERIES

The following list contains the most recent dissertations in the TRAIL Thesis Series. For a complete overview of more than 400 titles, see the [TRAIL website](http://www.rsTRAIL.nl): www.rsTRAIL.nl. The TRAIL Thesis Series is a series of the Netherlands TRAIL Research School on transport, infrastructure and logistics.

- Fang, P., *Development of an Effective Modelling Method for the Local Mechanical Analysis of Submarine Power Cables*, T2024/17, December 2024, TRAIL Thesis Series, the Netherlands.
- Zattoni Scroccaro, P., *Inverse Optimization Theory and Applications to Routing Problems*, T2024/16, October 2024, TRAIL Thesis Series, the Netherlands.
- Kapousizis, G., *Smart Connected Bicycles: User acceptance and experience, willingness to pay and road safety implications*, T2024/15, November 2024, TRAIL Thesis Series, the Netherlands.
- Lyu, X., *Collaboration for Resilient and Decarbonized Maritime and Port Operations*, T2024/14, November 2024, TRAIL Thesis Series, the Netherlands.
- Nicolet, A., *Choice-Driven Methods for Decision-Making in Intermodal Transport: Behavioral heterogeneity and supply-demand interactions*, T2024/13, November 2024, TRAIL Thesis Series, the Netherlands.
- Kougiatsos, N., *Safe and Resilient Control for Marine Power and Propulsion Plants*, T2024/12, November 2024, TRAIL Thesis Series, the Netherlands.
- Uijtdewilligen, T., *Road Safety of Cyclists in Dutch Cities*, T2024/11, November 2024, TRAIL Thesis Series, the Netherlands.
- Liu, X., *Distributed and Learning-based Model Predictive Control for Urban Rail Transit Networks*, T2024/10, October 2024, TRAIL Thesis Series, the Netherlands.
- Clercq, G. K. de, *On the Mobility Effects of Future Transport Modes*, T2024/9, October 2024, TRAIL Thesis Series, the Netherlands.
- Dreischerf, A.J., *From Caveats to Catalyst: Accelerating urban freight transport sustainability through public initiatives*, T2024/8, September 2024, TRAIL Thesis Series, the Netherlands.
- Zohoori, B., *Model-based Risk Analysis of Supply Chains for Supporting Resilience*, T2024/7, October 2024, TRAIL Thesis Series, the Netherlands.

- Poelman, M.C., *Predictive Traffic Signal Control under Uncertainty: Analyzing and Reducing the Impact of Prediction Errors*, T2024/6, October 2024, TRAIL Thesis Series, the Netherlands.
- Berge, S.H., *Cycling in the age of automation: Enhancing cyclist interaction with automated vehicles through human-machine interfaces*, T2024/5, September 2024, TRAIL Thesis Series, the Netherlands.
- Wu, K., *Decision-Making and Coordination in Green Supply Chains with Asymmetric Information*, T2024/4, July 2024, TRAIL Thesis Series, the Netherlands.
- Wijnen, W., *Road Safety and Welfare*, T2024/3, May 2024, TRAIL Thesis Series, the Netherlands.
- Caiati, V., *Understanding and Modelling Individual Preferences for Mobility as a Service*, T2024/2, March 2024, TRAIL Thesis Series, the Netherlands.
- Vos, J., *Drivers' Behaviour on Freeway Curve Approach*, T2024/1, February 2024, TRAIL Thesis Series, the Netherlands.
- Geržinič, N., *The Impact of Public Transport Disruptors on Travel Behaviour*, T2023/20, December 2023, TRAIL Thesis Series, the Netherlands.
- Dubey, S., *A Flexible Behavioral Framework to Model Mobility-on-Demand Service Choice Preference*, T2023/19, November 2023, TRAIL Thesis Series, the Netherlands.
- Sharma, S., *On-trip Behavior of Truck Drivers on Freeways: New mathematical models and control methods*, T2023/18, October 2023, TRAIL Thesis Series, the Netherlands.
- Ashkrof, P., *Supply-side Behavioural Dynamics and Operations of Ride-sourcing Platforms*, T2023/17, October 2023, TRAIL Thesis Series, the Netherlands.
- Sun, D., *Multi-level and Learning-based Model Predictive Control for Traffic Management*, T2023/16, October 2023, TRAIL Thesis Series, the Netherlands.
- Brederode, L.J.N., *Incorporating Congestion Phenomena into Large Scale Strategic Transport Model Systems*, T2023/15, October 2023, TRAIL Thesis Series, the Netherlands.
- Hernandez, J.I., *Data-driven Methods to study Individual Choice Behaviour: with applications to discrete choice experiments and Participatory Value Evaluation experiments*, T2023/14, October 2023, TRAIL Thesis Series, the Netherlands.
- Aoun, J., *Impact Assessment of Train-Centric Rail Signaling Technologies*, T2023/13, October 2023, TRAIL Thesis Series, the Netherlands.
- Pot, F.J., *The Extra Mile: Perceived accessibility in rural areas*, T2023/12, September 2023, TRAIL Thesis Series, the Netherlands.

- Nikghadam, S., *Cooperation between Vessel Service Providers for Port Call Performance Improvement*, T2023/11, July 2023, TRAIL Thesis Series, the Netherlands.
- Li, M., *Towards Closed-loop Maintenance Logistics for Offshore Wind Farms: Approaches for strategic and tactical decision-making*, T2023/10, July 2023, TRAIL Thesis Series, the Netherlands.